UNIVERSITÀ
DEGLI STUDI
DI PADOVA

Sede Amministrativa: Università degli Studi di Padova

Dipartimento di Principi e Impianti di Ingegneria Chimica «I. Sorgato»

SCUOLA DI DOTTORATO DI RICERCA IN
SCIENZA ED INGEGNERIA DEI MATERIALI
CICLO XXIII

ELECTROCHEMICAL SENSORS BASED ON SINGLE-WALLED CARBON NANOTUBES FOR BIOLOGICAL DETECTION

Direttore della Scuola: Ch.mo Prof. Gaetano Granozzi
Supervisore: Ch.mo Prof. Moreno Meneghetti
Supervisore: Dr. Nicola Elvassore

Dottorando: Francesco Lamberti

Abstract

In this work thesis we aim at discussing electrochemical biosensors based on single-walled carbon nanotubes for biological detection. The main strategy is to obtain modified electrodes with carbon nanotubes with two different classes of strategy. This can be realized in two ways: a surface modification strategy and a bulk modification strategy. The first one concerns the modification of patterned gold electrodes in which the tridimensionality is assured by the creation of a controlled forest of single-walled carbon nanotubes. The second strategy proposed is the modification of electrodes by means of a bulk doping of materials. We realized carbon nanotubes doped polyacrylamide hydrogels (HYs) acting as biosensors for glucose detection.

Finally examples for the integration of biosensing and microfluidic environments are proposed.

Electrochemical measurements (EIS, CV and CA) were performed in order to characterize samples and substrates. Also morphological measurements (AFM and SEM) were conducted to study topographic features of samples. Biocompatibility tests and electrical measurements were performed when treating with living systems.

Abstract

In questo lavoro di tesi vogliamo discutere biosensori elettrochimici modificati con nanotubi di carbonio a parete singola. La strategia principale è di ottenere elettrodi modificati con nanotubi di carbonio attraverso due classi diverse di modificazione. Ciò può essere realizzato in due modi: attraverso una modifica della superficie dell'elettro oppure attraverso una modifica della struttura del materiale. Per quanto riguarda la prima si tratta di una modificazione di elettrodi d'oro disegnati in cui la tridimensionalità è assicurata dalla creazione di una forest controllata di nanotubi di carbonio a parete singola. La seconda strategia proposta è la modifica di elettrodi per mezzo di doping di materiali. Si sono realizzati hydrogel (HYs) di poliacrilammide drogati con nanotubi di carbonio a parete singola in modo da funzionare come biosensori per il rilevamento di glucosio.

Infine vengono proposti esempi per l'integrazione dei biosensori in piattaforme mifcrofluidiche.

La caratterizzazione dei substrati e dei campioni è stata condotta per mezzo di misure elettrochimiche (EIS, CV e CA). Vengono eseguite inoltre misure di caratterizzazione morfologica (AFM e SEM) per studiare le proprietà topografiche dei campioni in esame. Nei casi in cui si è avuto a che fare di sistemi viventi sono state condotte prove di biocompatibilità e prove per il riconoscimento del segnale elettrico dalla superficie delle cellule.

To Chiara, my incredible love

Se sei a terra non strisciare mai
se ti diranno sei finito
non ci credere
G. Morandi, Uno su Mille ce la fa, 1999.

capio Falbo?

Non importa quanto vai piano,
l'importante è che tu non ti fermi
Confucio, VI sec. BC

Acknowledgements

23.33 del 28 gennaio 2011. Fine dei lavori. Puzzo come un cane (perchè non mi lavo di mio, mica per altro), il mio tesoro sta stirando magliette, jeans, robe.. Il tutto sotto lo sguardo attento della micetta bellissima che ci hanno dato in prestito e con ogni probabilità ci terremo. Che centra con i ringraziamenti sta roba? Niente, ma sono talmente fuso che scrivere castronerie è sicuramente più divertente che scrivere di nanotubi.
Alzo gli occhi e vedo la mia bellissima Chiara china sul ferro intenta a guardare "Grays Anatomy" e vedo il futuro bellissimo che ci attende: tieni duro Diamante quando la Gelmini capirà che ha fatto una cazzata saremo milionari. Come no!

Ringraziare il resto del mondo è fin troppo semplice e fastidioso: dallo Zio Ponzio che senza le sue inettitudini non mi avrebbero permesso di conoscere la Chiara, al Padova tutto (dagli ALN alla CAN B passando per la CAN PVO), all'AIA tutta che se non ci fosse bisognerebbe inventarla.

Poi vengono i miei *colleagues* che mai come in sti mesi sono sparsi per il mondo: da Elisa nella East Coast ad Ale nella West. Gli altri non serve, li ringrazio di persona che tanto sono tutti qui.. :)
Un grazie doveroso al Dr. Nelvas che mi ha fatto capire "come scrivere un lavoro scientifico in maniera decente (parole sue) el al caro Prof. Meneghetti, più grillo parlante che vero supervisore di tesi.
Un grandissimo grazie ai miei (ex) laureandi Marco, Martino e Franz che con i loro sforzi hanno fatto sì che questa tesi potesse prendere forma.

Finiamo ringraziando i parentadi vari che sono distribuiti in un qualche intorno di Padova (ormai vedo la città da distante) pié che altro perché non so

quanto hanno pagato per farmi arrivare alla fine di sto benedetto PhD.
Insomma, *xe finia sta fadiga!* E adesso?
Come al solito: aspettiamo che Nicola mi dica che posso mandare in stampa sto bel lavoretto che mi ha fatto faticar parecchio negli anni e che spero possa piacere a chi vuole leggerlo o se la cosa vi stanca troppo, spero almeno che la copertina sia di vostro gradimento.

Buona lettura! ... in LaTeX ovviamente!

Contents

List of Figures

1

Introduction

1.1 Aim of the work

The aim of this PhD work thesis is to study the development, production and characterization of electrochemical sensors based on single-walled carbon nanotubes for biological detection. The main strategy is to obtain modified electrodes with carbon nanotubes with two different classes of strategy. This can be realized in two ways: a surface modification approach and a bulk modification strategy. The first one concerns the modification of patterned gold electrodes in which the tridimensionality is assured by the creation of a controlled forest of single-walled carbon nanotubes. The second strategy proposed is the modification of electrodes by means of a bulk doping of materials. We realized carbon nanotubes doped polyacrylamide hydrogels (HYs) acting as biosensors for glucose detection.

We also studied the possibility of integrating these two strategies in a microfluidic platform by a preliminary research on platinum wires enzymes modified electrodes for online biosensing.

In conclusion, specific aims of the project are:

- Development of a robust protocol of oxidation of carbon nanotubes
- Electrochemical characterization of tridimensional modified electrodes
- Development of micro/nanostructured electrodes by softlitography, UV litography and chemical deposition techniques
- Development of enzymatic biosensors for glucose detection

- Comprehension of fluidodynamics in integrating biosensors in microfluidic environments
- Interfacing of carbon nanotubes modified electrodes with living biological systems.

A detailed outline of the whole work follows.

1.2 Project outline and Summary

The work can be divided into three distinct phases that go across the entire period of thesis (see Fig. 1.1):

1. Electrode developing: preparation of samples
2. Electrode characterization: measurements and validation
3. Applications in biologic environment: functionalisation with biomolecules

The first phase was spent in developing a robust synthesis protocol of self-assembled monolayers (SAMs) of single-walled carbon nanotubes (SWCNTs) and the creation/optimization of the experimental setup.
In the detail, I create by chemical approach SAMs of vertically aligned SWCNTs on gold surfaces. The optimization of this protocol leads me to obtain a control in the height of the forests (see Chapter 3) by tuning oxidation temperature bath of SWCNTs. As you can see further, the vertical coupling is achieved by covalent linking of carboxylated SWCNTs with the underlying cysteamine (CYS) SAM. The modification of the relative concentration of CYS on gold substrates allow us to control the spatial distribution of SWCNTs and as a consequence, electrochemical properties may change (see Chapter 4).
Gold electrode deposition also was realized in two different ways. Gold electrodes were created by sputtering metal on glass substrates and then they were micropatterned by means of soft lithographic techniques (Chapter 3). Also gold was deposited by PECVD (Physical Enhanced Chemical Vapor Deposition) on a titanium seed layer over glass substrate in order to optimize adhesion of metal: the patterning is therefore achieved by means of UV light patterning (Chapter 4 and 5).
Also electrochemical experimental set up is optimized in order to obtain several parallel

measurements that enhance reproducibility: signaling noise reduction and signal acquisition (see Chapter 3, 4 and 5).
The second stage is based on the characterization and validation techniques used during nanostructuring of electrodes.
In this step, atomic force microscopy (AFM) images are collected in order to study height controlling of forests (Chapter 3 and 4). Also a Raman characterization is provided both for what concerns surface modification of gold (Chapter 3) both for what concerns bulk modification of gold (Chapter 5). In this latter case micromaps are provided. Electrochemical measurements are also performed for inquiring kinetic properties of the modified electrodes when a redox probe is present (Chapter 4): cyclic voltammetries (CVs), electrochemical impedance spectroscopy (EIS) and chronoamperometry (CA) measurements were conducted. From CVs and EIS we obtain informations about the reversibility and the rate of response of the forests when height and density is tuned (Chapter 4); EI spectra of polyacrylamide hydrogels (HYs) modified with SWCNTs showed that carbon nanotubes may act as doping agent for making HYs electroconducting and CA scans of enzyme modified SWCNTs doped HYs were performed to detect glucose (Chapter 5). CA scans were finally performed in enzyme modified platinum microelectrodes working in microfluidic platforms for online detection of glucose (Chapter 6).
In the third and last phase I stuck together prepared electrodes to biological word: functionalisation of electrodes with biomolecules were done. I performed biocompatibility tests over SWCNTs doped HYs to check any toxicological effects of nanotubes doping (Chapter 5). Electrophysiological measurements were also performed in these samples: cardiomyocites were cultured on modified HYs and electrical signals are obtained (Chapter 5).
Also detection limits (DLs) of glucose detection of biosensors based on enzyme modified SWCNTs doped HYs (Chapter 5) and online detection with microelectrodes in microfluidic platforms were calculated (Chapter 6).
Thesis outline is organized as follows:

- Chapter 2: *Motivation of electrochemical biosensing with carbon nanotubes.* In this chapter the state of the art in modifying biosensors with carbon nanotubes is reviewed. Surface modification and bulk modification strategy are discussed. The perspective of integrating biosensors in microfluidic platforms is also discussed;

- Chapter 3: *Nanotubes oxidation temperature controls the height of single-walled carbon nanotube forests on gold micropatterned thin layers.* In this chapter a robust protocol of oxidation tuning bath oxidation temperature of nanotubes is shown. Carboxylated carbon nanotubes of different lengths and defects are created;

- Chapter 4: *Heterogeneous electron transfer parameters for forests with different density and height.* In this chapter electrochemical properties of single-walled carbon nanotubes forests with different heights and densities are studied. Wettability measurements are also provided in order to understand different topographic features of samples;

- Chapter 5: *Development of single-walled carbon nanotube-doped hydrogels for electrochemical biosensing.* In this chapter polyacrilamide hydrogels doped with carbon nanotubes were produced and modified with enzymes in order to detect glucose. Good detection limits are obtained. Heart cells were also cultured over samples for detecting electrical signals from the surface of cells;

- Chapter 6: *Sampling and biosensing of multi-analytes in microfluidic platforms.* This chapter is focused on integrating biosensors in microfluidic systems for effective measurements of multi-analytes. Effect of flow rate is studied in samples in which glucose or hydrogen peroxide is tuned.

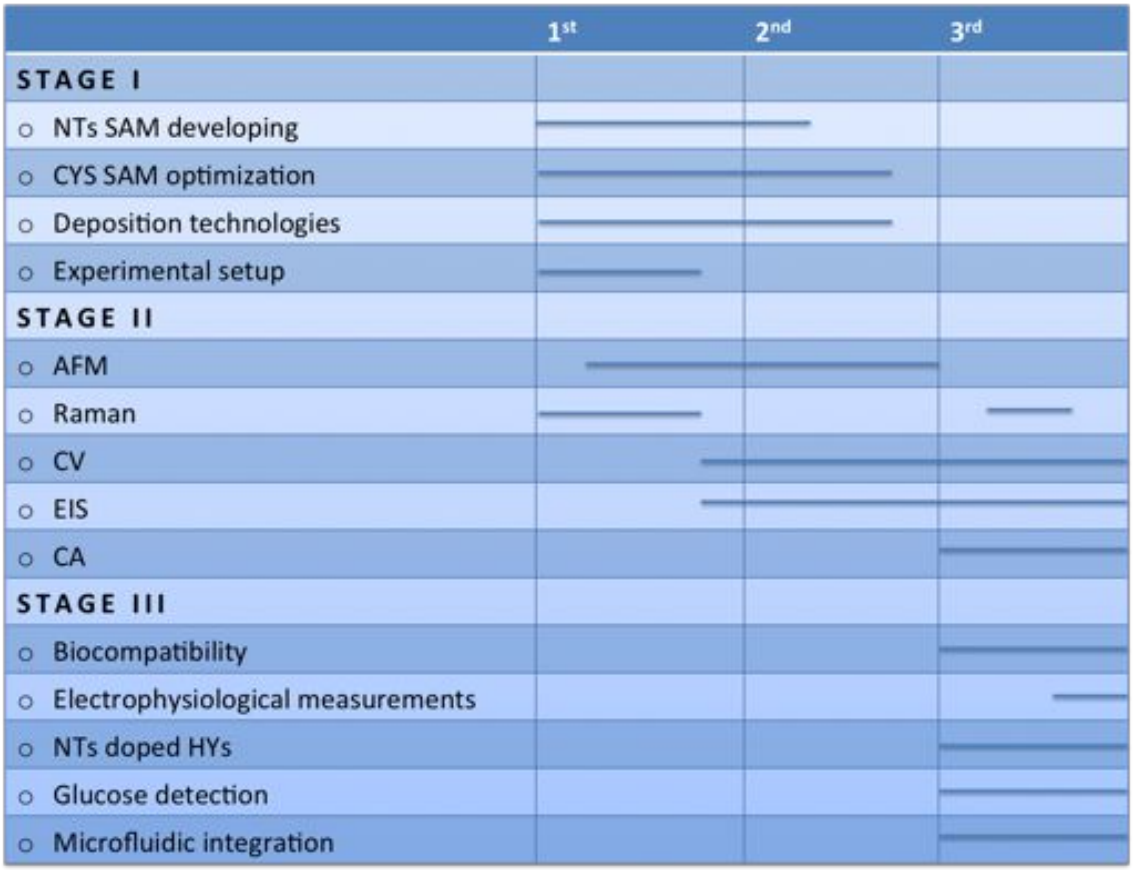

Figure 1.1: Timeline of PhD thesis development during the three years. - Each stage represents a step in developing the main project

2

Motivation of electrochemical biosensing with carbon nanotubes

In this chapter the state of the art in modifying biosensors with carbon nanotubes is reviewed. Surface modification and bulk modification strategy are discussed. The perspective of integrating biosensors in microfluidic platforms is also discussed. The present Chapter will be part of the book "Carbon nanotubes / Book 1" edited by InTech.

2.1 Electrochemical biosensing with carbon nanotubes

Carbon based electrodes have been commonoly used because of their cost, good electron transfer kinetics and biocompatibility. Recently carbon nanotubes (CNTs) have also been incorporated into electrochemical sensors.[1, 2, 3, 4, 5]

CNTs offer unique advantages including enhanced electronic properties, a large edge plane/basal plane ratio and a rapid electrode kinetics. In general, CNT-based sensors have higher sensitivities, lower limits of detection and faster electron transfer kinetics then traditional carbon electrodes. Many variables need to be tested and then optimized in order to create a CNT-based sensor. The performance can depend on the synthesis method of the nanotube, CNT surface modification, the method of electrode attachment and the addition of electron mediators.

Electrochemistry implies the transfer of charge from one electrode to another electrode. This means that at least two electrodes constitute an electrochemical cell to form a closed electrical circuit. However, a general aspect of electrochemical sensors is that the charge

transport within the transducer part of the whole circuit is always electronic. By the way, the charge transport in the sample can be electronic, ionic, or mixed. Due to the curvature of carbon graphene sheet in nanotubes, the electron clouds change from a uniform distribution around the C-C backbone in graphite to an asymmetric distribution inside and outside the cylindrical sheet of the nanotube. When the electron clouds are distorted, a rich π-electron conjugation forms outside the tube, therefore making the CNT electrochemically active [6]. Electron donating and withdrawing molecules such as NO_2, NH_3, and O_2 will either transfer electrons to or withdraw electrons from single-walled carbon nanotubes (SWCNTs). Thereby giving SWCNTs more charge carriers or holes, which increase or decrease the SWCNT conductance.[6]

Recent studies demonstrated that CNTs can enhance the electrochemical reactivity of important biomolecules[7, 8, 9, 10], and can promote the electron-transfer reactions of proteins (including those where the redox center is embedded deep within the glycoprotein shell).[11, 12] In addition to enhanced electrochemical reactivity, CNT-modified electrodes have been shown useful to accumulate important biomolecules (e.g., nucleic acids) [13] and to alleviate surface fouling effects (such as those involved in the NADH oxidation process).[8] The remarkable sensitivity of CNT conductivity to the surface adsorbates permits the use of CNT as highly sensitive nanoscale sensors. These properties make CNT extremely attractive for a wide range of electrochemical biosensors ranging from amperometric enzyme electrodes to DNA hybridization biosensors. To take advantages of the remarkable properties of these unique nanomaterials in such electrochemical sensing applications, the CNT need to be properly functionalized and immobilized. There are different ways for confining CNT onto electrochemical transducers. Most commonly, this is accomplished using CNT coated electrodes [13, 14, 15, 16, 17] or using CNT/binder composite electrodes [18, 19, 20]. The CNTs driven electrocatalytic effects and the increasing use of modified CNTs for electroanalytical applications have been recently reviewed [17].

Among the traditionally used electrode materials, CNTs showed better behavior than the others which also have good conducting ability and high chemical stability. CNT-based electrochemical transducers offer substantial improvements in the performance of amperometric enzyme electrodes, immunosensors and nucleic-acid sensing devices. The greatly enhanced electrochemical reactivity of hydrogen peroxide and NADH near the proximity or on the CNT-modified electrodes makes these nanomaterials extremely attractive for numerous oxidase- and dehydrogenase-based amperometric biosensors. For example, aligned

CNT "forest" can act as molecular wires to allow efficient electron transfer between the underlying electrode and the redox centers of enzymes. The CNT transducer can greatly influence for enhancing the response of the biocatalytic reaction product and provide amplification platforms carrying multiple enzyme tags.

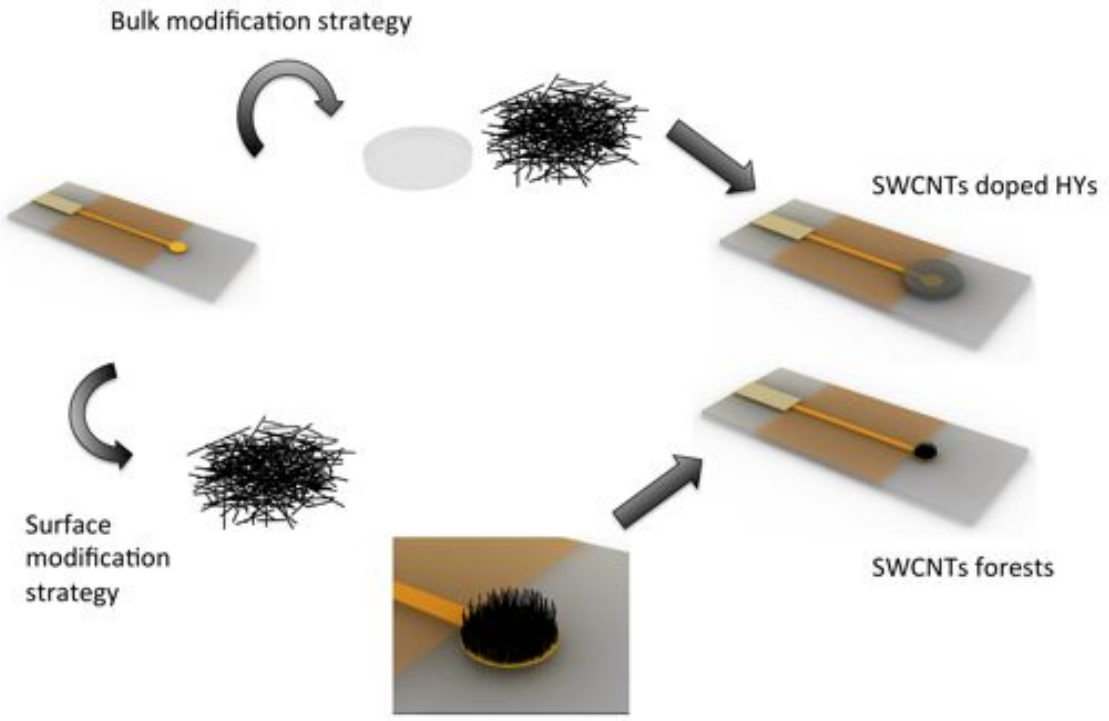

Figure 2.1: A schematic view of the strategies adopted in this work thesis. -

CNTs are generally used as doping in materials or biomaterials in two ways (Fig. 2.1):

- Via a surface modification strategy;
- via a bulk modification of materials.

The next two sections will provide a brief report of the state of the art of these two experimental strategies that form the principal targets of our work.

2.1.1 Surface modification strategy

It is extremely important to assemble SWCNTs on desired surface locations, with controlled density and orientation. The high order of SWCNT alignments can improve the performance of many nanotube-based devices. For example, SWCNTs can be used as field emitters in panel display, where vertically aligned nanotube arrays are highly desired.
Well-aligned nanoelectrode arrays are highly desirable to develop nano-scale electrochemical and bioelectrochemical sensors, though the high order of the nanoelectrode arrays is not prerequisite. In this application, vertically aligned carbon nanotubes are usually employed as nanoelectrodes due to their small diameter, high aspect ratio, and good conductivity. For example, vertically aligned MWNTs embedded in SiO_2 exhibited ultrahigh sensitivity for DNA detection[21]. Vertically aligned SWCNTs also showed good performance in electrochemical and bioelectrochemical devices[11, 22, 23, 24, 25]. Diao and Liu demonstrated that v-SWCNTs prepared by chemical assembly could be used as nanoelectrode arrays[22, 23] and the assembly density of SWCNTs had great effect on the electrochemical behavior of the nanotubes[23]. Gooding and coworkers demonstrated that v-SWCNTs are a good electrochemical system to study charge transfer properties between SWCNTs and redox proteins[11]. Rusling et al. accomplished highly sensitive electrochemical immunodetection of cancer biomarkers by using v-SWCNTs prepared by chemical assembly[24]. Moreover, it has been found that v-SWCNTs electrodes have a faster charge transfer rate compared to the randomly dispersed SWCNTs[25], indicating that, from the viewpoint of electrochemical studies, aligned SWCNTs are superior to unaligned SWCNTs.
The examples mentioned above clearly illustrate that vertically aligned carbon nanotubes may find a lot of applications in biosensing and the vertical orientation of nanotubes to the substrate provides additional advantages in practice. However, SWCNTs prepared by traditional chemical vapor deposition (CVD), arc-discharge, and laser ablation are nearly endless, randomly curled, and highly tangled. Due to the lack of order, these nanotubes cannot be used directly in most applications, especially in those applications that require perpendicular orientation to the substrates. Therefore, great efforts have been made to develop simple but effective methods for obtaining v-SWCNTs, and until now great progress has been achieved.

2.1.2 Bulk modification strategy

It is particularly surprising that only a few works discussing bulk biomaterials doped by carbon nanotubes are reported: they are normally used in tissue engineering as reinforcing agents [26, 27, 28, 29, 30, 31]. However a lot of papers in which there is an extended use of bulk modification of biomaterials has been reported in literature since the early Nineties [32, 33, 34, 35].

Among biocompatible materials, synthetic polymers are most frequently utilized in tissue engineering and cell culturing. They can be synthesized to be relatively nonadhesive, resorbable or tissuelike hydrogels but generally they are not electroconductive. On the other hand metals can provide high electrical conductivity but are not suitable for cell culturing application.

To achieve both features, the use of composites containing synthetic and naturally derived materials is of increasing interest [26]. In addition, soft drug delivery systems (materials that exhibit soft gel-like properties) have received increasing attention during the last decade.

Electrical conductivity is a desirable feature in composites to be used to support the growth of tissues such as cardiac muscle and neural tissue [36] in which electrical signals are propagated. An ideal interface between cells and artificial materials should promote adhesion and proliferation, and in the case where electrical stimulation is desired, have low electrical impedance. Ideally, interfacial biocompatibility and electrical charge transfer can be increased by using biomimetic and adaptive electrode materials that can seamlessly integrate with tissues once implanted [37].

Polymeric hydrogels with high water content and low surface tension [38] and [39] have been extensively used to mimic the natural extracellular matrix and promote cell growth.[40] Consequently, conducting gel coatings have been used to enhance the performance of implantable electrode.[41]

Polymer hydrogels are three-dimensional polymeric networks formed from highly hydrophilic monomers rendered insoluble by virtual, electrostatic or covalent crosslinking. Hydrogels imbibe large amounts of water. The result is an elastic network with water effectively filling the interstitial space of the network. When immersed and equilibrated in aqueous medium, cross-linked hydrogels assume their final hydrated network structure which brings into balance the forces arising from the solvation of the repeat units of the macromolecular chains that leads to an expansion of the network (the swelling force) and

the counter balancing elastic force of the cross-linked structure (the retractive force).
The imbibed water of a hydrogel may be free (freezable) or bound (non-freezable) [42, 43]. The hydrogel can accordingly easily change its size and shape in response to environmental stimuli and this is one of its intrinsic characteristics; effectively expelling or imbibing free water. Moreover, in so doing, hydrogels can also imbibe other monomeric, reactive and potentially polymerizable species into its interstices, essentially occupying its void volume and interacting with chain segments or pendant moieties of the host hydrogel.
Hydrogels have emerged since the early 50s as being of great importance in the biomaterials field.[44] Their unique characteristics, being of a soft elastomeric nature, serves to minimize mechanical and frictional irritation to the tissue bed, their low interfacial tension contributes to a reduction in protein adsorption and hence biofouling and cell adhesion, and their swelling capacity results in high permeabilities for low molecular weight drug molecules and metabolite.[45] These characteristics have allowed hydrogels to be used in biomedical applications that include biosensors, drug delivery systems, contact lenses, catheters, wound dressings and tourniquets. Of particular interest is their use as matrices for the immobilization and stabilization of enzyme.[46] This interest has lead to their parallel development as the biorecognition layer of potentiometric, conductometric, amperometric and fiber-optic based enzyme biosensors. Because of their high water content, hydrogel membrane layers and gel pads also find application as micro-bioreactors for the hosting and stabilization of biological molecules and for the conduct of biological reactions. There are multiple reports involving hydrogels that document their biocompatibility, biodegradability, dielectric relaxation and mass transport properties.
Poly(hydroxyethyl methacrylate)-based hydrogels are hydrolytically stable, may be engineered to possess similar water content and elastic moduli as body tissues, and exhibit good in vitro and in vivo biocompatibility.[47] Other types of naturally occurring, synthetic and hybrid hydrogels have been proposed and studied for the immobilization of biorecognition molecules and whole cells. Among these are agarose, alginates, polyvinylalcohol, poly(acrylate), collagen and gelatin, chitosan and hyaluronic acid.
Hydrogels are often utilized in tissue engineering when mass transport is required to and from a cell population, such as in cell encapsulation. The water content and mechanical properties of hydrogels can be tailored to be similar to that of a particular tissue; therefore the necessary transport of nutrients or cell products can occur. Also electrical properties may be important for integrations with sensors and actuators or electrically

active tissues such as cardiac muscle or neurons. These properties include conductivitiy, piezoelectric and charge storage properties. There are specific tissues in which electrical conductivity is an important functional feature, such as cardiac and neural tissue. It has also been suggested that electrical stimulation can cause physiological changes in a variety of cell type.[48] A number of recent studies have focused on the development of composite materials to enhance the properties of synthetic polymers commonly used in biomedical applications. Promising applications of such materials include their use as biomaterial scaffolds, sensors and delivery tools in the field of tissue engineering.[49]

2.1.3 Biosensing and microfluidics

The attraction of integrating an electrochemical detector module into microfluidics derives from its inherent portability and the easy fabrication of the microelectrodes. The instrumentation costs for this technique are also the lowest.
However, in order to utilize electrochemical detection in capillary electrophoresis separation, the interference resulting from high separation voltage needs to be eliminated first. The high electrophoretic voltage will raise the baseline of electrochemical detection and shift the redox potentials for the analytes. Hauser's group [50] has developed a microfluidic device for amino acids and carbohydrates based on electrochemical detection that tackled the high voltage field interference issue. In their study, a semicircular cross section separation channel 50 μm in width and 20 μm in depth was designed, with a significantly enlarged channel width at the far end near the working electrode. In this way, a small overall current was generated by the highly resistive, narrow separation channel as well as high voltage drop before approaching the working electrode. Furthermore, the enlarged channel width further reduced the local channel resistance and the electric field strength at that small current. As a result, the separation voltage that could cause interference to the detection was limited.[51] Another possible approach to eliminating any interference from the applied electrical field on the detection is to use a so-called decoupler in front of the detector. This consists of a porous material through which the solution can pass and make contact with the electrophoretic ground electrode [52].
The microfluidic device mentioned above also minimized the number of electrodes employed by using the electrophoretic ground electrode as the counter electrode of the electrochemical detector. Only a working electrode and an electrophoretic ground electrode were used for separation and detection. The feasibility of such simplification relies on the

stable potential from the electrolysis of water and the negligible amperometric current generated compared with the electrophoretic current. Incorporating electrodes in microfluidics is often also a technical challenge. Three electrodes are required to enable electrochemical detection with a highly resistive buffer. Whitesides' group [53] demonstrated a multiphase laminar flow patterning method of fabricating electrodes within microchannels. For a microscale system with a Reynolds number ¡ 2,000, the fluidic flow within the channels will be laminar in nature. Diffusional mixing of two or more streams of fluid in microscale features will dominate without turbulence. If there is a chemical reaction after the mixing of two streams of fluid, the reaction will only take place at the interface between the fluidic streams. In the work described by Kenis et al.[53], two streams containing components of an electroless silver-plating solution were diffusively mixed, but only at the fluidic interface, so that the silver was reduced and deposited at the position of the fluidic interface in a microchannel 200 μm in width. Although the dimensions of this silver reference electrode were not reported, a polymeric structure only 5 μm in width was deposited on glass by the same method. The study showed the potential of this method for fabricating ultramicroelectrode (UME), which is of significance to modern electrochemical studies.
There are three main types of electrochemical detection method: amperometry, potentiometry and conductometry. Electrochemical measurements only detect the electrical properties of analyte species undergoing redox reactions, so they are limited to electroactive species. The specific electrode potential can be employed to filter out compounds other than the analyte being detected. In combination with capillary electrophoresis separation, electrochemical detection often provides very good detection limits in microfluidics. Electrochemical detectors for detecting metabolic activity at the extracellular, single-cell level have recently been reviewed.[54]

3

Nanotubes oxidation temperature controls the height of single-walled carbon nanotube forests on gold micropatterned thin layers

In this chapter a robust protocol of oxidation tuning bath oxidation temperature of nanotubes is shown. Carboxylated carbon nanotubes of different lengths and defects are created. This work is published in Langmuir [55].

3.1 Abstract

We developed a simple methodology for a direct control of the height of carboxylated single-walled carbon nanotube (SWCNT) forests. We found that the important step is a good control of the oxidation temperature of the nanotubes. SWCNTs oxidation at different temperature was followed by Raman and X-ray photoelectron spectroscopies. Atomic force microscopy images showed that micropatterned self-assembled monolayers forests have average height from 20 to 80 nm using SWNTs oxidized in the temperature ranging from 323 to 303 K, respectively.

3.2 Introduction

Single-walled carbon nanotubes (SWCNTs) show promising results in different fields and various applications such as biosensors, polymeric carbon nanocomposites, conductive films, logic gates, scanning probes.[56, 57, 58, 59]

The arrangement of nanotubes in a SWCNT forest, i.e. a self assembled monolayer (SAM) of vertically oriented carbon nanotubes, have opened new perspectives in the development of new field effect transistors, electrochemical devices, immunosensors, hydrophobic materials and microfluidic devices.[60, 61, 62, 63]

Relevant for these applications is also the chemical functionalisation of carbon nanotubes, which allows to control the linking of active molecules to the nanotubes.[64] The functionalisation generated, obtained with oxidative processes, is the most common functionalisation generated on nanotubes because of the easy of further functionalisations using amidation or esterification processes.

$\tilde{T}$ Oxidative processes normally require strong acid mixtures treatments (nitric acid as the oxidant agent and sulphuric acid to help the oxidation) in water or, alternatively, nanotubes oxidation can be carried out at high temperature in various gases or combining this technique and wet treatments.[65, 66, 67]

However, in all cases, the two most important problems of SWCNTs oxidative treatments are related to the type of the produced functional groups (oxygenated species produced in particular in the hemifullerenic tube end) and the uncertainty of the SWCNTs shortening, i.e. the SWCNT length.

In particular, wet oxidative processes attack more strongly the tubes at their ends because of the more reactive emifullerene caps with their larger strain. These treatments produce open ends with relevant amounts of oxygenated species as carboxylic groups, phenols, ethers or aldehydes.[68, 69] Moreover, uncontrolled oxidative reactions generate SWCNTs with a wide length distribution which can strongly affect the properties of the SWCNTs-based application. For instance, the height of nanotubes in a SWCNT forest strongly influences the electrochemical responses of SWCNTs-modified gold electrodes.[70, 71] It was shown that the control of the length of the tubes allows an accurate control of most electrochemical properties.[23]

In this perspective, further downstream processing steps to select nanotubes with a given length are required.[72, 73, 74, 75, 76] and different techniques that use specific physi-

cal, chemical or electrical properties of SWCNT have been developed. For instance, Liu et al.[77] sorted nanotubes using a field-flow fractionation system which, however, produced the un-desired discarding of the most interesting nanotubes, i.e. those shorter than 100 nm. Electrophoresis was also employed to sort nanotubes, according to their relative mobility through a gel, in response to an electric field. This technique allowed to get both a length separation and a diameter selection, although the methodology is scalable with difficulty.[78] More recently, nanotubes sorting by length is based on ultracentrifugation;[79] in a density gradient medium, which successfully separate small amounts of nanotubes.

All this techniques represent an additional post-oxidative step which can be very expensive, time consuming, and they have intrinsic limitations in the process scale up to industrial production.

In this work we show that it is possible to control the length of the nanotubes only by controlling their oxidation and, therefore, without any further sorting step. Our methodology is based on an accurate temperature-controlled oxidation. Moreover, we show how such nanotubes can self assemble as nanotube forest with defined height on the surface of cysteamine-modified micro-patterned gold ultrathin films.

3.3 Results

Theoretical framework

Oxidative reactions are usually performed at isobaric conditions and, therefore, they depend on chemical composition and temperature of the system. While time of reaction and the chemical composition of a wet oxidative method is always well defined and specified, less attention is usually given to the control of the temperature. Moreover, most of such reactions are performed in ultrasonicating baths in which the time evolution of the local temperature is uncontrolled and unpredictable.

In order to rationally compare the role of the time and the temperature of reaction in the nanotubes oxidation process, we can get some indications by a simple semi-quantitative description of the reaction obtained by integrating the species mass balance for SWCNT carbon in time and assuming a first order reaction rate expressed by the Arrhenius' law for taking into account temperature dependence. A general expression for ϕ can be written

in term of dimensionless time, τ, and energy, ϵ:

$$ln(\phi) = -\tau \cdot exp(-\epsilon) \tag{3.1}$$

with $\tau = t \cdot k_0$ (t is time and k_0 is the pre-exponential frequency factor of the Arrhenius' law) and $\epsilon = E/RT$ (ϵ is the dimensionless energy, R the gas constant and T the temperature).

3.1a and 3.1b report the fraction of oxidized carbon, according to Eq. 3.1, as a function of temperature and time.

The isothermal temporal evolution of ϕ follows an exponential decay, whereas for fixed times, the ϕ shows a sigmoid-like behavior as a function of the oxidation temperature with almost a linear correlation around the inflection point.

This schematic representation highlights the poor feasibility of controlling the oxidative process tuning the reaction time, as usually done. In addition, it is clear that non-isothermal conditions can add large variability to the final products. On the other hand, by selecting a proper reaction time the kinetic of the process can be more easily controlled by adjusting the temperature of the oxidation.

SWCNT characterization

In order to obtain SWCNTs with defined length, we used an isothermal process, which produces a more controlled oxidation and, consequently, a more controlled shortening of their length. Raman analysis was used for determining the evolution of the density of defects on the nanotubes which can be related to the evolution of the oxidation and X Ray Photoelectron Spectroscopy (XPS) measurements to determine the nature of the oxygenated species produced on the nanotubes. The deposition of carboxylated SWCNT forests onto micropatterned gold surfaces provided a direct measurement of carbon nanotubes length through AFM characterisation. An isothermal oxidation process was obtained by equipping an ultrasonic bath with a refrigerate coil working at constant heat-exchange power and regulating the bath temperature by adjusting the power of an auxiliary heating resistance. Experiments at five different temperatures were performed within temperature uncertainties of $\pm$0.5K: 283 K, 293 K, 303 K, 313 K and 323 K.

SWCNTs (HiPco SWCNTs from Carbon Nanotech. - CNI) were cut according to the oxidation described in the literature.[77] Reactions were performed at different temperatures by fixing the time (3 h) and power of the ultrasonic bath as discussed in the Methods section.

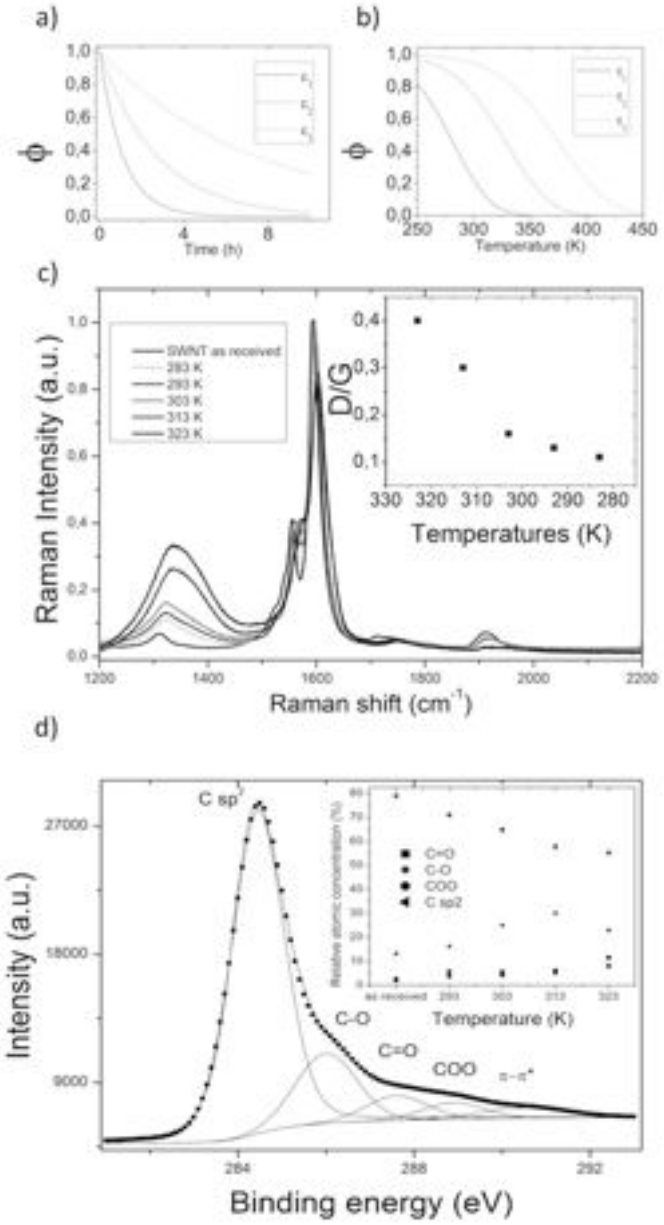

Figure 3.1: Rational of the work. - Time-dependence of ϕ according to equation 3.1 for different value of ϵ (ϵ values used are 240, 360 and 480) and E = 2000 J; b) Temperature-dependence of ϕ according to equation 3.1 for different value of τ (τ values used are 3600, 1100 and 22000) and k_0= 1 s^{-1}; c) Raman spectra (exciting line 633 nm) of SWCNT oxidized at five different temperatures. Inset reports the ratio of the D/G peak intensities as a function of temperature and the dotted line indicates the D/G ratio for the pristine nanotubes; d) X ray photoemission spectrum of carboxylated carbon nanotubes. The spectrum reveals that there are many partially oxygenated species in addition to -COO species. The inset graph shows the temperature dependence of the C sp^2 component and the corresponding enhancing of the oxygenated species.

Fig. 3.1c shows Raman spectra (exciting line of an He-Ne laser @ 633 nm, 0.85 mW, inVia Renishaw equipped with a Leika microscope) of the nanotubes oxidised at different temperature. The band at 1330 cm^{-1} (D-band) derives from a double resonance process with the participation of one phonon and of a scattering event produced by a defect. Its intensity is therefore related to the density of defects on the nanotube and one can clearly observe its increase for increasing oxidation temperatures. Since it was found that acid treatments oxidized and then digest the tubes from their ends,[57] it is reasonable to assume that the tubes would be shorter with increasing oxidation temperature. Three repeated experiments resulted in the same Raman spectra, demonstrating a high reproducibility for the isothermal controlled process.

Many functional groups may be generated at the surface of a nanotube when treated in oxidative conditions, and their atomic concentration can be analyzed by XPS measurements.

Fig. 3.1d shows the typical C sp^2 1s photoemission peak centered at about 284 eV. The deconvolution of the peak into the individual chemical shifted components allow us to obtain the contributions for all the oxygenated species present on the oxidized nanotubes.[80, 81, 82]

The inset to Fig. 3.1d shows that, when the oxidation temperature increases, C sp^2 1s peak intensity, at 284.6 eV, decreases (triangular symbols, while the peak intensity for carbon in carboxyl acids, at 290 eV, increases (circular symbols).

Another interesting feature of the oxidation kinetic is that the concentration of C-O carbons, related to phenols, pyrans, ethers, esters and anhydrides, diminishes after 313 K in favor of carboxyl carbons, showing that the oxidation process proceeds through several steps of oxidation. The reproducibility of the results shows that an accurate control of the temperature is very important for the oxidation process.

By means of Eq.3.1, in the Supporting Information we give a correlation between experimental XP results of the amount of C sp^2 1s with theoretical predictions.

SWCNT forests

The carboxylated SWCNTs produced at different oxidation temperatures were used to obtain self assembled monolayers (SAM) of different heights on micro-patterned gold surfaces. AFM topological analysis allowed to measure the height of the SAM (Fig. 3.2).

SAM were obtained on glass borosilicate substrates (Menzel) treated for 5 minutes under low vacuum atmospheric-air plasma (Harrick Plasma instrument) to remove organic

compounds so to enhance the hydrophilicity of the surface and to favour the subsequent gold adhesion.[83] Metal deposition on the treated glass surface was performed with an Edwards sputter coater for a few minutes in order to obtain a nanometric semitransparent thin gold film.

Selective gold etching with a micrometric precision, was obtained using a micro-structured agar stamp fabricated via replica molding on a silicon wafer obtained with standard lithographic techniques[84] and impregnated with gold etchant as reported by Kandere et al.[85]. After a few minutes of conformal contact between the gold coated surface and the

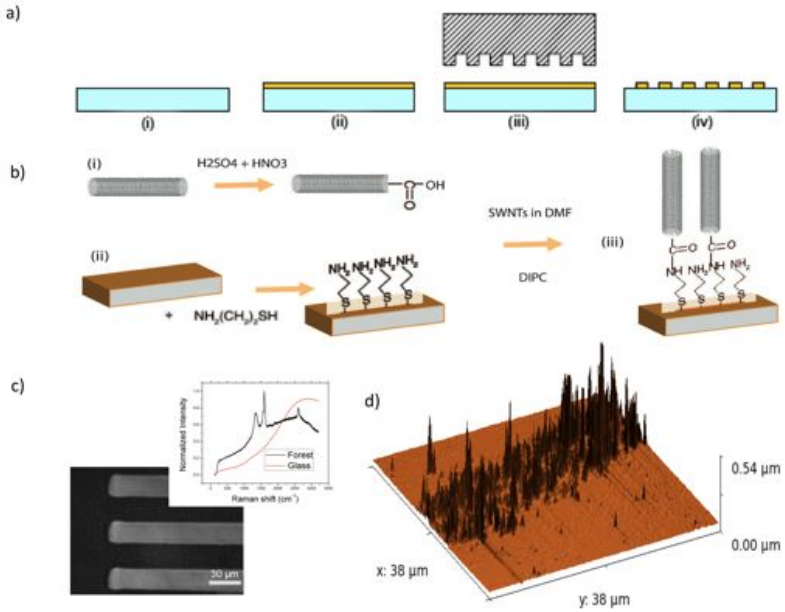

Figure 3.2: Schematic view of experimental for the work. - a) Schematic representation of a gold etching process: (i) clean glass substrate; (ii) gold sputtering; (iii) gold etching with an agar micropatterned stamp; (iv) resulting micropatterned gold surface; b) View of the preparation of SWCNTs forest: (i) strong acid treatment of the tubes; (ii) self-assembled monolayer (SAM) of cysteamine onto gold micropatterned surfaces; (iii) vertically aligned SWCNTs are coupled to the amine terminated thiols of the underlying SAM. c) Micrograph of gold substrates after micropatterning and SWCNTs deposition processes. The inset graph shows the Raman evidence of the micropatterning for glass and forests on gold substrates; (d) Atomic force microscopy 3D image of SWCNTs forests. No SWCNTs are observed on glass zones.

micro-structured agar stamp, the selective etching process allowed to transfer the desired micro-patterns on the gold surface (Fig. 3.2a).

To obtain SAM of SWCNTs, the micro-patterned gold substrates were first immersed in a 1mM cysteamine solution as described in the Methods section. In parallel, 1.2 mg of carboxylated SWCNTs were dissolved in 4 ml of N,N- Dimethylformammide (DMF 98%,

Fluka) and sonicated for 1 min. Then, the mixture was centrifuged for 5 minutes at 6000g in order to eliminate the aggregates. A few microliters of N-N'-Diisopropylcarbodiimide (DIPC, Sigma) were added to the supernatant followed by sonication for 15 minutes to allow nanotubes to covalently bind to the cysteamine with an amide bond. It is worth to recall that we used DIPC instead of the most commonly reported DCC (Dicyclohexylcarbodiimide) to avoid the formation of the typical DDC by-product (dicyclohexylurea), which is insoluble in almost all solvents. On the contrary, the DIPC by-product, the diisopropylurea, is rather soluble in organic solvents like DMF leaving the forests clean from unwanted products.

Finally, gold substrates were immersed in the DMF SWCNTs solution followed by strong rinsing with absolute ethanol and distilled water in order to remove nanotubes which were only adsorbed. Fig. 3.2c shows that SAM were selectively produced only on the gold coated surface. The inset shows that Raman spectra of SWCNT are observed only for the micropatterned gold surface. This result excludes unspecific SWCNT deposition on the un-coated glass. This methodology allows to estimate the SWCNT height within 5 nm

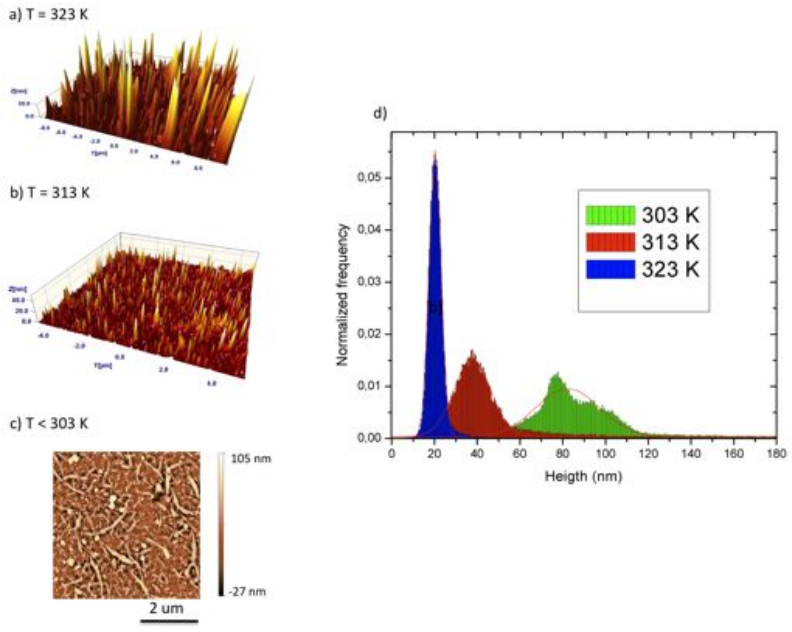

Figure 3.3: Results. - Atomic force microscopy 3D image of SWCNTs forests built at different temperature conditions: a) at 313 K; b) at 323 K; c) the AFM 2D image of randomly dispersed carboxylated SWCNTs treated at 283 K oxidation process; (d) normalized frequency of height of SWCNTs measured with AFM for three different temperatures. At 283 K and 293 K there is no evidence for SWCNTs forest.

accuracy, as reported in the Supporting Information.

Fig. 3.3a and Fig. 3.3b show AFM analysis of nanotubes forests obtained from batches of SWCNT oxidized at different temperatures (313 K and 323K). One finds that the forest of nanotubes oxidized at lower temperature (313 K) shows the larger heights as expected from their lighter oxidation. Fig. 3.3d reports the statistical analysis of the height of the peaks of the forests for the three cases in which they were obtained. One finds almost gaussian distributions peaked at 82 nm ($\pm$30), 38 nm ($\pm$17) and 20 nm ($\pm$6) with nanotubes oxidised at 303 K, 313 K and 323 K respectively. The tallest forest were obtained with the nanotubes oxidised at lower temperature as expected. It is interesting that we were not able to obtain forests with nanotubes oxidised at 283 K and 293 K. In this case (Fig. 3.3c) the AFM images show that the nanotubes were flat on the gold micropatterned surface. One can argue that the reason of such a behaviour derives from the fact that nanotubes oxidised at lower temperature are longer and show a low density of carboxylic groups, as suggested by XPS data, which do not favour the interaction among nanotubes and therefore their self assembling. The limiting of the forest height to less than 100 nm were also confirmed by other preparations.[86] It would be very interesting to investigate quantitative correlations between height and temperature.

Also, we do not provide higher oxidation temperatures than 323 K because smaller nanotubes would probably not detectable by AFM with respect to the average roughness of the gold surfaces.

The results of Fig. 3.2 show, therefore, that the accurate control of the oxidation temperature of SWCNT produces nanotubes with lengths which are inversely proportional to the temperature and with a narrow dispersion of their length. It is also worth to note that this temperature controlled-process does not require specific downstream purification steps which are always very expensive, time consuming, developed for small quantity, and, consequently, limiting the overall production rate.[87] Therefore, the process here proposed can be easily scalable for production of large amount of material without any additional separation step.

In conclusion, in this paper we proposed an efficient method to obtain carboxylated SWCNTs of controlled height using conventional strong acid oxidative reactions. The importance of controlling oxidation-temperature was supported by developing a simple schematic representation of the fraction of oxidized SWCNT carbon as function of reaction time and temperature. AFM images of self-assembled monolayers of nanotubes oxidized in a narrow

temperature interval (283K to 323 K) with height ranging from 82 ± 30 nm to 20 ± 6 nm allowed us to conclude that the length of the nanotubes can be related to the temperature at which the oxidations were operated. In addition, we observe that only for nanotubes shorter than 100 nm produced with oxidizing temperature higher than 300 K, SAM were successfully obtained.

It is very interesting to note how these results were achieved without other post processing steps such as ultracentrifugation or other fractionating systems.

The temperature control is a key factor for any reaction, but the importance of such a parameter was not considered before in the literature for the oxidation of carbon nanotube (anyway there are evidences in which nanotubes are treated with acids in gas phases[88]), probably for the difficulty of controlling such a parameter, within a sonicating bath, as required in the case of nanotubes. We showed that this is indeed a very important aspect for a fine tuning of the oxidation of such a material which results mandatory for obtaining micropatterned nanotube forests with controlled height.

3.4 Methods

Oxidation reaction step

For obtaining the complete carboxylation of the nanotubes, we treated 10 mg of single-walled carbon nanotubes, SWCNTs (Carbon Nanotechnologies, USA) in a sulfunitric mixture 3:1 (15 mL 95% v/v H_2SO_4 and 5 mL HNO_3 65% v/v, Sigma-Aldrich, USA) and ultrasonication. The power of the ultrasonic bath (CP 104, Ceia, Italy) is kept constant and equals to 500W for 3 h.

Temperature control was achieved through an external refrigerating bath (Lauda C6-CP, Triad Scientific, USA). Schematic representation is reported in Fig. 3.4, Supporting Information.

A refrigerating fluid passes through a coil immersed in the ultrasonic bath that was specifically designed to ensure efficient heat transfer.

A temperature probe immersed in the ultrasonic bath is used by the external cooling system to accurately control the temperature inside the bath by cooling or warming the refrigerating fluid. This simple experimental set up allows to achieve the desired process

temperature with a precision of ± 0.5 K.

Oxidations were performed at different process temperature (283 K, 293 K, 303 K, 313 K, 323 K).

After the oxidation reaction, the nanotubes were filtered with a 0.22 philic teflon membrane (Millipore, USA) in a a standard filtration system with distilled water until a neutral pH was reached.

Then a dry step in oven in low vacuum (133 Pa about) at 323 K for 12 h is needed for obtaining a thin and solid bucky paper film easily removable from the membrane.

Gold deposition and corrosion step

Borosilicate glass substrates (Menzel, Germany) were cleaned with absolute ethanol for 10 min followed by an atmospheric plasma treatment for 5 min ($2.5 \cdot 10^5$ Pa pressure in chamber) in order to remove organic compounds and to enhance the following gold adhesion.

Gold is then sputtered by means of a sputter coater (Edwards, USA): with a stylus profilometer (Alpha-Step IQ, KLA Tencor, USA) an average 5 nm gold film thickness is measured. AFM (VEECO, USA) shows a very low average roughness of ± 2 nm (Fig. 3.5, Supporting Information).

A silicon mold has been created following the procedure described elsewhere [84]. Briefly, the desired array was realised in digital form with Adobe Illustrator and consisted of several lines from 30 to 100 μm wide and tens of mm long. This pattern was printed onto an overhead transparency and used as a photomask. A standard photolitographic technique was employed for the fabrication of the master using a SU-8 photoresist (MicroChem, USA). The resist was spun (spin coater 150, CPK Industries USA) over a silicon wafer which was thermally treated, selectively polimerised by interposing the patterned photomask, and exposed to UV light (DAI 150, USA, λ= 365 nm) for 50 s. It was finally developed with 1-methoxy-2-propanol acetate (Sigma-Aldrich, USA).

The PDMS stamp was obtained via replica molding curing Sylgard 184 (Dow Corning, USA) on the pattern silicon master.

An agar (Agar Type 2, BioGermina, Italy) mold was then created following Kandere et al. [85]: an agar aqueous solution was prepared (5% in weight) and heated over its melting temperature (∼360 K) with continuos stirring in order to obtain a viscous pail yellow liquid.

The fluid was then deposited onto the surface of a silicon micropatterned stamp and left to

solidify in air. 20 μL of a Gold Etchant solution (Sigma-Aldrich, USA) drops were spilled in the agar stamp and after a few minutes one can gently put in contact the gold film for 10 s with the stamp. The micropatterned pattern was accurately transferred on the gold surface with a resolution of 5 μm.

3.5 Conclusions

In conclusion, in this work we proposed an efficient method to obtain carboxylated SWNTs of controlled height using conventional strong acid oxidative reactions. The importance of con- trolling the oxidation temperature was supported by developing a simple schematic representation of the fraction of oxidized SWNT carbon as a function of reaction time and temperature. AFM images of self-assembled monolayers of nanotubes oxidized in a narrow temperature interval (283-323 K) with height ranging from 82 (30 to 20 (6 nm allowed us to conclude that the length of the nanotubes can be related to the temperature at which the oxidations were operated. In addition, we observe that only for nanotubes shorter than 100 nm produced with oxidizing temperature higher than 300 K were SAMs successfully obtained.

It is very interesting to note how these results were achieved without other postprocessing steps such as ultracentrifugation or other fractionating systems. The temperature control is a key factor for any reaction, but the importance of such a parameter was not considered before in the literature for the oxidation of carbon nanotubes (anyway there are evidence in which nanotubes are treated with acids in gas phases), probably because of the difficulty of controlling such a parameter within a sonicating bath, as required in the case of nanotubes. We showed that this is indeed a very important aspect for a fine-tuning of the oxidation of such a material which results in being mandatory for obtaining micropatterned nanotube forests with controlled height.

3.6 Supporting Information

3.6.1 AFM

AFM images were collected using a VEECO Digital Instrument Dimensional D3100 with Nanoscope IV, and tubular scanner 100 X 100 X 6 μm.
Tips used were NSG01, nominal length 130 μm, width 35 μm, thickness 2 μm, resonance frequency 150 kHz and strength constant 5.5 N/m. Curvature radius was about 30 nm.
All measures were performed using the same parameters in tapping mode: scansion rate

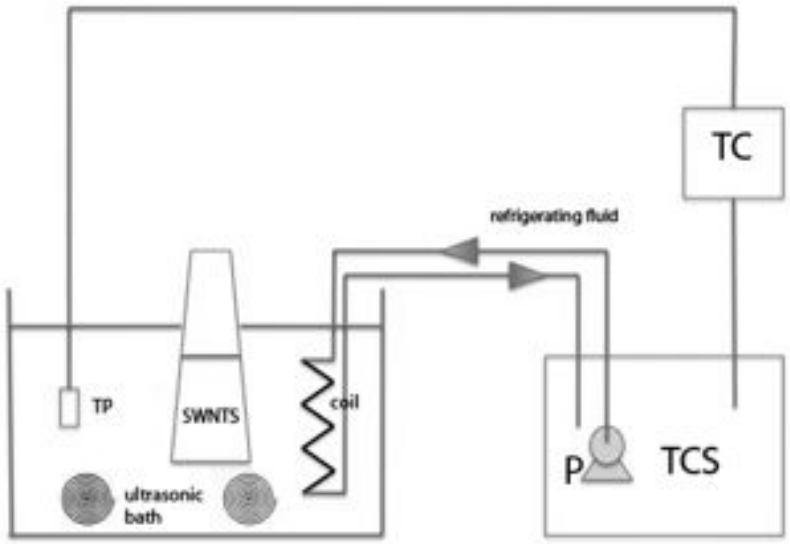

Figure 3.4: Schematic illustration of the experimental set up for the SWCNTs oxidation reactions. - TCS represents the temperature controlling system, TC stays for the temperature control, P the pump and TP is the temperature probe immersed in the ultrasonic bath. SWCNTS refers to the SWCNTs batch.

1 Hz, 512 lines x 512 points.
AFM analysis was achieved using Gwyddion 2.10 software and SPIP. Fig. 3d histogram was built collecting 20 profile lines and then making a statistic among the heights of the SWCNTs on the surfaces. This operation was repeated for every sample.

3.6.2 XPS

In order to study the thermal stability of the oxidized SWCNTs, we have performed x-ray photoemission measurements as a function of the annealing temperature.

3. NANOTUBES OXIDATION TEMPERATURE CONTROLS THE HEIGHT OF SINGLE-WALLED CARBON NANOTUBE FORESTS ON GOLD MICROPATTERNED THIN LAYERS

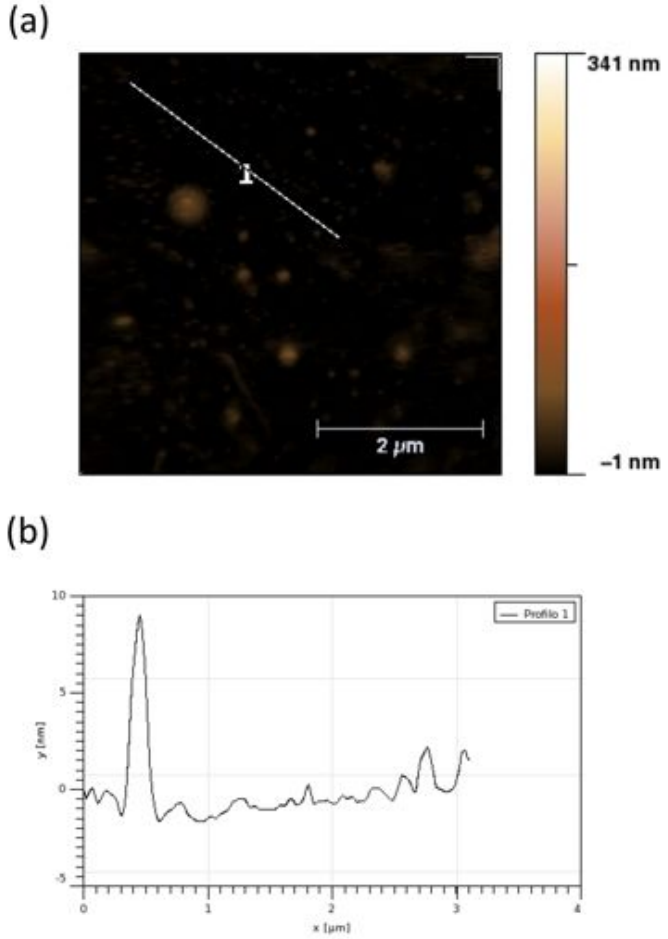

Figure 3.5: - a) AFM 2D image of a clean gold surface ready for patterning. (b) Line profile of a flat gold zone: the roughness is less than 2 nanometers.

The data were taken with a modified VG ESCALAB MKII operating at a base pressure of 10^{-6} Pa with a non monochromatized X-ray source (Mg Kα 300 W). The hemispherical electron analyzer was set to a pass energy of 20 eV and the final resolution was about 0.9 eV (considering both the source and the analyzer).
The SWCNTs were supported on a stainless steel holder and let to degas overnight, reaching a final pressure better than $5 \cdot 10^{-6}$ Pa. The samples have been heated resistively in ultra high vacuum (UHV) and maintained at the preset temperature for 10 min. A chromel-alumel thermocouple, spot-welded on the back of the sample holder, was used to monitor the temperature.
Fig. 3.6 of the Supporting Informations shows the intensity evolution of the chemical shifted components of the C 1s photoemission line after annealing in UHV at different temperatures. The main photoemission line has been fitted by five distinct components associates respectively to C-O, C=O, COO, C sp^2, π-π^* species, using mixed Gaussian-Lorentzian functions. Binding energies and full width at half maximum have been kept fixed to literature values.[80, 81, 82]
It can be seen that the oxidized SWCNTs are thermally stable up to 473 K, while for higher temperature, they are easily reduced as it is evidenced by the rapid increase of intensity of the C sp^2 component and the parallel reduction of the oxygen containing species. More in details, it can be noted that the most oxidized species (i.e C=O and COO) undergo to a rapid decrease and, eventually, they are almost completely eliminated, while the less oxygenated species (namely the CO component), even after the highest thermal treatment (873 K), still represents a significant fraction ($\sim$17%) of the carbon species.

3.6.3 Fitting

In order to obtain a real value of the activation energy of the process, we choose to fit XP results as a parameter for evaluating the enhancing of defects produced during various oxidations.
The values in Fig.3.7 are related to those obtained with XP measurements in Fig. 3.1d in which we normalized the values using the as received samples.
The results of the fitting are that using the equation 1, a value of about 7 kcal/mol K is achieved. This value is unique in literature, in our knowledge. In his work, Brukh et al.[89] found a value of 33 kcal/mol K: this is probably due to the fact that they oxidized carbon nanotubes in air (nitrogen and a small amount of oxygen to get a partially oxidant

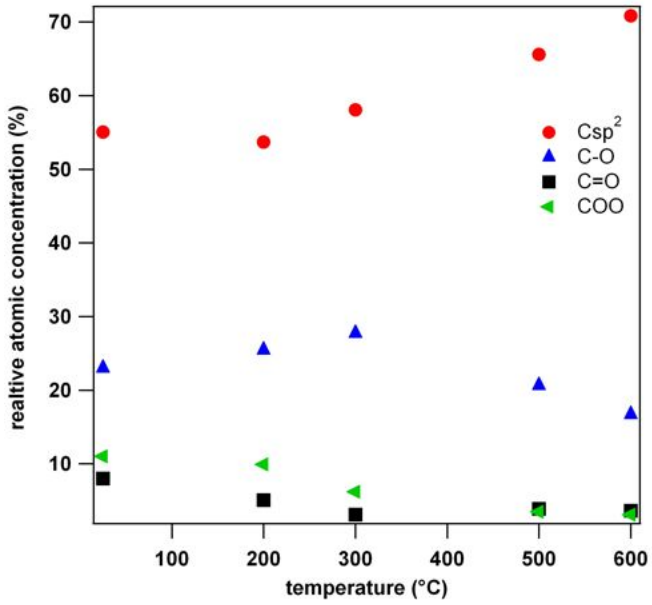

Figure 3.6: Relative atomic concentration versus temperature. - Data collected in a series of XPS experiments in which the samples are annealed. It is noted that C sp^2 values increase during the annealing while the oxygenated values decrease.

atmosphere) and not in sonicating wet conditions: is trivial to assume that our conditions are more favorable for shortening, so a minor value for the activation energy required is well accepted.

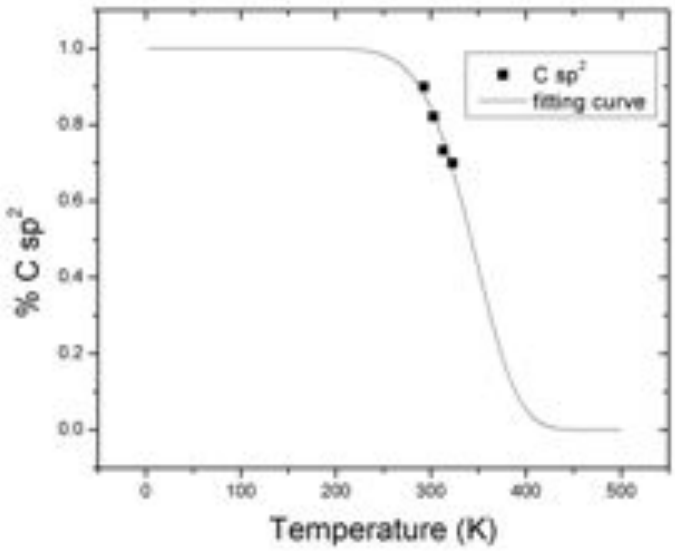

Figure 3.7: C sp^2 XP results are displayed in function of the temperature. - Dots are referred to experimental values, while the solid line represents the fitting curve using Eq.1 of the manuscript.

3. NANOTUBES OXIDATION TEMPERATURE CONTROLS THE HEIGHT OF SINGLE-WALLED CARBON NANOTUBE FORESTS ON GOLD MICROPATTERNED THIN LAYERS

4

Heterogeneous electron transfer dynamics for SWCNTs forests on patterned gold layers with different height and density

In this chapter electrochemical properties of single-walled carbon nanotubes forests with different heights and densities are studied. Wettability measurements are also provided in order to understand different topographic features of samples. The manuscript is to be submitted.

4.1 Abstract

We aim at investigating the electrochemical and morphological properties of SWCNTs forests with different height and density fabricated on patterned gold electrodes. Height of the forests is controlled tuning the oxidation temperatures (293, 303, 313 K) of SWCNTs shortening step. Carbon nanotubes density was adjusted developing cysteamine/2-mercaptoethanol (CYS/ME) self-assembled monolayers (SAMs) on gold at different ratios (1:3, 1:10, 1:100). Using electrochemical impedance spectroscopy (EIS), cyclic voltammetry (CV) and linear sweep voltammetry (LSV) heterogeneous electron transfer dynamics for hexamminoruthenium redox probe were investigated. Atomic force microscopy (AFM) and wettability measurements were collected in order to obtain topographical informations of samples.

Impedance spectra allow to calculate the apparent electron transfer rate constant for system kinetics, k_{app}, using a Randles modified circuit model as equivalent circuit. Values of k_{app} vary in the range from 5 10^{-3} s^{-1} to 2.5 10^{-2} s^{-1} for samples in which temperature is tuned.

AFM images show different spatial density for different ratio of insulating SAMs.

Wetting measurements reveal that different spatial density implies different topographical arrangements of nanotubes on the gold surface.

In conclusion the higher values of apparent electron transfer rate constants were found for the sample 1:3 CYS/ME with SWCNTs oxidized at 313 K.

4.2 Introduction

Vertical alignment of single-walled carbon nanotubes (SWCNTs) on flat surfaces has been recently reported as a promising perspective for sensing and biosensing technologies [86, 90, 91, 92].

In the recent past, the possibility of obtaining different electrochemical properties of such forests has been investigated by changing their main characteristics such as the length of insulating layer,[70] the length of the nanotubes[11], the quality of defects on nanotubes[25], the type of connectors (bamboo-like instead of SWCNTs[93]) and the element of the underlying electrode (silicon[94, 95] or carbon[96] instead of gold).

Heterogeneous electron transfer (HET) kinetics were studied both for directly anchored species like ferrocene[95, 97] and biomolecules[71, 98] both for HET dynamics in which were investigated in the outer-sphere redox probe[97]. The question of obtaining complete informations of such electrochemical modified electrodes is still opened because, in our knowledge, an answer to the need of controlling the electrical properties of the connectors is lacking.

When treating nanotubes with acid mixtures it is well known that defects of different number and quality are produced on the caps and also on the sidewalls [99]. In our previous work,[55] we reported the effect of temperature in oxidizing single-walled carbon nanotubes: we shown that checking the temperature of treatment instead of the time would increase the reproducibility and allow to control also the quality of defects produced. It

is also known that different lengths and defects would affect electronic properties of nanotubes [100].
Therefore, a comparative study on the effect of the length and the density of nanotubes on vertically aligned SWCNTs modified electrodes to our knowledge is lacking and it would be interesting in order to ameliorate the knowledge of electrochemical properties of such substrates. As a matter of fact, people have recently shown that the lack of order in samples in which the perpendicular orientation is needed could limit the applications: examples are in photoelectric conversion[24] and in electrochemical sensing [101] in which the sensitivity of electrodes is enhanced by controlling the density of the forests.
For this reason, in this new work, we aim at studying electrochemical properties such as HET dynamics of carboxylated SWCNTs forests at different heights and densities. The vertical control is monitored by tuning the length of carbon nanotubes used for the fabrication of forests and the spatial control is determined by varying the concentration of the underlying insulating self-assembled monolayer of cysteamine for controlling the density. We use patterned gold layers as working electrodes. Wettability measurements also help to understand how solvation effects affect topological outcome of vertical alignments on modified electrodes.

4.3 Results

In Fig. 4.1 a schematic view of the fabrication process is presented. In panel a) SWCNTs are oxidized at different oxidation temperatures (293 K, 303 K and 313 K), whereas in panel b) a schematization of gold deposition and gold modification is shown. Cysteamine (CYS) has been chosen as linking bridge between nanotubes and gold and diluted it with 2-mercaptoethanol (ME) causing a different surface density. In panel c) it is shown the formation of the forest via a carbodimmide activation as described elsewhere [11, 22, 23, 55, 102].
In Section 4.4 complete informations about these steps are presented.
Electrochemical Impedance Spectroscopy (EIS) was used to follow the electron transfer kinetics occurring at the gold modified electrodes in which SWCNTs forests at different oxidation temperature (i.e. different height) have been built up. The EIS measurements were performed at the formal potential of the redox probe (E1/2 about -0.10 V vs Ag/AgCl

4. HETEROGENEOUS ELECTRON TRANSFER DYNAMICS FOR SWCNTS FORESTS ON PATTERNED GOLD LAYERS WITH DIFFERENT HEIGHT AND DENSITY

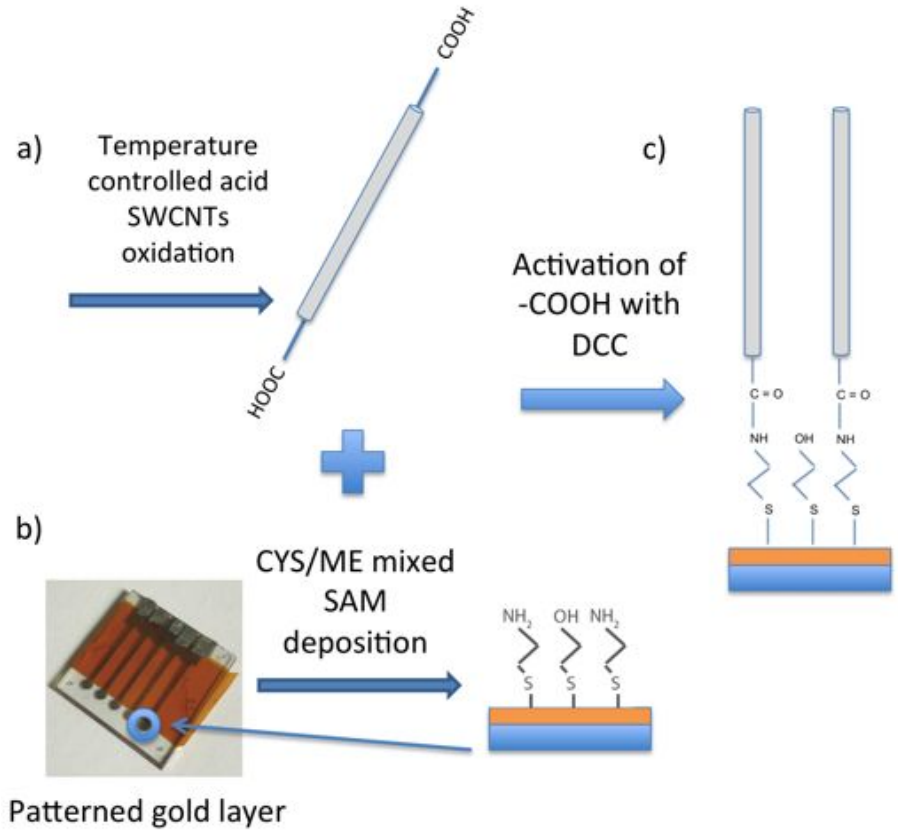

Figure 4.1: A schematic showing the steps involved in the fabrication of vertically aligned carboxylated SWCNTs self-assembled monolayers. - A) SWCNTs are initially oxidated following procedure described in [55] leading to carboxylic functions at the ends of the nanotubes. B) A patterned gold layer is created over a glass substrate followed by the formation of a mixed self-assembled monolayer of cysteamine and mercaptoethanol. C) Then a covalent coupling of is performed by activating the acid ending functions with carbodiimide as reported elsewhere.

for the redox couple hexamminoruthenium (III) / (II)).
In Fig. 4.2 EIS outcomes for samples at different temperatures are shown. Comparison of Nyqvist plot and Bode phase plot of samples are shown in panel a) and b). 293 K sample produces a resonance peak at 100 Hz about and it is noted that enhancing temperature, the peak reduces its intensity till reaching the shape of gold sample. It is only a qualitative comparison of different AC properties of these samples.
A more quantitative result can be obtained by fitting these values using equivalent circuit models. We chose Randles modified circuit model (Fig. 4.2c) in which we can study the outer-sphere redox probe: R_s represent the uncompensated resistance solution, C is the capacitance of the double layer, R_{ct} is the charge transfer resistance and Q is the constant phase element.
The EIS data were satisfactorily fitted with the modified Randles equivalent circuit model (solid lines in Fig. 4.2 a and b) and relative errors of fitting data are displayed in Fig. 4.6 in Supporting Information.

The heterogeneous electron transfer dynamics in a redox probe is investigated by evaluating the apparent electron transfer rate constant (k_{app}) of each of the modified electrodes. This is be given by equation 4.1 [97]:

$$k_{app} = \frac{1}{4}\frac{RT}{n^2F^2AR_{ct}C} \tag{4.1}$$

where n is the number of electrons transferred, F is the Faraday constant, R is the ideal gas constant, T is the Kelvin temperature, A is the electrochemical determined area of the electrode, the R_{ct} value is the main output of the fitting and C is the concentration of the redox probe.
Electrochemical area is determined using Randles-Sevcik theory[103] applying it on LSV measurements at different scan rates (from 10 mVs^{-1} to 200 mVs^{-1}) and obtaining a value of 0.304 cm^2).
As we can see from Figure 4.2d theres a diminution of R_{ct} value of one order of magnitude for samples with higher bath oxidation temperature (right y axis) and consequentially an higher value of k_{app} (left y axis) thus producing a more rapid redox reaction at the electrodes.
It agrees with the thesis expressed in a recent work[104] by Parekh and coworkers in which

4. HETEROGENEOUS ELECTRON TRANSFER DYNAMICS FOR SWCNTS FORESTS ON PATTERNED GOLD LAYERS WITH DIFFERENT HEIGHT AND DENSITY

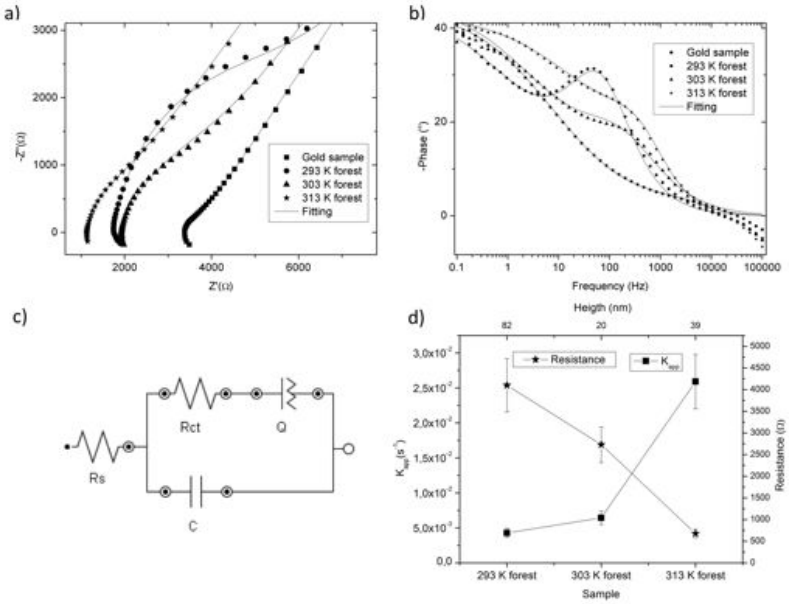

Figure 4.2: EIS outcomes - a) Nyqvist plot a) and Bode phase plot b) of samples at different temperatures: dotted lines represent experimental data whereas solid line represent fitting results. c) is the circuit model used for fitting data. *Rs* is the uncompensated resistance solution, *Rct* is the charge transfer resistance, *C* is the capacity related to the double layer and *Q* is the constant phase element. d) graphs kinetic behavior for different working conditions of this paper: squares stay for the the kapp values estimated following eq., stars are related to fitted Rct values. Height values of nanotubes in top x axis are reported in [55]. Supporting electrolyte: 10 mM KNO3; Potential applied: -0.10 V ref. Ag/AgCl; Redox species: 0.5 mM hexamminoruthenium (III).

they shown treating carbon nanotubes thin films with nitric acid slows down the associated sheet resistance. This is could be explained by a semiconductor-metallic transition is achieved when treating nanotubes with oxidants, without destroying the conjugated structure of the nanotubes: defects produced act as doping for semiconductive nanotubes that become metallic and consequentialy, more conductive.

In our previous work [55], we shown that enhancing bath oxidation temperature would cause enhancing of number of defects (enhancing of D-band in Raman spectra of samples), so it would be possible that 313 K nanotubes are doper than 293 K nanotubes.

The results also agree with Gooding's work [11] in which they fabricated SWCNTs forests with different heights (nanotubes were oxidized controlling time instead of temperature); these forests were covalently functionalised with enzym and the heterogeneous electron transfer was studied. They determined that shorter SWCNTs probably do not add significant electrical resistance.

Our study is then focalized to obtaining kinetic informations on samples in which the

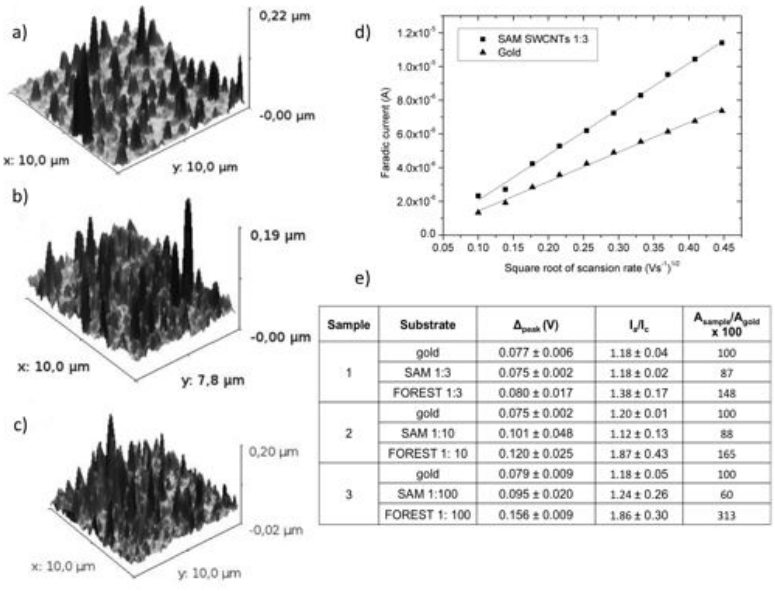

Sample	Substrate	Δ_{peak} (V)	I_a/I_c	A_{sample}/A_{gold} x 100
1	gold	0.077 ± 0.006	1.18 ± 0.04	100
	SAM 1:3	0.075 ± 0.002	1.18 ± 0.02	87
	FOREST 1:3	0.080 ± 0.017	1.38 ± 0.17	148
2	gold	0.075 ± 0.002	1.20 ± 0.01	100
	SAM 1:10	0.101 ± 0.048	1.12 ± 0.13	88
	FOREST 1: 10	0.120 ± 0.025	1.87 ± 0.43	165
3	gold	0.079 ± 0.009	1.18 ± 0.05	100
	SAM 1:100	0.095 ± 0.020	1.24 ± 0.26	60
	FOREST 1: 100	0.156 ± 0.009	1.86 ± 0.30	313

Figure 4.3: Summary of the outcomes for CV and LSV measurements for 313 K treated SWCNTs forests produced varying the insulating SAM - a), b) and c) show 3D AFM images for 1:3, 1:10, 1:100 mixed CYS/ME SAM respectively; d) represents LSV results for Sample 1; e) shows the electrochemical results for different electrode modifications. Supporting electrolyte: 10 mM KNO3; Scan rate: 50 mVs^{-1}; Redox species: 0.5 mM hexamminoruthenium (III). LSV were performed from 10 mVs^{-1} to 200 mVs^{-1}.

density varies. We chose to fix the oxidation temperature (313 K, the best in terms of

electrochemical answer) and tuning the density by diluting CYS with ME: three different relative concentrations are obtained (1:3, 1:10, 1:100 CYS/ME ratios) as discussed in 4.4 Section.

Initially AFM, CV and LSV measurements are performed. In Figure 4.3 a), b) and c) Atomic Force Microscopy 3D images of samples at different density are displayed in which is evident that diminishing the concentration of CYS, the order of the SWCNT SAM is lowered. This lack of order reflects on the electrochemical efficiency of electrodes. In Fig. 4.3e one can see that while the insulating layer do not affect reversibility (δ_{peak} is quite similar), nanotubes modification is very prominent: δ_{peak} value for FOREST 1:100 sample is doubled with respect to FOREST 1:3 sample, thus producing slower reaction rates at the electrodes surfaces. Also we can estimate A_{sample}/A_{gold} ratio comparing electrochemical determined area for samples with respect to electrochemical area for gold electrodes using Randles-Sevcik theory (Figure 4.3d: areas for more diluted SAMs are greater than the others.

This is not surprising in fact this reflects the lack of reversibility in the diluted samples: we think that these samples are so disordered that a long range vertical alignment is no more preserved and random bundles of nanotubes are deposited through the surfaces.

In order to explain the reason why diminishing the relative concentration of CYS enhancing the number of nanotubes deposited on the surface of the electrodes, contact angle measurements are performed. A drop of SWCNTs solution is deposited on modified electrode and contact angles is measured as explained in 4.4 section. Supporting informations are available for this technique.

In Figure 4.4a, b, c and d are shown micrographs representing the drops for each sample and table in panel e summarizes the obtained data fitting images. It is noted that diminishing CYS the sample become more hydrophilic thus leading to a more disordered forest: we think that because of nanotubes do not totally dissolve into NMP, they can precipitate for gravity at the bottom of the drop leading the nanotubes to adsorb on the surface of gold. But, since the drop for hydrophilic samples is smoother, nanotubes can adhere better to substrate and may destroy long range vertical alignment and damaging electrochemical reversibility.

Also heterogeneous electron transfer dynamics can be studied samples at different spatial density.

In Figure 4.5a Nyqvist plot for Sample 1 is presented. The inset shows a zoom in the low

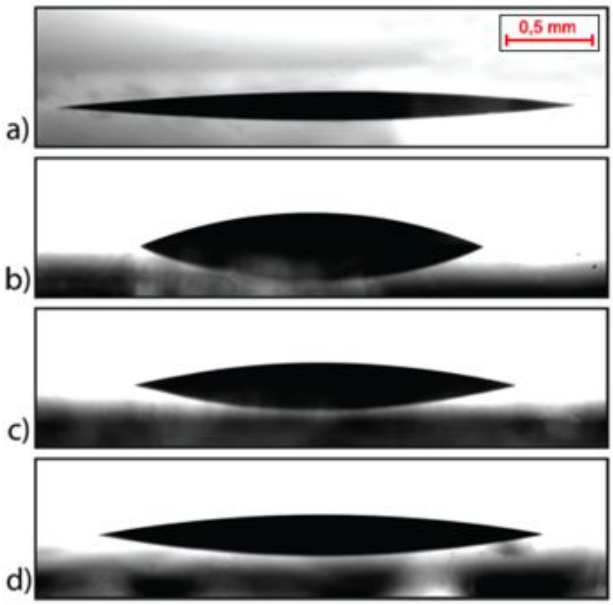

e)

Sample		Angle (°)
a)	Gold	4 ± 1
b)	1:3	20 ± 1
c)	1:10	13 ± 1
d)	1:100	11 ± 1

Figure 4.4: Contact angle measurements for gold layers modified with different SAMs. - Micrographs representing clean gold electrode, a), gold is modified with 1:3 CYS/ME SAM, b), with 1:10 CYS/ME SAM c) and with 1:100 CYS/ME SAM, d). e) summarizes the values for contact angles obtained by fitting images.

resistance range.

Panel b summarizes EIS outcomes for samples at different density and it is noted that kapp value for sample 3 is in the middle between sample 1 and 2. We explain that linking wettability measurements: diluting SAM enhances the diminution of surface tension with respect to CYS samples in which an high surface tension is present. The result is that forests-like self-assembled monolayer is peculiar of samples in which the surface tension is maintained high and further studies have to be done for understanding if surface tension property of susbtrates affects thermodynamics or kinetics in building SAMs.

We can conclude that sample 1 (FOREST 1:3) is the specimen in which electrochemical reversibility and topological features are the best.

4.4 Methods

SWCNTs oxidation

SWCNTs (HiPCo, Carbon Nanotechnologies, USA) are purified and shortened using our

4. HETEROGENEOUS ELECTRON TRANSFER DYNAMICS FOR SWCNTS FORESTS ON PATTERNED GOLD LAYERS WITH DIFFERENT HEIGHT AND DENSITY

a)

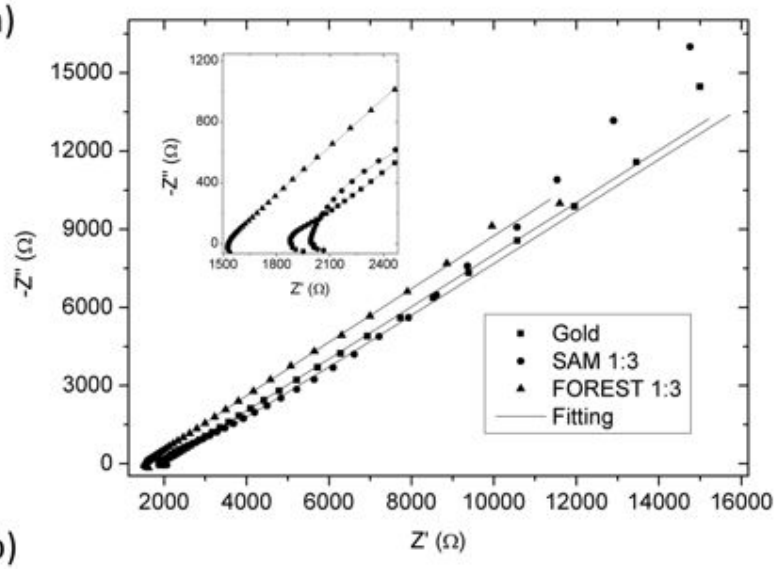

b)

Sample	Substrate	k_{app} (s^{-1})	Relative decreasing (%)
1	gold	5.21×10^{-2}	-
	FOREST 1:3	3.78×10^{-2}	27
2	gold	4.61×10^{-2}	-
	FOREST 1:10	6.10×10^{-3}	87
3	gold	5.21×10^{-3}	-
	FOREST 1:100	2.40×10^{-3}	54

Figure 4.5: EIS results for Sample 1 - Dotted lines represent experimental data, solid lines depict fitted values using model in Fig. 2c. The inset graph shows a zoom at low values of resistance. B) summarizes EIS fitted outcomes.

previous temperature controlled protocol (ref) in which we demonstrated that using temperature is preferable with respect to choose time for shortening in order to obtain more repetible results. 10 mg of single-walled carbon nanotubes, are added in a sulfunitric mixture 3:1 (15 mL of 95% v/v $H2\,SO4$ and 5 mL of $HNO3$ 65% v/v, Sigma-Aldrich, USA) and sonication. The power of the ultrasonic bath (CP 104, Ceia, Italy) was kept constant at 500 W for 3 h.

We set three different bath temperature: 293 K, 303 K and 313 K. Shortened nanotubes are filtered with porose membrane (0.45 μm pores diameter, Millipore, Italy) and washed untill neutral pH is reached.

Patterning and modification of gold layer

Borosilicate glasses (Menzel, Vetrotecnica, Italy) cleaned in a piranha solution (3 : 1 v/v concentrated $H2\,SO4$ to 30% $H2\,O2$, Sigma-Aldrich, Italy) for 5 minutes, followed by rinsing with distilled water and acetone. A step in oven at 400 K till drying is complete follows.

So every glass slide is positioned on the spin coater rotating plate (WS-650 MZ-23, Laurell) and covered with 1mL of negative photoresist (SU-8 2000, MicroChem, USA) every 25 mm of substrate diameter. The speed of the spin coater is set at 2000 rpm for 30 seconds to obtain a final thickness of 6 μm.

The resist is then soft baked on a level hotplate (368 K for 2 minutes). The photoresist is finally exposed to UV light (OAI 150, USA, $lamda$ = 365 nm) at an exposure energy of 110-140 mJ/cm^2 with a patterned photomask.

The slides are post exposure baked at 368 K for 2 minutes. To develop the photoresist, i.e. to remove it from the not lighted regions, the slide is completely immersed in 1-methoxy-2-propanol-acetate for 2-3 minutes. The development is blocked with isopropyl alcohol (Carlo Erba reagents, Italy). At the end the slide is rinsed with distilled water and dried.

A 20 nm gold thickness film is realized on slides by PECVD (PORTA 900s, Plasma Electronics-Antec) after a titanium predeposition in order to optimize gold adhesion. Deposition parameters are given in Supplementary Informations for completeness.

After the formation of the gold film, slides are treated with commercial remover (Remover PG, MicroChem, USA) under sonication at 350 K and rinsed with distilled water to eliminate the photoresist. Thus only the gold layer remains on the glass surface.

Patterning of gold electrodes provides five separated lines that can be used as five different working electrodes for statistical. Gold electrodes have a diameter of 3 mm. Gold

lines are covered with polyamide insulating tape (Kapton, Dupont, France) to prevent line shorting once the glass slide is immersed in the electrolyte solution. Moreover the ends of lines are covered with small strips of electro-conductive scotch (aluminium foil with nickel nanoparticles inside the glue). A line-selector allows to chose the desired line.
Mixed self-assembled monolayer of 2 mM cysteamine and 2-mercaptoethanol (Sigma-Aldrich, Italy) at different concentrations are created on glass clean substrates: 1:3, 1:10, 1:100 ratios are chosen and slides are put in immersion for 2 h.

SWCNTs forests formation

Finally shortened carbon nanotubes and modified gold substrates are put together in order to obtain SWCNTs forests following procedure described elsewhere [55]. 4 mg of carboxylated SWCNTs are dissolved in 15 mL NMP (1-methy-2-pirrolidone, Sigma-Aldrich, Italy). Then 0.5 mg/mL of DCC (Dicyclohexylcarbodiimmide, Sigma-Aldrich, Italy) are added to SWCNTs solution followed by sonication for 15 min to allow the nanotubes to covalently bind to the cysteamine with an amide bond.
Therefore gold substrates are immersed in SWCNTs solution for 3 h.

Electrochemical measurements

CV and EIS measurements were carried out with Metrohm AUTOLAB potentiostat/galvanostat PGSTAT302N, equipped with FRA2 module for impedance analysis (0.1 Hz to 10 kHz) managed by software Nova 1.6. Reference electrode used was a Ag/AgCl electrode (Amel Instruments, Italy), counter electrode a Mettler Toledo Pt electrode. Supportying electrolyte used was KNO3 10 mM (pH 7) and redox species used was 0.5 mM hexamminoruthenium (III), Sigma-Aldrich. EIS measurements were performed biasing the sample with -0.1 V referred to reference electrode.

4.5 Conclusions

In this work we have discussed electrochemical properties and morphological implications in modifying patterned gold electrodes with carboxylated SWCNTs forests using mixed insulating self-assembled monolayers of cysteamine and 2-mercaptoethanol as bridge between nanotubes and gold.
Density (varying insulating SAM) and height (varying oxidation temperature) effect on fabrication steps were investigated by means of electrochemical impedance spectroscopy,

cyclic voltammetry, linear sweep voltammetry and wettability measurements. We showed that a low level of 2-mercaptoethanol and small forests are the best conditions for obtaining high response and well-ordered SWCNTs forests.

For such reasons, in order to wide range application in sensing, electrochemical modified electrodes with self-assembled monolayers of carbon nanotubes have to be produced paying attention to all the components used for fabricating it from type of insulating layer to length of nanotubes for do not affect sensing efficiency.

4.6 Supporting Information

4.6.1 EIS outcomes

In Fig. 4.6 we show EIS fitted parameters related to Figure 4.1 of the manuscript. R_s represent the uncompensated resistance solution, R_{ct} the charge transfer resistance, Q is the constant phase element and N is the exponential of the phase element that can assume values from -1 (an ideal inductor) to 1 (an ideal capacitor).
It is evident how N values in the last column are close to 0.5 that it is related to a Warburg impedance which is associated with the domain of mass transport control arising from the diffusion of ions to and from the electrode—solution interface.
N_{dl} values are close to 1 that it is the common value for an ideal capacitance for the double layer (Cdl).

Sample	Substrate	Δ_{peak} (V)	I_a/I_c	A_{sample}/A_{gold} x 100
1	gold	0.077 ± 0.006	1.18 ± 0.04	100
	SAM 1:3	0.075 ± 0.002	1.18 ± 0.02	87
	FOREST 1:3	0.080 ± 0.017	1.38 ± 0.17	148
2	gold	0.075 ± 0.002	1.20 ± 0.01	100
	SAM 1:10	0.101 ± 0.048	1.12 ± 0.13	88
	FOREST 1: 10	0.120 ± 0.025	1.87 ± 0.43	165
3	gold	0.079 ± 0.009	1.18 ± 0.05	100
	SAM 1:100	0.095 ± 0.020	1.24 ± 0.26	60
	FOREST 1: 100	0.156 ± 0.009	1.86 ± 0.30	313

Figure 4.6: Summary of EIS fitted parameters related to Fig. 4.1 - Values in parentheses refer to EIS fitted errors.

4.6.2 Wettability measurements

The apparatus in Fig. 4.7 consists in a: motorized syringe pump (Ultra Micro Pump II, World Precision Instruments), collimated light and a telecentric telescope mounted on CCD camera. The sample-holder and the CCD camera are assembled on micrometer translators controlled by computer. The collimated light combined to the telecentric telescope reduces the problems of shadows and reflections, which are usually present with standard optical systems. The procedure foresees that a drop (volume $\sim$ 0.25 ml) is produced with the syringe pump and been it a small volume it doesnt fall down for gravity. At this point its possible to find the correct focus distance and gently deposit the drop on

the surface.

For each image, the drop profile was fitted with a polynomial function of degree 4, as in

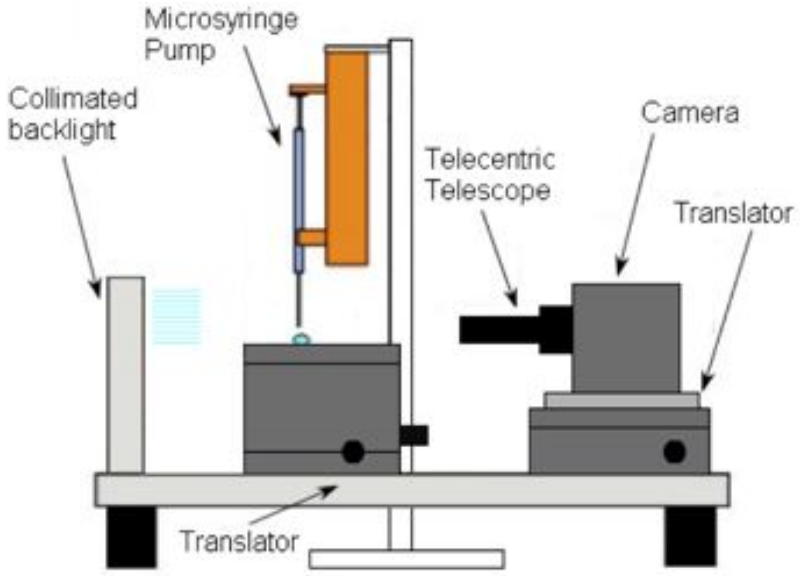

Figure 4.7: A schematic view of the apparatus for angle contact measurements. -

Fig. 4.8 and the error fitting procedure was typically less than ± 1. At least five drops for each sample were typically analyzed to obtain statistically sound results. Then, the averages were taken as representative contact angles and the standard deviations as errors, which were around ± 1.

Figure 4.8: Image representing the error fitting procedure used for determining angle contact values in Fig. 4.5d of the manuscript. - Red and blue circles establish chosen zone of drop for performing fitting.

4. HETEROGENEOUS ELECTRON TRANSFER DYNAMICS FOR SWCNTS FORESTS ON PATTERNED GOLD LAYERS WITH DIFFERENT HEIGHT AND DENSITY

5

Development of single-walled carbon nanotube-doped hydrogels for electro-chemical biosensing

In this chapter polyacrilamide hydrogels doped with carbon nanotubes were produced and modified with enzymes in order to detect glucose. Good detection limits are obtained. Heart cells were also cultured over samples for detecting electrical signals from the surface of cells. The work is to be submitted.

5.1 Abstract

Cell cultures integrated biosensors request an engineered interface between cells and electrodes that can be biocompatible, highly permeable to metabolites, with elastic properties as living tissues and could allow electronic flow from the center of the biomediator (i.e. the redox center) to the underlying electrode. For this reason, here we develop how making electroconductive a biocompatible insulating polyacrilammide hydrogel for the further applications as biosensor for glucose or electrical signaling from cells.
Conductivity is achieved by doping with single-walled carbon nanotubes (SWCNTs) at different concentrations. Electrochemical impedance spectroscopy (EIS) and cyclic voltammetry (CV) were used to characterize these soft samples. Chronoamperometry (CA) is performed for calibrating the biosensor. Biocompatible test were also performed in order to study eventual citotoxical effect of nanotubes.

EIS spectra reveal that data of sample at different doping level can be fitted with three different equivalent circuit models: this implies that three different electrical behavior are established. CV scans show that redox probe can enter the doped HYs at different time depending on the degree of doping.
An enzyme, GOx (Glucose Oxidase), is adsorbed in doped HYs by electrophoresis, in order to realize a composite glucose biosensor: a very low detection limit is reached (15 uM) for 0.85 wt% sample.
Futhermore, electrical signaling from cardiomyocytes were collected using doped HYs as conducting layer. In conclusion we realize an electroconductive polyacrylamide soft HY by doping with SWCNTs and further we make a glucose biosensor inserting GOx by electrophoresis obtaining an up-to-date value of detection limit. Also electrical signaling from cultured cardiomyocytes was collected.

5.2 Introduction

Electroconductive biomaterials are of great interests in such fields as biosensing, medicine, tissue engineering and biology. [105, 106, 107] The open problems are the demand of having a substrate that can assure smart electrical and mechanical properties and also the permeability of metabolites to and from the cell cultures [108].
It is the interface the most important element during the engineering of a biomaterial: it should promote the adhesion and proliferation of a cell and have a low electrical impedance if needed. Many efforts have been produced for answering to these questions. People first tried to build synthetic polymers [38, 39, 109, 110] but they are normally not conductive and so not suitable for cell culturing application.
Electrical conductivity is achieved by the creation of conducting gel coatings [106] used to enhance the performance of implants.
Many literature has been produced about the development of polymeric hydrogels (HYs) [111, 112]. HYs can be acrylamide, vinilpirrolidone, collagen or ialuronic acid based. Thanks to their biocompatible properties and their simple chemistry that can mimic natural systems they have been reached a prominent position among the other biomaterials [44].
These characteristics have allowed hydrogels to be used in biomedical applications that include biosensors, drug delivery systems, contact lenses, catheters, wound dressings, tourni-

quets and enzyme stabilizators [112].
In our previous works we have demonstrated that cells cultured on a micropatterned polyacrylamide HY stamp can grow following geometrical borders [84, 113]. Also the possibility of doping HYs with electroconductive materials without modifying bulk mechanical and structural properties is nowadays achieved in order to perform cell culturing and physiological measurements of cardiac, muscular and neural cells [41, 48, 114]. Gong was the first that was able to study the conductive electron transfer of a complex salt into an HY structure [115]. People are used to insert in the HY structure conductive polymers in bulk form or in nanoparticles form such as polyaniline or polypirrole [116], metals (copper and gold) [117], and carbonaceous materials such as graphite and carboxylated single-walled carbon nanotubes (SWCNTs) [118, 119].
Doping with carbon nanotubes allows people to create electroconductive materials lowering of at least one order of magnitude the amount of dopants: normally doping levels are about of 40-50% in weight for what concerns polymers and metals [117] but exploiting electric properties of nanostructures, only 4% of doping is necessary [120, 121]. It is estimated that alignment of the nanotube phase could produce improved mechanical and electrical properties at loadings as low as 0.1 wt.
(manca il pezzo sulle misure sui cardio)

5.3 Results

So in the first part of this work we produced conducting SWCNTs doped polyacrylamide HYs (SWCNTS-HYs). Fig. 5.1d Electrochemical Impedance Spectroscopy (EIS) measurements were performed in order to understand electrical properties of the interfaces. Different circuit models for conductivity at various degrees of doping are presented. The second part of the paper focuses on a smart application of these modified electrodes. Chronoamperometry measurements are performed in samples in which Glucose Oxidase (GOx) has been inserted3.1e and a good detection limit of glucose with compared to what presents in literature is obtained. Also biocompatibility tests were performed.
When carbon nanotubes are inserted into a polymeric structure like HYs, different levels of doping can be fulfilled. Fig. 5.1 When concentration of dopants is low, nanotubes do not affect electronic and mechanical properties of sample (Fig. 5.1a), if the concentration enhances, a phase separation system may occur (Fig. 5.1b), so when the concentration is

sufficient enough (Fig. 5.1c), bulk properties of samples may change dramatically. Our hypothesis is that when nanotubes can migrate in the HY and they can feel each other, a percolation path is created and electronic conductivity is so possible. A Raman study of the effect of doping on the HYs is presented in Supplementary Information (see Fig. 5.11).

In this latter case if redox reactions occur in the bulk of the sample, electrons can be detected and collect to the underlying electrode, revealing redox probes. Seven different

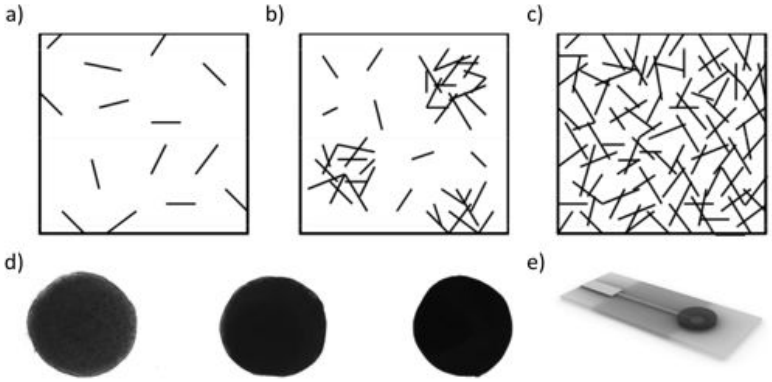

Figure 5.1: Schematic representation of the three distinct situations of SWCNTs doped Hys. - low doping, a), medium doping , b), and high doping. Micrographs showing SWCNTs doped Hys at three distinct concentrations (0.1 wt%, 0.5 wt% and 0.85 wt%), d). Picture representing homemade patterned gold electrode modified with SWCNTs doped HY in which GOx has been inserted by electrophoresis producing a biosensor for the detection of glucose.

types of SWCNTs doped-hydrogels - gold composite electrodes were tested. Carbon nanotubes loading were: 0 wt%, 0.1 wt%, 0.25 wt%, 0.375 wt%, 0.5 wt%, 0.64 wt% and 0.85 wt%. In order to obtain relevant statistic informations three HYs for every doping level were tested.

Fig. 5.2 shows an overlay of Nyqvist plots for all samples and relative circuit models for fitting experimental data. It is evident that two different circuit models have to be used for fitting data in a satisfactory way: HYs with a medium level of doping must be fitted with a different equivalent circuit model. Bode phase plots will provide a quantitative outcome for understanding better what it is happening in such samples. Fig. 5.3 shows Bode phase plots for data shown in the previous figure. Electrodes with nanotubes concentration between 0 wt% and 0.25 wt% (Fig. 5.3a) exhibit only one resonance peak. The intensity of the peak decreases as nanotubes concentration increases and also a shift to lower frequency (from 2-3 Hz to 0.4 Hz) can be observed.

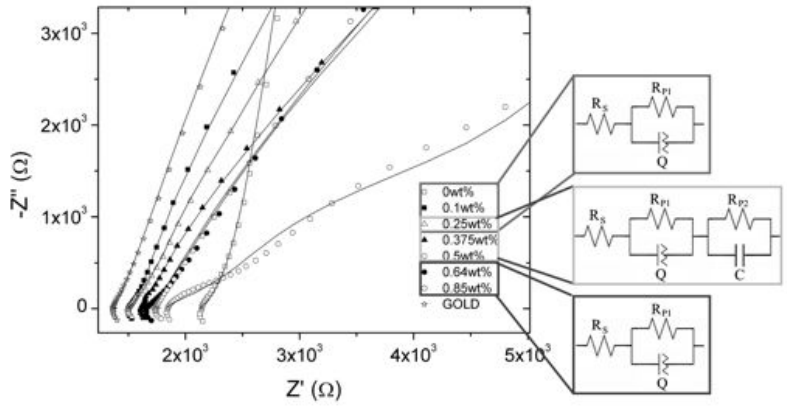

Figure 5.2: Nyqvist plot of samples in this paper. - The insets show the different equivalent circuit models used for fitting (Randles cell). Rs is the electrolytic solution, Rpx the two polarization resistance, Q the constant phase element in replacement of C that represents the double layer capacity.

On the contrary for 0.375 wt% and 0.5 wt% (Fig. 5.3c) composite electrodes a new resonance peak appears at a lower frequency (about 0.07 Hz). The intensity of this peak increases as nanotubes concentration increases.

Phase for electrodes with 0.64 wt% and 0.85 wt% (Fig. 5.3b) have a shape similar to that of electrodes with low nanotubes concentration, in fact the peak at low frequency disappears and only one peak at about 1 Hz remains.

Data were fitted in order to have a quantitative comparison. Curves with only one resonance peak can be fitted with $R_S(R_{P1}Q)$ circuit. On the other hand curves with two resonance phenomena can be fitted only with $R_S(R_{P1}Q)(R_{P2}C)$ circuit, where R_{P1} is associated to resonance peak at higher frequency and R_{P2} is associated to resonance peak at lower frequency. For every kind of composite electrodes, the mean values for $R_{P1,2}$ and standard deviations are collected (see 5.6).

Electrodes modeled with the same equivalent circuit $R_S(R_{P1}Q)$ can be compared. ANOVA tests were performed in order to get a comparison between mean values for R_P (Fig. 5.13 of Supplementary Information).

Then we plotted R_{P1} mean values for composite electrodes with $R_S(R_{P1}Q)$ equivalent circuit against SWCNTs concentration in Fig. 5.3d. The horizontal band shows upper and lower values of R_{P1} for homemade gold electrode without hydrogel.

In panel e), we show the trend for samples with medium doping level both for R_{P1} and R_{P2} values.

Considering impedance and phase plots, we can summarize the results of the first part

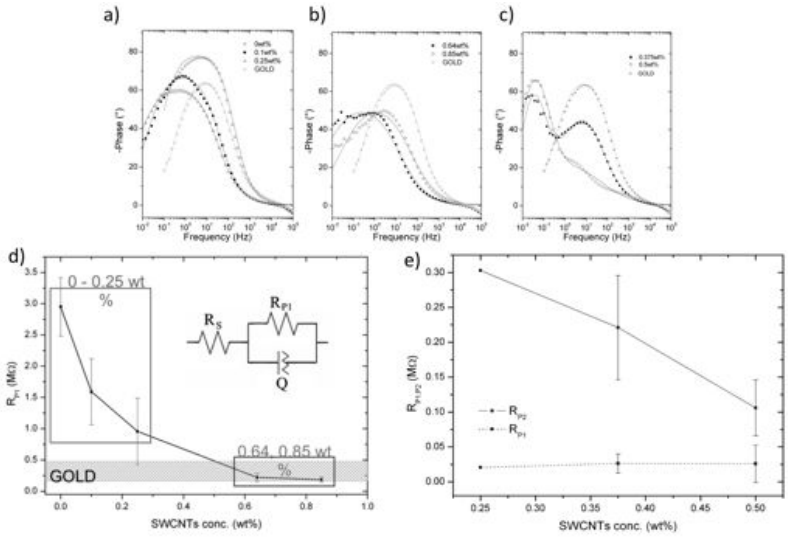

Figure 5.3: Resistance outcomes. - In panel a), b) and c) are displayed Bode phase plots for samples in Fig. 5.2. Panel d) shows Rp1 versus the degree of doping in the Randles equivalent circuit doped HYs while panel e) shows Rp1 and Rp2 versus doping in Randles modified equivalent circuit doped HYs.

for the work by attesting that three different conductive behaviors take place. Between 0 wt% and 0.25 wt%, we think that nanotubes cannot create a percolation pattern because their concentration is too low (or null). SWCNTs are too far from each other so electrons cannot flow through them. However a slight decrease in resistance takes place as concentration increases because the distance between nanotubes decreases. So the resonance mechanism should be due to hydrogel matrix that acts as a dielectric between gold surface and electrolytic solution.

On the contrary for 0.375 wt% and 0.5 wt%, nanotubes can create an electroconductive pattern but only in regions where SWCNTs concentration is higher enough. So the new resonance mechanism at low frequency could be due to the overpotential that electrons suffer when they have to cross the interface between regions with high and low nanotubes concentration. Instead the phase peak at high frequency should describe the same resonance mechanism than HYs with nanotubes 0-0.25 wt% concentrations produced.

Finally when nanotubes concentration is high enough, a uniform electroconductive pattern is created throughout the total volume of hydrogel and only a single resonance mechanism takes place. So in this case, hydrogel acts as a conductive material because of CNTs doping. In order to get information about the reversibility of the reactions and if any species could penetrate polymeric structure, and to know the particular mechanisms that

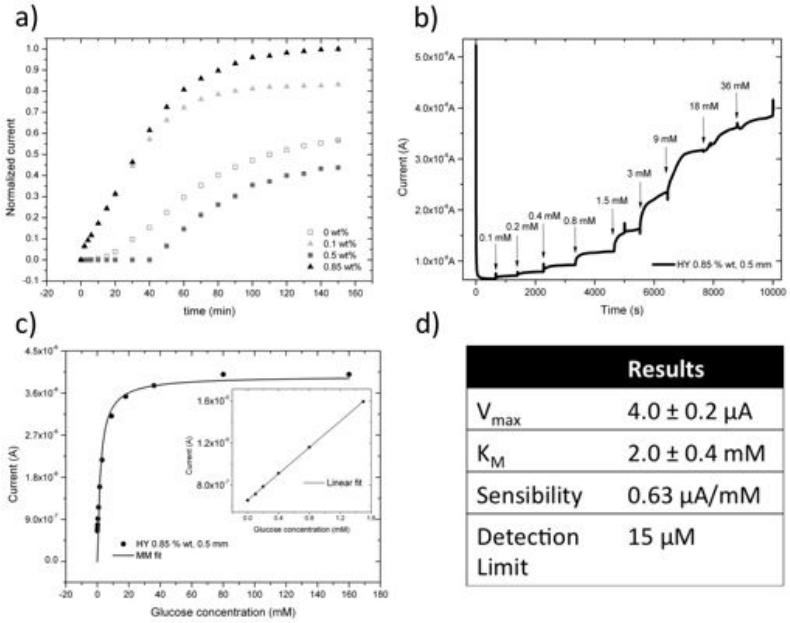

Figure 5.4: Chronoamperometry outcomes. - In panel a) faradic normalized current versus time. Each data point refers to a single CV experiment. WE: SWCNTs doped HYs at different degree of doping; Electrolytic solution: 10 mM KNO3 ; Redox probe: 0.5 mM FcMet. In panel b) a CA measurement of SWCNTs doped GOx-HY 0.85 wt%. Potential applied: +0.7 V ref. Ag/AgCl. Arrows refer to the injection of glucose, the target. In panel c) fitting with Michaelis-Menten kinetic equation referred to data in panel b); the inset shows a zoom in the range of low values of concentration. Panel d) summarizes fitting results.

happen in the 0.25 wt% - 0.5wt% range, CV measurements were also performed.
Scans were conducted in the range of 0-0.5 V vs Ag/AgCl electrode at a scan rate of 0.1 V/s. Several measurements were taken for every composite electrode after pre-set times. The modified electrodes were let immersed in the electrolytic solution containing the redox molecule (ferrocenemethanol) and a CV was collected when necessary.
In Fig. 5.4a we show the faradic intensities of the anodic peaks for every CV at fixed time and SWCNTs concentration normalized to the greater value collected for 0.85 wt% sample after 150 min. Initial time point (0 min) corresponds to that of the immersion in the electrolyte solution.
0 wt% sample (i.e. without SWCNTs) and 0.5 wt% sample exhibit sigmoidal shape in which the faradic current is almost null for some minutes, then increases smoothly and finally reaches a saturation value. 0.1 wt% and 0.85 wt% samples instead show a different behavior, in fact faradic current immediately increases. This suggests that these HYs could provide a conductive pattern that allows the direct transfer of electrons produced by ferrocenemethanol oxidation. However, different saturation currents are reached, suggesting that 0.85wt% sample provides a better electroconductivity. On the other hand, 0.5wt% sample exhibits a behavior different from others doped-HYs, like it happened for EIS measurements: steady-state current reached at 160 min is quite less than the value of 0 wt% sample revealing a quasi-insulating behavior. In Supplementary Information an in-depth study of this phenomenon is provided.
We think that insulating properties of 0-25-0.5 wt% HYs are dues to a phase separation that occurs inside the HY during polymerization and that creates a microstructure composed of clusters of carbon nanotubes surrounded by hydrogel matrix with a low content of nanotubes. Electrons have to spend a lot of energy to cross the matrix by jumping between clusters and thus decreasing the electroconductivity and providing a new resonance mechanism.
So EIS and CV results give reason to believe that an electroconductive pattern is provided by SWCNTs doping but, because of phase separations phenomena, the conductivity is good only in precise ranges of carbon nanotubes concentration.
The second aim of our work is to realize an enzymatic amperometric biosensor for glucose exploiting the realized conductive HY. Enzyme is inserted into the 0.85 wt% HY by electrophoresis and chronoamperometries were performed as described in Methods section. The results are shown in Figure 5.4b.

Michaelis-Menten kinetics equation [122] was used to fit experimental data as described in Fig. 5.4c. Table in panel d) show a good value for detection limit and sensitivity that are fixed to 15 uM and respectively, interesting values if compared to what present in literature for similar biosensors [123, 124]. Biocompatibility tests were also performed

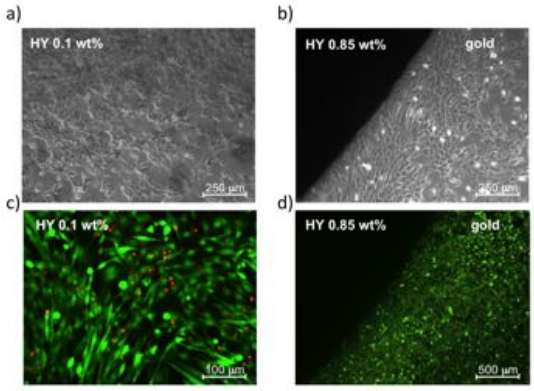

Figure 5.5: C2C12 Live and Dead vitality test. - In panel a) and c) cells are deposited on 0.1 wt% HYs while in panel b) and d) on 0.85 wt% HYs.

in order to reveal the toxicity of carbon nanotubes as dopants for HYs. It is well known that HYs are suitable substrates for culturing cells. As described elsewhere[84] they can provide tunable mechanical properties similar to that of biological tissues. This lays the foundation for a possible application for HYs, for example cells could be easily grown up on the HY surface and then tested if a glucose detection is needed. Vitality tests were performed by growing up C2C12 cells on HYs as described in Methods section and in Supplementary Information.

Cells photographed after 5 days showed a normal morphology and growth rate, both on the surface (Fig. 5.5a) than near the edge of the HY (Fig. 5.5b). Cytoplasmic protrusions are visible, demonstrating that cells are adherent to the surface.

To test also the vitality of cells, we made Trypan blue and Live/Dead assay after the same culturing time.

Live/Dead assay of Fig. 5.5c and d, shows that cells had a good rate of vitality (green spots are living cells). Only a few cells (i.e. red spots) seem to be dead, but their number

is low and normal.

Doped HYs were used for detecting electric signals from cells. Cardiomyocytes (see Section 5.6 for protocols) were seeded on doped HYs and electrical properties of the system was characterized by EIS and CA.

In Fig. 5.6a it is shown Nyqvist plot for samples on which living and dead cardiac cells are present. Data were fitted accordingly to [125] with equivalent circuit model in Fig. 5.6d, in which R_S is the uncompensated resistance solution, $R_G and Q_{dl}$ are the equivalent elements related to the gold electrode, R_H is the resistance of the HY and $R_{cell}Q_{cell}$ are the equivalent electric elements of the cell layer and give good agreement with experimental values. The shape of the curve reveals a good electric contact between cell layer and the underlying conductive HY. In panel a) it is also shown the Nyqvist plot associated to a dead layer of cells on the modified doped HY: impedance values are high with respect to the previous ones.

In panel b), Bode phase plot, interestingly it is shown that a resonance appear at 100 Hz

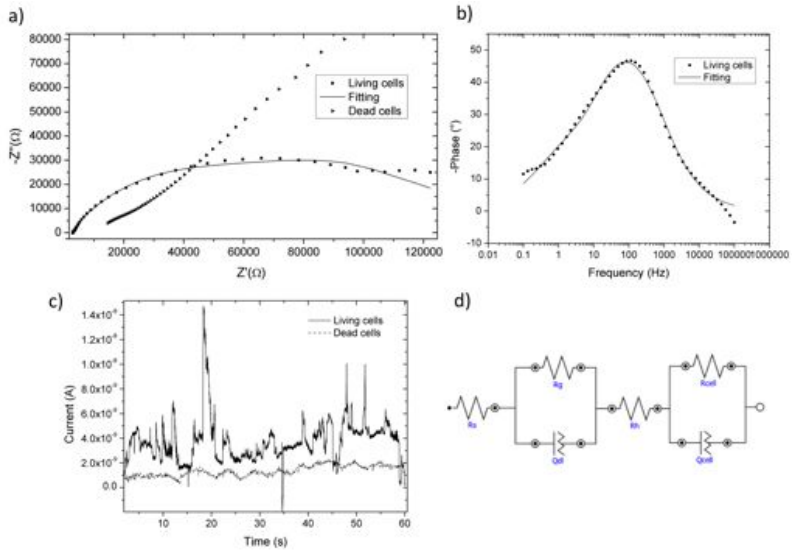

Figure 5.6: Detection of electrical activity from cardiac cells. - In panel a) Nqvist plot of living and dead cells are shown; in panel b) Bode phase plot of living cells; c) CA measurement of living and dead cells. All measurements were performed in recording solution (see Section 5.6) biasing at OCP ref. to Ag/AgCl electrode.

revealing electric phenomena on the surface of the cells of the order of 1-10 ms

This results is quite remarkable because the resonance frequency observed only in presence of living cells is consistent with the scale of cell membrane depolarization mechanisms.

In panel c), CAs of living and dead cells are presented. Solid line shows electric activity from the surface of the cells whereas dead cells do not reasonably show any signal.
This results are very encouraging and further study are required for correlating the physiological cell activity to the amperometric analysis.

5.4 Methods

Poly(acrylamide/bisacrylamide) (Poly(AA/BIS) is a copolymer of two monomer: acrylamide (AA, Sigma-Aldrich, Italy) that composes the principal polymer chains and N,N-Methylene Bisacrylamide (BIS, Sigma-Aldrich, Italy) that is the cross-linking agent. The copolymerization of BIS results in the bridge in which four chains of polyacrylamide come together in a irreversible covalent connection creating a 3D-network structure.

Treatment on glass coverslips with silane-glutaraldehyde

In order to ensure a uniform and prolonged adhesion of hydrogel to glass a specific functionalization of the glass surface is necessary.
The treatment protocol developed consists of a surface modification with silane and glutaraldehyde (Sigma-Aldrich, Italy). A full detailed description of this step is described in Supplementary Information.

Preparation of polyacrylamide hydrogels

To realize poly(AA/BIS) hydrogels, acrylamide solution (40wt% in pure water solution, SIGMA) was added to N,N-Metilen-bis-acrylamide powder (Sigma) and milliQ water in a 1.5 ml Eppendorf. The mix ratio (w/w) of acrylamide:bis-acrylamide was always 29:1.
Exploiting fabrication of high resolution proteins gels [126], chemical polymerization is used for obtaining hydrogel chains as full discussed in Supplementary Information.

Water suspension of nanotubes

100mg of CoMoCat SWCNTs (Sigma Aldrich, Italy) as received were added to 10mL of milliQ water to form 1 wt% suspension of SWCNTs.
Also 20mg/mL of Sodium Cholate (SC, 99% Sigma-Aldrich, Italy) as surfactant agent were added to the solution.

Homemade gold electrodes

Measurements were performed using homemade gold electrodes. These electrodes consist of a nanometer-thick film of gold deposed on a glass slide through Plasma-Enhanced

Chemical Vapour Deposition (PECVD) after a photolithography treatment on the glass surface and a deposition by PECVD of a nanometric seed layer of titanium to enhance adhesion of gold. Deposition steps are deeply presented in Supplementary Informations.

Cleaning procedures

Produced gold electrodes undergo a cleaning procedure that consists of several CVs. Cleaning is suspended when a reproducible scan has been reached. Scans were performed from 0 V to 1.5 V vs Ag/AgCl at a scan rate of 0.1 V/s in H_2SO_4 2% v/v solution for homemade gold electrodes.

Preparation of SWCNTs-doped hydrogels

Aqueous suspensions of carbon nanotubes were used to made poly(AA/BIS) SWCNTs-doped HYs. The tested technique consists of using carbon nanotubes suspensions in the preparation of the pre-polymer solution (see Supporting Information for protocol preparation).

The electrophoretic migration of glucose oxidase from aspergillus niger (GOx, Sigma-Aldrich, Italy) inside HYs was obtained by electrophoresis, applying a constant potential of +0.7 V for 30 minutes, in 20 mL of PBS 1X enriched with 0.25 mg/mL of GOx. With these conditions GOx can propagate inside the HY for a length not less than 500 um [127]. Biosensor were then rinsed with milliQ-water and stored at 4 C.

Measurements and fitting

Electrochemical impedance spectroscopy measurements were performed using a potentiostat/galvanostat (Autolab PGSTAT302N, Metrohm, EcoChemie, The Netherlands) managed by software NOVA 1.6 and equipped with a FRA2 module for frequency analyzer. The classic three electrodes cell scheme was used: he homemade gold electrode acts as working electrode, a Ag/AgCl electrode (Amel Instruments, Italy) as reference and a Mettler Toledo Platinum cylindrical electrode used as counter electrode. Potential applied was +0.7 V referred to the reference, electrolytic supporting solution was KNO3 10 mM. Frequency scan range was established between 0.1 Hz to 100 kHz. Fitting of spectra were performed using equivalent circuits provided by manager software.

Cyclic voltammetries were conducted between 0 and 0.5 V referred to the reference. Redox probe used was ferrocene methanol (Sigma-Aldrich, Italy) at 0.5 mM concentration.

Chronoamperometries were performed at fixed potential of +0.7 V vs Ag/AgCl electrode. Concentrations from 0.1 to 160 mM of glucose (Glucosata solution) were tested. Supporting electrolyte used was PBS 1x (Invitrogen, Italy).

Biocompatibility tests - Seeding and Culture of C2C12 cells

Biocompatibility test were done. Trypan blu and Live/Dead assays were conducted (see Supporting Informations for further details).

5.5 Conclusions

Single wall carbon nanotubes (SWCNTs) in sodium cholate (SC) aqueous suspensions were successfully used to make doped poly(acrylamide/bisacrylamide) hydrogels (HYs). Electrical properties of SWCNTs-doped hydrogels were studied through electrochemical impedance spectroscopy (EIS) and cyclic voltammetry (CV) on SWCNTs-doped hydrogels gold surface working electrodes.

Three different impedance behaviors were obtained for three different concentration ranges of SWCNTs. Considering a possible phase separation involving SWCNTs in the polymeric matrix, the conducting mechanism, found in the medium range of doping, can be associated to the overpotential that electrons must exceed when they have to cross the interface between regions with high and low SWCNTs concentration. Increasing SWCNTs concentration, the tendency to form two phases inside the matrix diminishes because distance between clusters of nanotubes diminishes and electrons can jump more easily: we think that at his point the conductive pattern is forming.

An amperometric enzymatic glucose biosensor based on 0.85wt% SWCNTs-doped hydrogel and GOx was finally created and a subsequent Michaelis-Menten calibration is performed by chronoamperometry experiments. The biosensor showed an high detection limit of 15.2 ?M glucose concentration with compared to what presents in literature. A value of sensitivity of 626 nA/mM is found. These results make this device suitable for glucose detection on living cells systems in which the value of glucose concentration detectable is 5 mM about and a good time of response is needed.

Biocompatibility test with positive outcomes are finally performed. SWCNTs-doped hydrogels, rinsed with water and PBS 1X, did not shown any cytotoxic effect on C2C12 murine myoblasts morphology after 5 days.

5.6 Supporting Information

5.6.1 Supporting Methods

Chemical polymerization

1/100 v/v Ammonium Persulfate, 5% solution (APS, Sigma-Aldrich, Italy) and 1/1000 v/v N,N,N,N-Tetramethylethylenediamine (TEMED, Sigma-Aldrich, Italy), are added to the prepolymer solution.

APS in water produces $S_2O_8{}^{2-}$ $2SO_4{}^{-}$ free radicals that initiate the reaction. TEMED catalyzes the reaction because it exists as free radical in solution. The higher is the concentration of TEMED, the faster will be the polymerization. It also would be better to degas the pre-polymer solution before adding APS and TEMED because oxygen can inhibit the initiator. However in this case it is not necessary because the concentration of monomer is high.

So the ready solution has to be rapidly transferred to the PDMS mold and then covered with a coverslip like in photopolymerization. In this way it takes about 15 minutes to reach the complete polymerization of little cylindrical hydrogels at room temperature.

Water suspension of SWCNTs

Sodium cholate (SC) is an ionic surfactant, it can be removed by dialysis and can also be successfully used for carbon nanotubes dispersion. At concentrations above 2mM, SC will form micelles having M.W. 900 to 1200. The small size of the micelles allows themselves to be easily removed by dialysis or by gel filtration.

The compound was ultra-sonicated with a 13 mm diameter titanium tip (Bandelin Sonopuls HD 2200) for 60 min at 40W in an ice bath to prevent the overheating of suspension. The power of the ultra-sonicator was kept not too high to prevent an excessive shortening of nanotubes and consequently a deep modification of their bulk properties. Then the resulting suspension was decanted for some days. It appeared of a black colour.

Deposition processes

Photolithography

Squared glass slides (borosilicate glass, 40x40 mm, 1 mm thick, Vetrotecnica, Italy) are immersed in a piranha solution (3:1 v/v, concentrated H_2SO_4 : 30% H_2O_2) for 5 minutes. Because the mixture is a strong oxidizer, it removes most organic matter and it also hydroxylates the surface making it hydrophilic. Then they are rinsed with distilled water and acetone and dried in an oven in air at 400 K till drying is complete. Each glass

slide is then positioned on the spin coater rotating plate (WS-650 29MZ-23, Laurell) and covered with 1mL of photoresist (SU-8 2000, MicroChem, USA) every 25 mm of substrate diameter. The speed of the spin coater is set at 2000 rpm for 30 seconds to obtain a final thickness of 6 ?m. The SU-8 product consist of chemically amplified, epoxy- based negative resists with high functionality, high optical transparency and are sensitive to near UV radiation. Cured films or topography are highly resistant to solvents, acids and bases and have excellent thermal stability, making it well suited for permanent use applications. After that the resist is soft baked on a level hotplate set at 368 K for 2 minutes to relax the polymer structure and thus to reduce internal tensions.

So the photoresist is exposed to UV light (λ = 365 nm, OAI 150) at 110 - 140 mJ/cm^2. At this stage a photo-mask is put over the glass slide. In the black regions UV light will not reach the photoresist and so it will not crosslink.

Slides are then newly put on a level hotplate set at 368 K for 2 minutes. In this post exposure bake stage the regions that were exposed to UV light can reticulate. After 1 minute an image of the mask should be visible on the surface.

To develop the photoresist, i.e. to remove it from the not lighted regions, the slide is completely immersed in 1-methoxy-2propanol-acetate (Sigma-Aldrich, Italy) for 3 minutes. The development is blocked with isopropyl alcohol. At the end slides are rinsed with distilled water and dried.

Plasma-Enhanced Chemical Vapor Deposition (PECVD)

PECVD is a process used to deposit thin films from a gas state (vapor) to a solid state on a substrate. Chemical reactions are involved in the process, which occur after creation of a plasma of the reacting gases. The plasma is generally created by RF (AC) frequency or DC discharge between two electrodes, the space between which is filled with the reacting gases.

Two different layers are deposited on the glass slides covered with the photoresist mask, using PECVD (PORTA 900s, Plasma Electronics-Antec): first a 50 nm thick titanium layer is deposited on the glass to provide a good mechanical adhesion to glass. Then a second gold layer of about 15-20 nm is deposited over the titanium layer. PECVD can provide a gold surface for these homemade electrodes much purer than that of commercial gold electrode. Parameters used for the depositions are displayed below (Fig. 5.7). After the deposition, the gold-coated glass slides are treated with the remover through sonication at 350 K and rinsed with distilled water to eliminate the photoresist. Thus only the

	Titanium layer	Gold layer
Current on target	2A	30mA
Atmosphere of deposition	93 sccm Ar	93 sccm Ar
Current on substrate	150 W	150 W
Rotational speed of sample holder	4 rpm	4rpm
Deposition time	6 min	100 s
Distance between target and substrate	12 cm	12 cm
Thickness (by profilometer)	50 nm	15-20 nm

Figure 5.7: Deposition parameters for PECVD steps. -

gold layer remains on the glass surface (Fig. 5.8). In the available configuration these

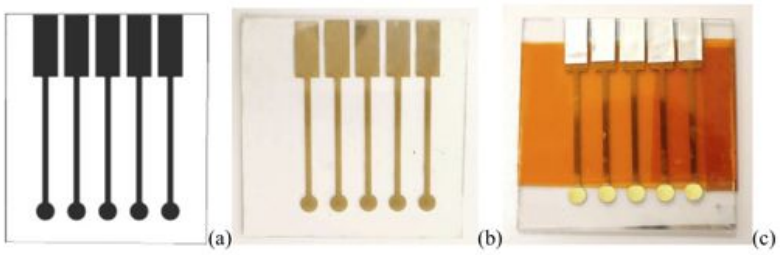

Figure 5.8: Patterning of the homemade electrode - a) photomask; b) gold coated glass; c) finished homemade gold electrode

homemade gold electrodes provides five separated lines that can be used as five different working electrodes. Gold electrodes have a diameter of 3 mm. Gold lines are covered with polyamide insulating tape (Kapton) to prevent line shorting once the glass slide is immersed in the electrolyte solution. Moreover the ends of lines are covered with small strips of electro-conductive tape (aluminium foil coated with Ni NPs-doped glue) that allows connecting it to the potentiostat-galvanostat through a clip for each line. A line-selector allows to chose the desired line without opening or moving the electrochemical cell.

HYs preparation

100 mg of AA powder were dissolved in 100 ?L of milliQ-water resulting in a final volume of 180 ?L.

To further increase the SWCNTs concentration, the 1wt% carbon nanotubes suspension was heated in order to evaporate water. A 1.5 mL Eppendorf was filled with 1mL of 1wt% nanotubes suspension and put on a hot place. The resulting nanotubes suspensions had a maximum 1.33wt% concentration because a too long heating could damage nanotubes. Firstly Eppendorf were filled with BIS powder, AA solution and SC solution in the right

quantities (Fig. 5.9).

Then SWCNTs suspension were added to the pre-polymer solution (Fig. 5.10).

CNTs wt%	AA 40% (µL)	AA 100% (µL)	BIS(mg)	2wt% SC in H_2O (µL)
0.1	250		3.5	200
0.25	250		3.5	125
0.375	250		3.5	62.5
0.5	250		3.5	
0.64		180	3.5	
0.85		180	3.5	

Figure 5.9: Compositions doped hydrogel prepolymer solutions -

SWCNTs-doped HYs were then chemically polymerized on glass coverslips pre-treated with APTES and glutaraldehyde. Photo-polymerization was not applicable to the SWCNTs-doped HYs because nanotubes acted as a black filter absorbing light radiation and preventing polymerization even after a long exposure time. This caused burns and excessive drying on the surface while not complete polymerization of lower layers of hydrogel.

Preparation of GOx/SWCNTs-doped poly(AA/BIS)/gold biosensor

CNTs wt%	1wt% CNTs in H_2O (µL)	1.33wt% CNTs in H_2O (µL)
0.1	50	
0.25	125	
0.375	187.5	
0.5	250	
0.64	320	
0.85		320

Figure 5.10: Additions of carbon nanotubes suspensions -

0.5 mm thick cylindrical SWCNTs-doped HYs were polymerized on homemade gold electrodes. Homemade gold electrodes were pre-treated with APTES-Glut but only on the glass surface that surrounds the gold spot to improve adhesion of HYs without damaging the gold surface.

Biocompatibility tests - Seeding and Culture of C2C12 cells

Cultures of C2C12 cells were used to test two different types of SWCNTs-doped hydrogels:

- hydrogels with 20% w/v AA, AA/BIS 29:1 and 0.1% SWCNTs

- hydrogels with 20% w/v AA, AA/BIS 29:1 and 0.85% SWCNTs

In both cases chemical polymerization method with APS and TEMED was used.
After polymerization, cylindrical hydrogels with 0.5 ?m thickness and 20 mm, were rinsed with distilled water for three times to remove all residual monomer and free nanotubes traces.
Moreover they were rinsed with PBS 1X to cause the swelling of the hydrogel useful to remove further traces of nanotubes from hydrogel pores. After that hydrogels were sterilized with an UV lamp for 15 min working inside a sterile hood.
Subsequently, every hydrogel was put in a compartment of a multiwell and sprinkled with some drops of a protein accession solution (laminin-collagen) on the top face. After 2-3 minutes the protein solution was removed. Afterwards 3 ml of cell culture medium with 3x105 C2C12 cells (murine myoblast cell line) were put in every well, primarily sprinkling the top face of the hydrogel to favour the cell seeding on the surface of the hydrogel.
Samples were maintained in the incubator (Heraeus BBD 6220) at 310 K in an atmosphere of 5% CO2 and 95% relative humidity for three days, and then they were analyzed with Trypan blue and LIVE/DEAD assays to have information about the viability and cellular proliferation.

Trypan blue assay

Live cells or tissues with intact cell membranes are not colored. Since cells are very selective in allowing the entry of compounds that pass through the membrane, in a viable cell trypan blue is not absorbed; however, it pass through the membrane of damaged cell. Hence, dead cells are shown as a distinctive blue color under a microscope.
First of all, it is necessary to remove all the culture medium with a Pasteur pipette. cells were then fixed filling every well with 4% paraformaldehyde (PFA, Sigma) phosphate buffer solution for 7 min. Samples were rinsed with PBS 1X and a drop of Trypan Blue 1X solution was put on each cell culture. After 5 minutes the Trypan solution was removed washing twice with PBS 1X to make microscopy analysis.

LIVE/DEAD assay

Live cells are distinguished by the presence of ubiquitous intracellular esterase activity, determined by the enzymatic conversion of the nonfluorescent cell-permeant Calcein AM to the intensely fluorescent Calcein. The polyanionic dye Calcein is well retained within live cells, producing an intense uniform green fluorescence in live cells (EX/EM λ = 495 nm/λ = 515nm).

Ethidium homodimer-1 (EthD-1) enters cells with damaged membranes and undergoes a 40-fold enhancement of fluorescence upon binding to nucleic acids, thereby producing a bright red fluorescence in dead cells (EX/EM 495 nm/ 635 nm). EthD-1 is excluded by the intact plasma membrane of live cells. The determination of cell viability depends on these physical and biochemical properties of cells. It was found that Calcein AM and ethidium homodimer are optimal dyes for this application.
Cell culture medium were completely removed from the wells and the cell cultures were rinsed with PBS 1X twice. Wells were then filled with PBS 1X solution of 3 μM calcein AM and 3 μM ethidiumhomodimer-1. After 45 minutes at room temperature cell culture were washed twice in PBS 1X and analyzed with a fluorescence microscope (Leica DMI6000-B).
Electrical signaling from cells and breeding/culturing protocol specifications
Cardyomyocites are from 0-3 days neonatal rats Sprague Dawley that are breeded under legislative regulations in experimental animals after authorization of University Ethical Commitee of Experimentation on Animals (C.E.A.S.A.) of University of Padua. Cells were seeded on sterilized HYs (sterilization occurs with ethanol 100% immersion, subsequent rinsing with milliQ water and storing in sterile PBS for 12 h) at a cellular density of 300'000 cells/HY. Since polyacrilamide is cellular repellent, it was needed to functionalise HY surface with an adhesion protein. It was used laminine (BD, 354232) at 100 μg/mL concentration. Laminine solution was deposited on HY, whose surface was previously dried with vacuum pump and incubated for 2 min at room temperature. The protein is then removed.
EIS measurements and chronoamperometries with cells were conducted in recording solution (NaCl 125 mM, KCl 5 mM, Na_3PO_4 1 mM, $MgSO_4$ 1 mM, Hepes 20 mM, $CaCl_2$ 2 mM, Glucosio 5.5 mM a pH 7.4 con NaOH).

5.6.2 Supporting Results

Raman measurements
Raman spectroscopy was carried out to get information about the dispersion of SWCNTs. A 15x15 μm squared area was scanned on three humid hydrogels with three different concentrations of SWCNTs (0.1wt%, 0.5wt% and 0.85wt%). A Raman/SNOM confocal spectrometer (Alpha 300S, Witec) equipped with a He-Ne laser (λ = 633 nm) and a 10X

lens was used.

Spectra were integrated 10 times for each point in the G-band peak interval (between 1585 and 1597 cm^{-1}). Then data were normalized on the maximum and minimum peak intensity collected throughout the three HYs and plotted as a function of x-y spatial coordinates obtaining three comparable microRaman maps of the surface of the hydrogels. The specific Raman activity of carbon nanotubes allows a qualitative comparison between their concentrations in different doped-hydrogels, by considering the Raman radiation coming from the volume near the surface.

Surface maps (Fig. 5.11 were easily obtained for humid hydrogels. The same maps for the transversal sections were not obtained because the cut surfaces were too rough to achieve a good focus on them at 10X magnification.

The intensity of the G-band peak provided by CNTs were used to compare the amount of nanotubes present in the three samples. Maps in 5.11 are normalized on the maximum intensity of the G-band throughout the three HYs. So darkest regions correspond to zone at low level of doping. All maps show a good color uniformity that confirms a

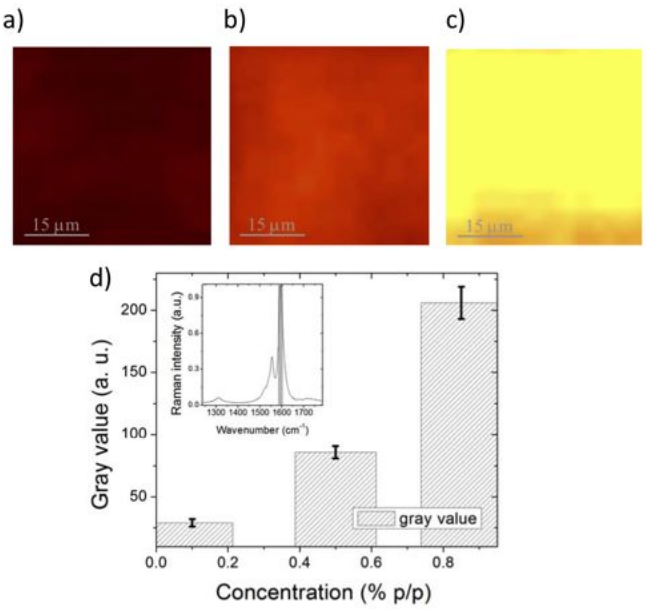

Figure 5.11: MicroRaman maps of the surface of 0.1wt%. - a), 0.5wt% b) and 0.85wt% c) SWCNTs-doped hydrogels and mean intensities against SWCNTs concentration d).

good degree of dispersion on a micrometric scale. Only some slight variations to lighter color (i.e. increment in intensity) appear, meaning that CNTs concentration is a little bit

higher in those regions. In agreement with micrographs (Fig. 5.12) these could be regions where CNTs are more aggregated, thus more concentrated than in the rest of the hydrogel surface.

In Fig. 5.11d the mean intensity of the G-band peak for every map is plotted as a function of CNTs theoretical concentration. The graph shows that increasing nanotubes concentration, the surface concentration increases too as it was expected.

Micrographs (Fig. 5.12) of HYs were taken with a OLYMPUS inverted steromicroscope coupled with a camera, at a magnification of 10X and fixing light intensity and other optical parameters. This gave the possibility to compare the microstructure of HYs with different SWCNTs concentrations. Micro pictures of both the surface and of the transversal section of HYs were taken.

EIS measurements

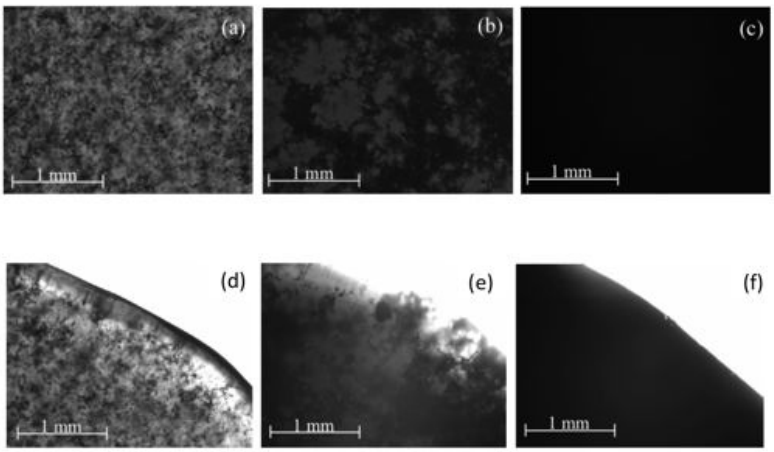

Figure 5.12: MicroRaman maps of the surface of 0.1wt%. - (a), 0.5wt% (b) and 0.85wt% (c) SWCNTs-doped hydrogels. Top view and transversal view.

Below we present summarizing table referring to Fig. 5.3 in the manuscript (Fig. 5.13). Standard errors are calculated on the base of three repetitive measurements.

Electrodes treated within the manuscript were also statistically characterized by means of analysis of variance (ANOVA).

ANOVA test in fact provides a statistical test of whether or not the means of several groups are all equal. It generalizes t-test to more than two groups. Box chart plot of Fig. 5.13b shows mean values, the smallest observation (sample minimum), lower quartile, median, upper quartile, and largest observation (sample maximum) for every sample.

CV measurements

Referring to Fig. 5.4a of the main manuscript, we show in the figure below (Fig. 5.14) the evolution of the anodic peaks with time for the four samples. The same curves show that for 0 wt%, 0.1 wt% and 0.85 wt% HYs, the capacitive current increases with nanotubes loading and with time. Also for 0.5 wt% sample the area gets larger but it is much greater than others from the beginning. Since a linear shape like 0.5wt% is specific for an insulating layer (a quasi ohmic response is given), thus confirming the fact that in such conditions these samples are less conductive than the others as EIS results predicted.

CA measurements

As shown in Fig. 5.15, a glucose biosensor made with HY without SWCNTs does not provide any current peak both with low glucose addition even with higher glucose concentration. In biosensor without nanotubes, H2O2 cannot reach immediately the gold surface and so any current is provided.

a)

SWCNTs conc. (wt%)	Circuit	R_{P1} mean (Mohm)	St. Dev.	R_{P2} mean (Mohm)	St. Dev.
0	$R_S(R_{P1}Q)$	3.0	0.47	Not present	
0,1	$R_S(R_{P1}Q)$	1.6	0.53	Not present	
0,25	$R_S(R_{P1}Q)$	0.96	0.53	Not present	
0,25	$R_S(R_{P1}Q)(R_{P2}C)$	0.021		0,30	
0,375	$R_S(R_{P1}Q)(R_{P2}C)$	0.026	0.014	0,22	0,075
0,5	$R_S(R_{P1}Q)(R_{P2}C)$	0.026	0.027	0,11	0,027
0,64	$R_S(R_{P1}Q)$	0.22	0.065	Not present	
0,85	$R_S(R_{P1}Q)$	0.19	0.040	Not present	
GOLD	$R_S(R_{P1}Q)$	0.32	0.16	Not present	

b)

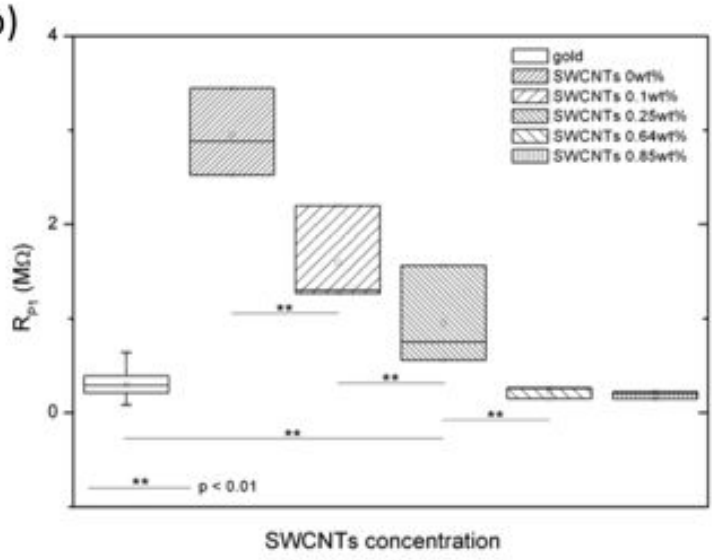

Figure 5.13: Statistics for electric measurements. - a) Mean resistances for modified HYs studied in the work referring to Fig.3 of the main manuscript; b) ANOVA box plot for the samples.

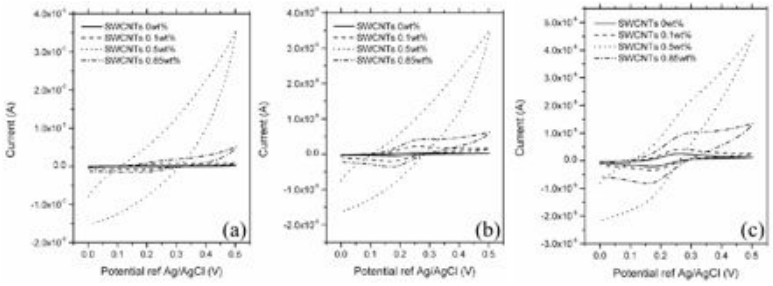

Figure 5.14: Comparison between voltammograms. - CVs in 10mM KNO3, 500?M FcMetOH aqueous solution for SWCNTs-doped hydrogels - gold surface composite electrodes after 6 min (a), 30 min (b) and 150 min (c)

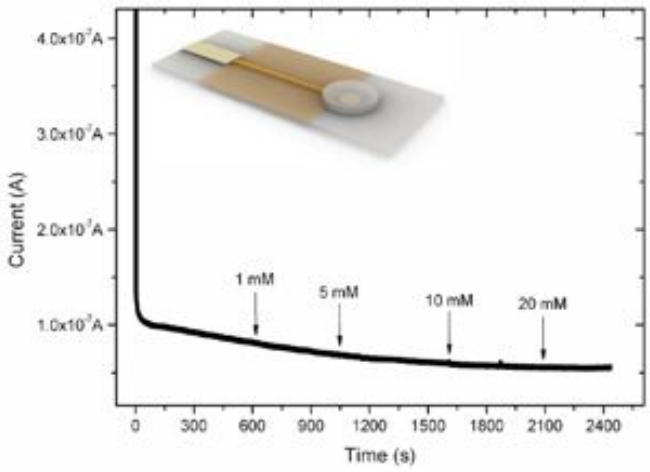

Figure 5.15: Chronoamperometry on GOx-HY with 0wt% SWCNTs concentration. - Successive glucose additions are reported on the graph with arrows.

6

Sampling and biosensing of multi-analytes in microfluidic platforms

This chapter is focused on integrating biosensors in microfluidic systems for effective measurements of multi-analytes. Effect of flow rate is studied in samples in which glucose or hydrogen peroxide is tuned. The manuscript is to be submitted.

6.1 Abstract

Microscale technologies are emerging as powerful tools for many tissue engineering and biological studies. By reducing the operational dimensions of a conventional macro-fluidic-based system down to the micro scale, one can not only reduce the sample volume, but also access a range of unique characteristics, which are not achievable in conventional macro-scale systems. In this work a sampling and biosensing of multi-analytes will be presented. The aim of this work is to integrate the Lab on a Chip approach to the biosensor to in line detection of metabolite concentration by the use of a sample unit.
Chronoamperometries of hydrogen peroxide glucose in various concentration will be performed during fluid perfusion at different flow rates and concentrations using a platinum wire imbibed with an enzyme, Glucose Oxidase, GOX.
Flow rate affects hydrogen peroxide and glucose detection in different way: a phenomenological explanation is given. Also time of response effect causes the need to realize a

sampling unit that enables the decoupling of process flow rate to biosensing flow rate: an integrated microloop is realized.

6.2 Introduction

Miniaturization can expand the capability of existing bioassays, separation technologies and chemical synthesis techniques. Although a reduction in size to the micrometer scale will usually not change the nature of molecular reactions, laws of scale for surface per volume, molecular diffusion and heat transport enable dramatic increases in throughput [128]. Due to the significant differences in several physical phenomena between microscale and macroscale devices, microfluidic technology provides unique functionality, which was not possible in previous studies using traditional techniques [129].

During the last few years, integrating biosensors into microfluidic systems has been reported as a promising perspective because it allows the downscaling of the average dimensions of the sensing device with consequent provision of a range of fundamental features that accompany system miniaturization such as reagent consumption, high temporal resolution due to rapid mixing, high throughput, enhanced analytical performance, less waste, low unit cost, reduced energy consumption, and reduced dimensions when compared to macroscale techniques [130, 131].

Biosensors have been included in many applications as reported in literature: from biomedical applications in particular in system biology [132, 133, 134] and high-throughput biological screening [135] to cell analysis [136] and environmental monitoring [137].

Continuous on-line monitoring of multiple-analyte has paramount importance in optimizing and controlling bioprocesses: for instance combination of glucose and lactate measurement can be related to oxygen-dependent metabolic activity [138, 139, 140]. For this reason, it is requested an online measurement and miniaturization of the devices [141, 142].

Normally, amperometric detection of hydrogen peroxide produced by the enzymes glucose oxidase (GOx) and lactate oxidase (LOx) immobilized at the surface of working electrodes is chosen as the biosensor principle.

As reported, there are many works in which biosensors and metabolic detection stick together in microfluidics [143, 144]. Recently, systems in which extracellular and intracellular metabolites from cells can be electrochemically detected were fabricated [145] or

people tried to monitor glucose [146] or lactose [147] consumption in the subnanoliter volume range, or again, a multiparameter cell population measurement microfluidic chip is proposed [148].
In such sense, open questions are how continuous flow rate affects sensitivity, dispersion of the reagents in the microtubes[149] and response time because of the development of integrated biosensors and microfluidic chip [150]. Both in chemistry [151] both in biology [152] continuous flow conditions are important: Natarajan et al. tuned experimental conditions to optimize protein deposition in continuous flow [152].
Nevertheless in our knowledge an in-depth study of how flow rate can modify biosensor activity when miniaturized is still lacking.
Also, for optimal analysis control, it is convenient to realize systems in which decoupling of sampling and analysis is allowed. A sampling unit integrated in the same microfluidic platform can further enhance analysis performances and outcomes exploiting miniaturization. This task could be assisted by the use of valves or pneumatic microfluidic technologies as reported in literature [153, 154].
Pumps and valves allow flowing regulation, on/off switching and can help to reduce sampling problems such as concentration out of linearity, required dilution, undesirable side effects like dirty and pH buffering. Also analyte detection require optimal flow rate conditions that can be different from sampling ones [155].
In this work we aim at investigating the role of continuous flow rate on the hydrogen peroxide electrochemical detection in enzyme-modified electrode integrated in microfluidic channels. Moreover, as a proof of concept, a microfluidic sampling unit may be added for decoupling bioprocess downstream outlet from the biosensor stream for optimal metabolite detection.

6.3 Results

Microfluidic platform is realized following protocol discussed in Section 6.4. In Fig. 6.1 we show a schematic view of the microchannel and of the biosensor. In panel a) a lateral view is depicted: a 250 μm height channel and 2 mm cylindrical chambers were fabricated. The flow inlet and outlet are put at the two lateral extremities of the polymeric structure. Three narrow conical channels (Fig. 6.1b and c) are created for storing the electrodes

as we can see from the top view. In panel d), a scanning electron microscopy image is presented showing the final active part of the biosensor produced by Prof. P. A. Serra's group [156]: the polyurethane coating is about 8 μm thick and covers Pt/Ir wire.
Biosensors prior to be integrated in the microfluidic platform has to be fully calibrated.

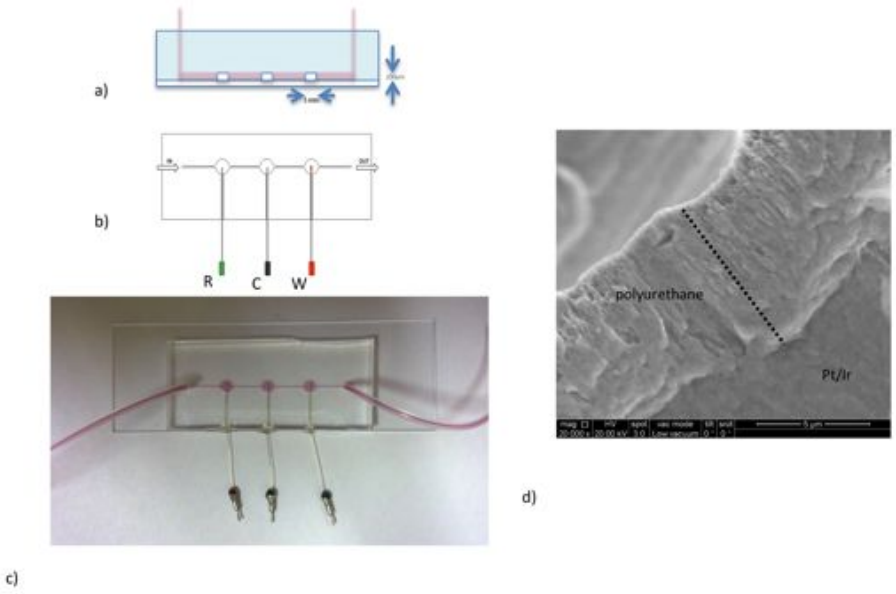

Figure 6.1: Schematic view of the microfluidic platform and its components. - a) Lateral and b) top view of the microfluidic channel. R is the reference electrode, C the counter and W the working electrode, the biosensor. c) picture representing the microfluidic system. Red fluid is used as example. d) SEM image showing lateral section of the active part of the biosensor: polyurethane membrane coats Pt/Ir wire.

Repetitive chronoamperometries experiments were performed in static conditions. Michaelis-Menten enzymatic kinetic equation allows to obtain main parameters for characterizing the biosensor [122]: as shown in Fig. 6.2, V_{max} value is (210 $\pm$ 3.2) nA and K_M is (4.1 $\pm$ 0.2) mM. The biosensor shows a linearity response within 1-5 mM range of concentration and all following experiments were conducted in this range.
Flow rate effects on hydrogen peroxide online detection have been studied under controlled perfusion. we show that varying the concentration of redox substrate the current enhances (Fig. 6.3): higher H_2O_2 concentration shows higher value of current collected at the electrode.
On the other hand, current shows only small ranges at flow rate variations for the same concentration. However, the inset graph shows that there are big variations of current with respect the flow rate when the current is normalized. Modification of the flow rate

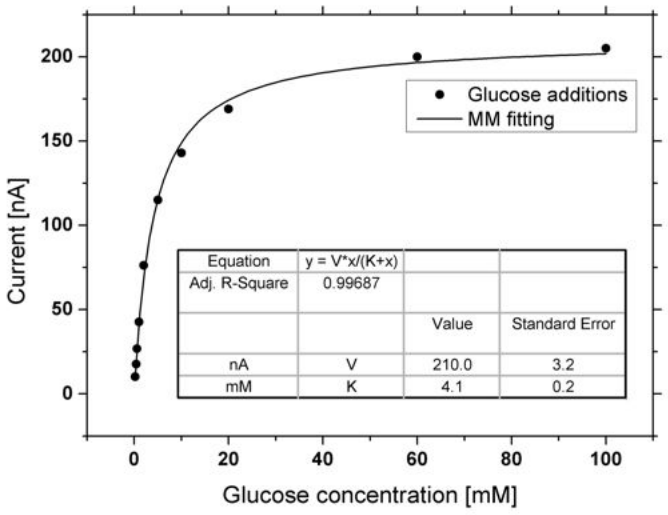

Figure 6.2: Static calibration of Pt biosensor. - Current versus glucose concentration additions and Michaelis-Menten kinetic equation calibration shows that the response of the biosensor can be considered linear till 4 mM

produces in the range between 10 μL/min and 100 μL/min, a significative variation in the current for both the samples.

For high flow rates, the curves tend to reach the same asymptotic value; This is why under 100 μL/min flow rate values, fluidodynamic regime is diffusion-limited whereas over 100 μL/min the limiting phenomenon is the concentration of samples and current becomes independent from flow rate (convection dominated in a mass transport regime.

Glucose online detection has been performed in biological medium samples using range flow rates between 1 μL/min and 50 μL/min (see Section 6.4 for further details). Chronoamperometries were performed. As shown in Fig. 6.4a, current detected is proportional to the concentration of samples. In the inset graph we show that normalizing current to maximum current detected for each sample, 1 mM values for very low flow rate values are bigger than for 5 mM values.

Flow rate affects the current detected: bigger is the flow rate, lower is the current.

For understanding how flow rate affects online detection of glucose, hydrogen peroxide chronoamperometries were performed in the same experimental conditions. In Fig. 6.4b blue triangles represent hydrogen peroxide trend tuning flow rate values. It is shown that enhancing flow rate, hydrogen peroxide gets high current values with respect to glucose behavior (red triangles).

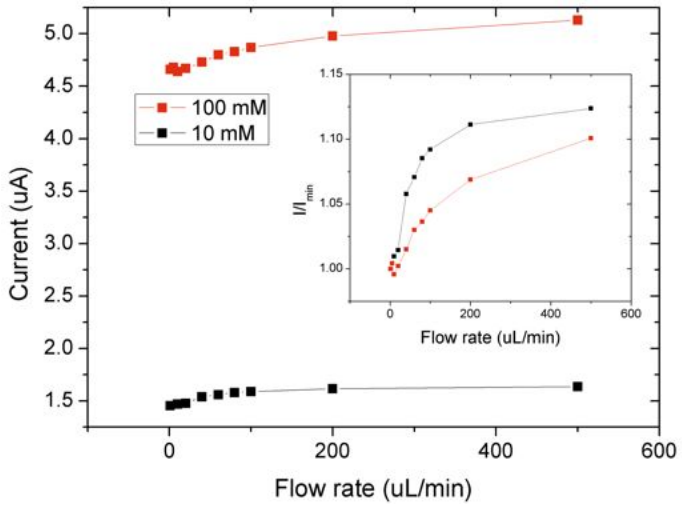

Figure 6.3: Effect of flow rate in hydrogen peroxide online detection. - The graphs shows current collected at the electrode versus flow rate. The effect of flow rate seems to be independent with respect to the flow rate but if we graph normalized current we can show how it enhances.

This is probably due stripping of hydrogen peroxide stripping from the surface of the biosensor. In the case in which there is only hydrogen peroxide in the channel, an enhancement of the current is achieved because more hydrogen peroxide is carried to the surface of the wire where redox reaction takes place. In the case in which glucose has to be oxidized by the enzyme, an intermediate reaction occurs. Hydrogen peroxide is produced after glucose oxidation and it could be either washed out in the medium or react on Pt surface producing detectable current. From our results it seems clear that the intermediate hydrogen peroxide reduce the overall efficiency of the glucose detection.

It is therefore convenient to calculate the efficiency of the system (Fig. 6.4b right y axis): ratio $I_{glucose}/I_{H_2O_2}$ estimates the real capability of the biosensor to detect glucose. Only for low flow rate values the efficiency is good.

Also time of response is important in such biosensors: in Fig. 6.4c, we show that flow rate affects time of response. A quick response is achieved only for low flow rate values. This behavior is quite in contrast to what we have found in the above paragraph: we need low flow rate values to obtain high current values.

For obviating this peculiar problem we have realized an integrated sampling system that prevents the user to use the same flow rate for processing and for biosensing.

In Fig. 6.5 we show the system we fabricated for solving the decoupling problem. In panel a) an image of the microloop: the flow enters (‘in‘) ’the main channel if pumps are active

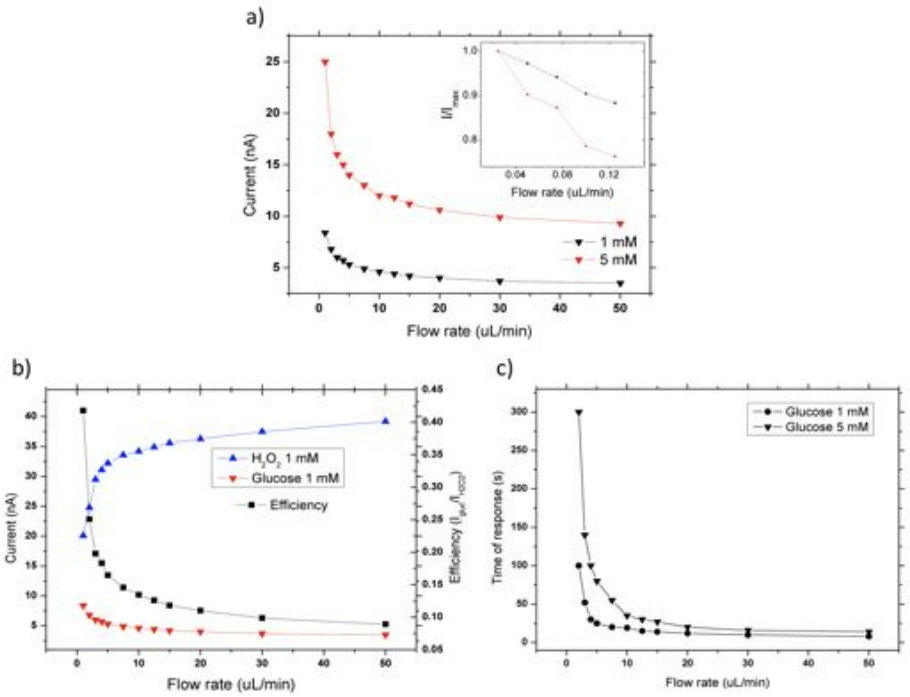

Figure 6.4: Effect of flow rate in glucose online detection and efficiency estimation of the system. - a) The graph shows how current response is highly dependent to the flow rate with respect to the previous experiment with hydrogen peroxide. The inset shows how flow rate variation is quite linear in the range of small flow rates; b) Comparison between two behaviors: the efficiency is high for low flow rate values; c) Time of response of the biosensor: the biosensor answers quickly for high values of flow rate.

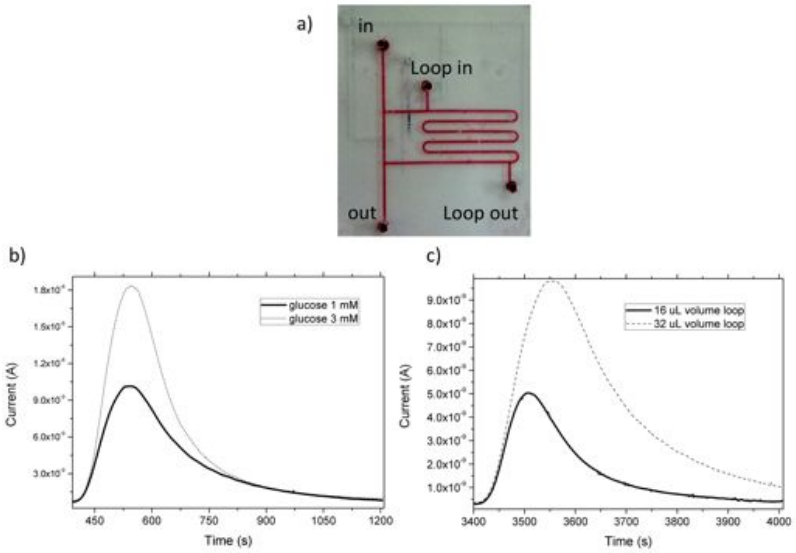

Figure 6.5: Sampling system - a) Image showing the microfluidic loop used for solving decoupling problems; b) CA measurement at different glucose concentration and c) CA at different volume concentration.

and passes straight till exit ("out')'. In case of pumps are inactive the flow passes through the loop that has been previously charged (by the entrance "loop in") with the detectable species and drives it to the exit of the "out". Loop volume can be adjusted by changing the dimensions of spirals. We chose two volume loops: 16 and 32 μL. Further details are discussed in Section 6.6.

In panel b) CA measurement shows the current detected when it used a fixed loop. In panel c) the same measure performed at fixed concentration (1 mM) but varying the volume loop. The comparison between the two graphs show how the transient shape of the curves is the same for samples in which concentration is the same (Fig. 6.5c) as expected but it differs significantly when the concentration changes (Fig. 6.5b).

6.4 Methods

Microbiosensors

The biosensors used in this work were projected and realized by Prof. P. A. Serra's group of University of Sassari [156].

The amperometric biosensor is composed by a cylindrical microelectrode of Pt/Ir 90%/10%.

The diameter of the wire is 0.125 mm and the length is 40 mm. The active element (the end of the wire) is coated with a thin film of polyterimmide that is imbibed by the enzyme, Glucose Oxidase, GOx from *Aspergillus Niger*. Finally the wire is coated with polyurethane film. Teflon is used for insulating.
The biosensor is stored at 150 K in order to preserve catalytic functionalities.

Chronoamperometry measurements and chemicals

Chronoamperometry measurements were performed using a potentiostat/galvanostat (AUTOLAB, PGSTAT 128N EcoChemie, The Nederlands) and managed by Nova 1.6 Software. All measures were conducted using biosensors as working electrode or Pt wires as necessary. Counter electrode was a Pt wire and reference was a pseudoreference in Ag/AgCl. Measurements were conducted biasing the working electrode at 0.7 V referred to the pseudoreference electrode. Static measurements were performed in usual electrochemical commercial cells. Supporting electrolytes used were PBS 1x (Vetrotecnica, Italy) or 1 mM Dulbecco Modified Medium High Glucose (DMEM High Glu, 4.5 mg/L D-Glucose, Invitrogen, Italy) and 5 mM Dulbecco Modified Medium Glucose free (DMEM Glu Free, Invitrogen, Italy). 50 % hydrogen peroxide solutions were prepared by diluting 80% hydrogen peroxide (Sigma-Aldrich, Italy) in distilled water. All solutions were sterilized and put in incubator at 300 K in order to prevent bacteria formation inside the aliquots.

Microfabrication - Photolitography

Photolitographic techniques were used to build microfluidic platforms. Photomasks were designed with AUTOCAD 2D 2010 (Autodesk, USA) and printed in transparence photo mask (8000 dpi). Silicon wafers (5" Siltronic) were treated under atmosferic plasma (Harrick Plasma, USA) for 2 minutes in order to remove organic molecules on the surface and making it hydrophilic. As regards the biosensing platform, a coating with negative photoresist (SU-8 2100, MicroChem Corp. USA) was made on the wafer using a spin coater (WS-650-23, Laurell Technologies Corporation, USA) to obtain 250 μm of thickness. After a soft baking the photo resist was exposed at UV light treatment ($\lambda = 365$ nm, OAI 150, USA). An expose bake followed the exposure treatment. The development was achieved in methoxymetacrilate (Sigma-Aldrich, Italy) and further rising with Isopropanol. An hardbaking treatment was done from 338 K to 433 K at 120 K/h for 2 h. For the sample chip 2 molds were needed. For the firs mold (Flow layer [157]), after a treatment under HDMS vapor, 2 layer of positive photoresist SRR 620-7 were spun to obtain a total high

of 36 μm. After the baking, at least 3 hours for rehydratation were needed before exposure. Development with Microposit MF 319 (Rohm & Haas) and further rising with water complete the development. Hard baking from 298 K to 463 K with 10 K /h ramp was needed to obtain rounded channels. At the end of the hard baking under profilometer the high was between 30-40 μm. Another mold was made for the control layer with SU8-2100 to obtain square channels 100 μm high.

Microfabrication - Softlitography Polydimethylsiloxane (PDMS, Sigma-Aldrich, Italy) was used for molding in the ratio of 10:1 (base:cure agent). The two compounds were mixed, stirred and degassed before baking. The mold was covered with the liquid PDMS and then cured in oven at 353 K for 2 h. The chip was peeled and linked to a borosilicate glass (Vetrotecnica, Italy) by plasma treatment (30 s 70W 30mbar).

In the sample unit a 150 μm high liquid PDMS (10:1 base:cure agent) was spun on the flow mold and baked at 353 K to 30 min. The control mold was covered with a thick layer of liquid PDMS and baked for 30 min at 353 K. After this time the chip was peeled. Its bottom surface covered with the cure agent and aligned on the flow mold. At this point, once bonded together, they were put in the oven for 2 hours. The two layers chip was then peeled and bonded via plasma treatment to a borosilicate glass. The simple unit and the biosensing unit were connect using tubing (Tygon).

The biosensors were integrated into the microfluidic platform by hand under a stereo microscope (Leica Microsystems, Italy) and then fixed by insertion of an UV glue (DYMAX Corp., USA) polymerized in situ directly in contact with the electrodes using a UV lamp for 5 sec (DYMAX 3067, USA). In this way the watertight was guaranteed.

Flow rate regulation

Fluid enliven within the channels is realized by using a syringe pump (PHD 22/2000 HPSI, Harvard Apparatus, USA). It is provided of a multi-rack holder for 10 syringes storing. Syringes used were 3 mL and 5 mL from Becton, Dickinson and Company, USA.

Sampling unit

The elastomer used is Sylgard 184 (Dow Corning, USA), composed of two parts. Part "A" contains a polydimethylsiloxane bearing vinyl groups and a platinum catalyst; part "B" contains a cross linker containing silicon hybrid (Si-H) group, which form covalent bond with vinyl group. Sylgard 184 is normally used at a ratio of 10 A : 1 B.

The top layer is cast thick (about 5 mm) for mechanicals stability, whereas the other layer is cast thin.

The thin layer was created by spin-coating the mixture on a microfabricated mold at 1000 rpm for 60 sec, yielding a thickness of 60 μm. Each layer was separately baked: the thin layer at 283 K for 90 min and the other layer at 353 K for 60 min.
Molds were patterned photoresist on silicon wafer. For the flow layer SPR 220-7 photoresist (Rohm & Haas, USA) was spun at 800 rpm, patterned with a transparency film as a mask, and developed to yield inverse channel of 30 μm in height. When baked at 463 K for 3 hours, the photoresist reflows and the inverse channels become rounded. For the control layer SU8-2100 (MicroChem Corp., USA) photoresist was spun at 3000 rpm, exposed with the control mask and developed to obtain channel of 100 μm height.

6.5 Conclusions

In this work we realized a microfluidic platform in which microstructured biosensors were integrated for online detection of metabolites and especially for glucose. In the first phase we performed chronoamperometries measurements (CAs) in static conditions in order to test the performance of the biosensor.
Online monitoring is fulfilled by optimal engineering of the microfluidic platform realized by means of microfabrication techniques.
We think at the most important variable for online detection the flow rate and studies of its effect on biosensing system have been conducted.
We chose as target probe for our proof of concept study oxygen peroxide and glucose in different concentrations.
CAs reveal that hydrogen peroxide and glucose have different behaviors: enhancing flow rate in hydrogen peroxide samples, current enhances while the contrary appears when glucose is added in the microflow. We explain this fact by hypothesizing that flow rate influences the quantity of hydrogen peroxide that can reach the underlying electrode from the outer sphere box.
For this reason efficiency of system measurement is calculated: under 1 μL/min values of low rate the efficiency is at the maximum. Also time of response is important but diminishing flow rates, time for having responses get longer: an optimization of the two parameters is needed.
For resolving troubles in times elongation, we proposed an integrated loop sampling system

in which we can decouple process flow rate from sensing flow rate. We shown that different loop volume do not affect current transient behavior during online detection of analytes.

6.6 Supporting Information

Signaling

Using soft lithography technique membrane microvalves can be produced. A basic microfluidic device is composed of two elastomer layers (Fig. 6.6a). One layer contains channels for flowing liquids (flow layer), and the other one contains channels that deflect the membrane valve into the flow channel and stop liquid flow when pressurized with air or liquid (control layer, CL). Using microvalves it has been developed a sampling unit for the injection of an accurate sample amount. In this way at the specific injection time the device is able to inject the sample downstream the system, for example in the culture unit or in the biosensor unit. The prototype developed is shown in Fig. 6.6d. Joining the sampling unit to the culture chamber it will be able to produce a established impulse in quantity and time. The quantity is determined by the channels length (volume) as shown in Fig. 6.6b. In Fig. 6.6b and c is reported the fluid-dynamic validation of the culture chamber impulse: there is a uniform advancing front and a homogeneous loading in the microfluidic distribution system.

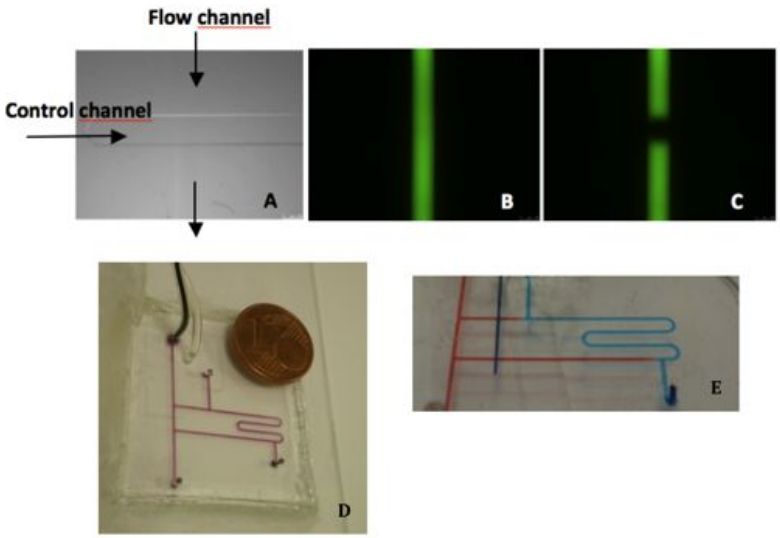

Figure 6.6: Loop description - Flow channel (150 μm wide and 36 μm high) and control channel (250 μm wide and 100 μm high) in phase contrast, a) and in fluorescence with CL pressure 0 bar, b) and 1 bar, c; Sampling device d); the sample volume is in light blue and under pression the CL in blue.)

6. SAMPLING AND BIOSENSING OF MULTI-ANALYTES IN MICROFLUIDIC PLATFORMS

7

Conclusions

During this period of thesis, I worked on the development of single-walled carbon nanotubes (SWCNTs) biosensors for electrochemical detection of analytes.

Biosensors were produced starting from gold electrodes on glass substrates. The optimization of metal deposition led to obtain a nanometric gold film created by PECVD technique on predeposited titanium thin layer which allowed to enhance the adhesion of the gold on glass. The patterning was achieved by photolithographic processes as described in Chapters 4 and 5.

Carbon nanotubes act as doping agent for the modification of the prepared electrodes. Two different approaches have been discussed in this thesis (see Chapter 2: the first one concerns the vertical surface modification of gold electrodes by means of covalently self-assembling of SWCNTs ("forests") and the second one is a bulk modification strategy in which a polyacrilamide hydrogel (HY) has been doped with SWCNTs.

Sensors based on nanotubes forests presented different electrochemical properties: it is well know from literature that different lengths of nanotubes and different oxygenated species at the ends of nanotubes may affect electrical properties thus influencing performances of modified electrodes (and therefore the sensors).

For this reason we aimed firstly at developing a robust protocol of modification of SWCNTs for preparing electrodes that posses different electrochemical properties (Chapter 3). We tuned bath oxidation temperature in order to obtain shorter carboxylated SWCNTs as the temperature increased. We explained this choice by demonstrating that the oxidative process has a strong dependence within the temperature with respect to the time. Atomic force microscopy (AFM) images of shorted carboxylated SWCNTs forests revealed

that bigger is bath temperature shorter is the forest of nanotubes. Raman spectra also revealed that carboxylated SWCNTs are more defective when temperature is increased thus confirming AFM outcomes.

In a successive work we studied the effect on electrochemical properties of forests in which height and density of the forests are tuned (Chapter 4). The control in density is achieved by changing the relative amount of cysteamine by diluting it with 2-mercaptoethanol, a species that is quite inert to the covalently attack of carboxylated nanotubes.

Cyclic voltammetries (CVs) and electrochemical impedance spectroscopy (EIS) measurements shown that shorter is the forest, faster is the redox reaction that occur at the surface of the modified electrode. Nevertheless linear sweep voltammetries (LSVs) and AFM images of samples in which cysteamine is very diluted (i.e. forests are theoretically less dense), shown that carbon nanotubes forests were disordered and nanotubes deposited in each case on the substrates.

For this reason wettability measurements with SWCNTs solution drops were conducted in samples in which density of cysteamine is tuned: we shown that there was a strong hydrophobic behavior in samples in which cysteamine concentration was maximum. This confirmed the idea that a drop of SWCNTs solution with low contact angle (i.e. hydrophilic samples and low surface tensions) affect deposition of nanotubes on the surface (and of course electrochemical properties) because of difference in surface tensions.

In conclusion, electrodes modified with self-assembling of nanotubes can act as electrochemical sensors (or biosensors if a biomolecule is linked to the nanotube) and a good knowledge of their morphological (such as height and density) and chemical (numbers and quality of defects) properties are needed in order to obtain reproducible results.

This work has to be recognized as a great effort for understanding bulk and functional properties of modified surface electrodes: for the rapid applicability of such devices, people have to pay attention to all features of these peculiar electrodes. Vertical assembling of SWCNTs requirements the knowledge of chemical and morphological properties of nanotubes and also the awareness that modifying hydrophilic substrates can affect electrical properties.

We then spoke about bulk modification strategies by means of bulk modification of an hydrogel with SWCNTs (Chapter 5).

In this work we realized single-walled carbon nanotubes doped polyacrilamide HYs in order to make them electroconductive. This problem comes from the request of a biocompatible

substrate in which cells can be cultured and of an electrical material that can be used as biosensor for metabolites detection.
HYs are very promising in this sense: their elastic properties (such as stiffness) are quite similar to those of living tissues and this allows cells to proliferate very well.
EI spectra shown that two different behaviors appear when doping concentration is tuned. A phase separation occur when nanotubes are in small number inside the gel matrix, while when the concentration is high enough, electrons can percolate through the nanotubes and an electroconductive material is realized.
Small amount of nanotubes are sufficient to make HYs electroconductive thanks to peculiar electrical properties of carbon nanotubes.
Then we realized a glucose biosensor by inserting an enzyme, GOx, Glucose Oxidase from *Aspergillus Niger*, by electrophoresis technique into the modified HY: chronoamperometries (CAs) and calibrations with Michaelis-Menten equation gave very low detection limits with compared to what present in literature and good sensitivity values.
Electrical signaling is finally revealed via EIS and CA measurements on doped HYs in wich cardia cells were seeded.
Also bulk modification strategy as surface modification can assure the realization of good biocompatible substrates for biosensing. This work is very promising for future applications in the field of tissue engineering because conductive biocompatible substrates with very low content of dopants (minor 1% in weight) have been realized. Both biosensing applications (glucose or other metabolites detection) and electrical cellular activity are destined to become a point of reference for people who want to perform electrophysiological measurements in complex living systems.
The last work is focused on the possibility of integrating carbon nanotubes biosensors based like forests in microfluidic environments. This could lead to ameliorate the entire biosensing system exploiting well known microfluidic properties: enhancing time of response, less waste, more sensitivity and so on.
For this reason we aim at, in this final work (Chapter 6), developing a biosensing multi-analytes microfluidic platform in which metal wires act as electrodes.
A platinum wire coated with GOx enxyme provided by. Prof. P.A. Serra from University of Sassari, Italy, was used as working electrode. An *ad hoc* microfluidic platform has been realized for the biosensors. Studies on the effect of flow rate in detecting glucose have been conducted. CAs shown that for optimal outcomes, people have to balance the effect of

flow rate and time of response: in fact, when the flow rate enhances diminishes the time of response but also the current collected.
A sampling unit, a microloop, is therefore inserted in the microchannel in order to decouple process flow rate to biosensing flow rate optimal conditions.
Finally, integration of biosensing and lab-on-a-chip approach has been investigated: future perspectives are focused on industrial application. Low cost and small time of responses are the base in economic progress in Science world.

References

[1] GL Che, BB Lakshmi, ER Fisher, and CR Martin. **Carbon nanotubule membranes for electrochemical energy storage and production**. *Nature*, **393**(6683):346–349, MAY 28 1998. 7

[2] PJ Britto, KSV Santhanam, A Rubio, JA Alonso, and PM Ajayan. **Improved charge transfer at carbon nanotube electrodes**. *Advanced Materials*, **11**(2):154–157, JAN 22 1999. 7

[3] JK Campbell, L Sun, and RM Crooks. **Electrochemistry using single carbon nanotubes**. *Journal of the American Chemical Society*, **121**(15):3779–3780, APR 21 1999. 7

[4] HX Luo, ZJ Shi, NQ Li, ZN Gu, and QK Zhuang. **Investigation of the electrochemical and electrocatalytic behavior of single-wall carbon nanotube film on a glassy carbon electrode**. *Analytical chemistry*, **73**(5):915–920, MAR 1 2001. 7

[5] JX Wang, MX Li, ZJ Shi, NQ Li, and ZN Gu. **Electrocatalytic oxidation of 3,4-dihydroxyphenylacetic acid at a glassy carbon electrode modified with single-wall carbon nanotubes**. *Electrochimica Acta*, **47**(4):651–657, NOV 1 2001. 7

[6] M. Meyyappan. *Carbon Nanotubes: Science and Application*. CRC, Usa, 2005. 8

[7] Q Zhao, ZH Gan, and QK Zhuang. **Electrochemical sensors based on carbon nanotubes**. *Electroanalysis*, **14**(23):1609–1613, DEC 2002. 8

[8] M Musameh, J Wang, A Merkoci, and YH Lin. **Low-potential stable NADH detection at carbon-nanotube-modified glassy carbon electrodes**. *Electrochemistry Communications*, **4**(10):743–746, OCT 2002. 8

[9] V. Erokhrin, M. Kumar Ram, and O. Yavuz. *The New Frontiers of Organic and Composite Nanotechnology*. ELSEVIER, 2008. 8

[10] S. Andreescu, J. Njagi, and C. Ispas. *The New Frontiers of Organic and Composite Nanotechnology*. ELSEVIER, 2008. 8

[11] J.J. Gooding, R. Wibowo, J. Liu, W. Yang, D. Losic, S. Orbons, F.J. Mearns, J.G. Shapter, and D.B. Hibbert. **Protein electrochemistry using aligned carbon nanotube arrays**. *Journal of the American Chemical Society*, **125**(30):9006–9007, 2003. 8, 10, 34, 35, 39

[12] X Yu, D Chattopadhyay, I Galeska, F Papadimitrakopoulos, and JF Rusling. **Peroxidase activity of enzymes bound to the ends of single-wall carbon nanotube forest electrodes**. *Electrochemistry Communications*, **5**(5):408–411, MAY 2003. 8

[13] J Wang, AN Kawde, and M Musameh. **Carbon-nanotube-modified glassy carbon electrodes for amplified label-free electrochemical detection of DNA hybridization**. *Analyst*, **128**(7):912–916, 2003. 8

[14] J Wang, M Musameh, and YH Lin. **Solubilization of carbon nanotubes by Nafion toward the preparation of amperometric biosensors**. *Journal of the American Chemical Society*, **125**(9):2408–2409, MAR 5 2003. 8

[15] JHT Luong, S Hrapovic, D Wang, F Bensebaa, and B Simard. **Solubilization of multiwall carbon nanotubes by 3-aminopropyltriethoxysilane towards the fabrication of electrochemical biosensors with promoted electron transfer**. *Electroanalysis*, **16**(1-2):132–139, JAN 2004. 8

[16] Lijun Liu, Fu Zhang, Fengna Xi, and Xianfu Lin. **Highly sensitive biosensor based on bionanomultilayer with water-soluble multiwall carbon nanotubes for determination of phenolics**. *Biosensors and Bioelectronics*, **24**(2):306–312, OCT 15 2008. 8

[17] Deepa Vairavapandian, Pornnipa Vichchulada, and Marcus D. Lay. **Preparation and modification of carbon nanotubes: Review of recent advances and applications in catalysis and sensing**. *Analytica chimica acta*, **626**(2):119–129, SEP 26 2008. 8

[18] J Wang and M Musameh. **Carbon nanotube/teflon composite electrochemical sensors and biosensors**. *Analytical chemistry*, **75**(9):2075–2079, MAY 1 2003. 8

[19] MD Rubianes and GA Rivas. **Carbon nanotubes paste electrode**. *Electrochemistry Communications*, **5**(8):689–694, AUG 2003. 8

[20] B Sljukic, CE Banks, C Salter, A Crossley, and RG Compton. **Electrochemically polymerised composites of multi-walled carbon nanotubes and poly(vinylferrocene) and their use as modified electrodes: Application to glucose sensing**. *Analyst*, **131**(5):670–677, 2006. 8

[21] Jun Li, Hou Tee Ng, Alan Cassell, Wendy Fan, Hua Chen, Qi Ye, Jessica Koehne, Jie Han, and M. Meyyappan. **Carbon Nanotube Nanoelectrode Array for Ultrasensitive DNA Detection**. *Nano Letters*, **3**(5):597–602, 2003. 10

[22] P. Diao, Z. Liu, B. Wu, X. Nan, J. Zhang, and Z. Wei. **Chemically Assembled Single-Wall Carbon Nanotubes and their Electrochemistry**. *ChemPhysChem*, **3**(10):898–991, 2002. 10, 35

[23] P. Diao and Z. Liu. **Electrochemistry at chemically assembled single-wall carbon nanotube arrays**. *J. Phys. Chem. B*, **109**(44):20906–20913, 2005. 10, 16, 35

[24] Xin Yu, Bernard Munge, Vyomesh Patel, Gary Jensen, Ashwin Bhirde, Joseph D. Gong, Sang N. Kim, John Gillespie, J. Silvio Gutkind, Fotios Papadimitrakopoulos, and James F. Rusling. **Carbon nanotube amplification strategies for highly sensitive immunodetection of cancer biomarkers**. *Journal of the American Chemical Society*, **128**(34):11199–11205, AUG 30 2006. 10, 35

REFERENCES

[25] Alison Chou, Till Bocking, Nagindar K. Singh, and J. Justin Gooding. **Demonstration of the importance of oxygenated species at the ends of carbon nanotubes for their favourable electrochemical properties**. *Chemical Communications*, **7**:842, 2005. 10, 34

[26] Rebecca A. MacDonald, Brendan F. Laurenzi, Gunaranjan Viswanathan, Pulickel M. Ajayan, and Jan P. Stegemann. **Collagen-carbon nanotube composite materials as scaffolds in tissue engineering**. *Journal of Biomedical Materials Research Part A*, **74A**(3):489–496, 2005. 11

[27] B.S. Harrison and A. Atala. **Carbon nanotube applications for tissue engineering**. *Biomaterials*, **28**(2):344–353, 2007. 11

[28] G. Gruner. **Carbon nanotube transistors for biosensing applications**. *Analytical and bioanalytical chemistry*, **384**(2):322–335, 2006. 11

[29] N. Aoki, A. Yokoyama, Y. Nodasaka, T. Akasaka, M. Uo, Y. Sato, K. Tohji, and F. Watari. **Cell culture on a carbon nanotube scaffold**. *Journal of Biomedical Nanotechnology*, **1**(4):402–405, 2005. 11

[30] B.L. Allen, P.D. Kichambare, and A. Star. **Carbon Nanotube Field-Effect-Transistor-Based Biosensors**. *Advanced Materials*, **19**(11):1439–1451, 2007. 11

[31] A. Abarrategi, M.C. Gutiérrez, C. Moreno-Vicente, M.J. Hortig
"uela, V. Ramos, J.L. López-Lacomba, M.L. Ferrer, and F. del Monte. **Multiwall carbon nanotube scaffolds for tissue engineering purposes**. *Biomaterials*, **29**(1):94–102, 2008. 11

[32] D.Y. Wang, Y.Y. Chang, C.L. Chang, and Y.W. Huang. **Deposition of diamond-like carbon films containing metal elements on biomedical Ti alloys**. *Surface and Coatings Technology*, **200**(7):2175–2180, 2005. 11

[33] S.I. Stupp and P.V. Braun. **Molecular manipulation of microstructures: biomaterials, ceramics, and semiconductors**. *Science*, **277**(5330):1242, 1997. 11

[34] A. Krajewski, A. Ravaglioli, A. Bertoluzza, P. Monti, MA Battaglia, A. Pizzoferrato, R. Olmi, and A. Moroni. **Structural modifications and biological compatibility of doped bio-active glasses**. *Biomaterials*, **9**(6):528–532, 1988. 11

[35] L. Dai, J. Lu, B. Matthews, and A.W.H. Mau. **Doping of conducting polymers by sulfonated fullerene derivatives and dendrimers**. *J. Phys. Chem. B*, **102**(21):4049–4053, 1998. 11

[36] DG Jones, ER Anderson, and KA Galvin. **Spinal cord regeneration: Moving tentatively towards new perspectives**. *Neurorehabilitation*, **18**(4):339–351, 2003. 11

[37] Sarah M. Richardson-Burns, Jeffrey L. Hendricks, Brian Foster, Laura K. Povlich, Dong-Hwan Kim, and David C. Martin. **Polymerization of the conducting polymer poly(3,4-ethylenedioxythiophene) (PEDOT) around living neural cells**. *Biomaterials*, **28**(8):1539–1552, MAR 2007. 11

[38] SG Zhang. **Fabrication of novel biomaterials through molecular self-assembly**. *Nature Biotechnology*, **21**(10):1171–1178, OCT 2003. 11, 50

[39] L.M. Pakstis, B. Ozbas, K.D. Hales, A.P. Nowak, T.J. Deming, and D. Pochan. **Effect of chemistry and morphology on the biofunctionality of self-assembling diblock copolypeptide hydrogels**. *Biomacromolecules*, **5**(2):312–318, 2004. 11, 50

[40] Matthew R. Hynd, John P. Frampton, Natalie Dowell-Mesfin, James N. Turner, and William Shain. **Directed cell growth on protein-functionalized hydrogel surfaces**. *Journal of neuroscience methods*, **162**(1-2):255–263, MAY 15 2007. 11

[41] DH Kim, M Abidian, and DC Martin. **Conducting polymers grown in hydrogel scaffolds coated on neural prosthetic devices**. *Journal of biomedical materials research part A*, **71A**(4):577–585, DEC 15 2004. 11, 51

[42] Anthony Guiseppi-Elie. **Electroconductive hydrogels: Synthesis, characterization and biomedical applications**. *Biomaterials*, **31**(10):2701–2716, APR 2010. 12

[43] Yingjun Wang, Guoxin Tan, Shujiang Zhang, and Yanxia Guang. **Influence of water states in hydrogels on the transmissibility and permeability of oxygen in contact lens materials**. *Applied Surface Science*, **255**(2):604–606, NOV 15 2008. 1st International Symposium on Surface and Interfaces of Biomaterials, Chengdu, PEOPLES R CHINA, OCT 05-07, 2007. 12

[44] R.V. Ulijn, N. Bibi, V. Jayawarna, P.D. Thornton, S.J. Todd, R.J. Mart, A.M. Smith, and J.E. Gough. **Bioresponsive hydrogels**. *Materials Today*, **10**(4):40–48, 2007. 12, 50

[45] H Li, DQ Wang, BL Liu, and LZ Gao. **Synthesis of a novel gelatin-carbon nanotubes hybrid hydrogel**. *Colloids and surfaces B-Biointerfaces*, **33**(2):85–88, JAN 15 2004. 12

[46] C Jimenez, J Bartrol, NF deRooij, and M KoudelkaHep. **Use of photopolymerizable membranes based on polyacrylamide hydrogels for enzymatic microsensor construction**. *Analytica chimica acta*, **351**(1-3):169–176, SEP 30 1997. 12

[47] S Abraham, S Brahim, K Ishihara, and A Guiseppi-Elie. **Molecularly engineered p(HEMA)-based hydrogels for implant biochip biocompatibility**. *Biomaterials*, **26**(23):4767–4778, AUG 2005. 12

[48] X Cui, V A Lee, Y Raphael, J A Wiler, J F Hetke, D J Anderson, and D C Martin. **Surface modification of neural recording electrodes with conducting polymer/biomolecule blends**. *J Biomed Mater Res*, **56**(2):261–72, Aug 2001. 13, 51

[49] S Brahim, D Narinesingh, and A Guiseppi-Elie. **Interferent suppression using a novel polypyrrole-containing hydrogel in amperometric enzyme biosensors**. *Electroanalysis*, **14**(9):627–633, MAY 2002. 13

[50] MA Schwarz, B Galliker, K Fluri, T Kappes, and PC Hauser. **A two-electrode configuration for simplified amperometric detection in a microfabricated electrophoretic separation device**. *Analyst*, **126**(2):147–151, 2001. 13

[51] RS Martin, AJ Gawron, BA Fogarty, FB Regan, E Dempsey, and SM Lunte. **Carbon paste-based electrochemical detectors for microchip capillary electrophoresis/electrochemistry**. *Analyst*, **126**(3):277–280, 2001. 13

[52] MA Schwarz and PC Hauser. **Recent developments in detection methods for microfabricated analytical devices**. *Lab on a Chip*, **1**(1):1–6, 2001. 13

[53] PJA Kenis, RF Ismagilov, and GM Whitesides. **Microfabrication inside capillaries using multiphase laminar flow patterning**. *Science*, **285**(5424):83–85, JUL 2 1999. 14

[54] RA Yotter and DM Wilson. **Sensor technologies for monitoring metabolic activity in single cells - Part II: Nonoptical methods and applications**. *IEEE Sensors Journal*, **4**(4):412–429, AUG 2004. 14

[55] F. Lamberti, S. Agnoli, M. Meneghetti, and N. Elvassore. **Nanotubes Oxidation Temperature Controls the Height of Single-Walled Carbon Nanotube Forests on Gold Micropatterned Thin Layers**. *Langmuir*, **26**(13):11344–11348, 2010. 15, 34, 35, 36, 38, 39, 44

[56] YP Sun, KF Fu, Y Lin, and WJ Huang. **Functionalized carbon nanotubes: Properties and applications**. *Acc. Chem. Res.*, **35**(12):1096–1104, DEC 2002. 16

[57] E. T. Thostenson, Z. F. Ren, and T. W. Chou. **Advances in the science and technology of carbon nanotubes and their composites: a review**. *Compos. Sci. Technol.*, **61**:1899–1912, 2001. 16, 20

[58] B. Mahar, C. Laslau, R. Yip, and Y. Sun. **Development of carbon nanotube-based sensors - A review**. *IEEE Sens. J.*, **7**:266–284, 2007. 16

[59] P. Avouris, Z. H. Chen, and V. Perebeinos. **Carbon-based electronics**. *Nature Nanotech.*, **2**:605–615, 2007. 16

[60] J. Im, I. H. Lee, B. Y. Lee, B. Kim, J. Park, W. Yu, U. J. Kim, Y. H. Lee, M. J. Seong, E. H. Lee, Y. S. Min, and S. Hong. **Direct printing of aligned carbon nanotube patterns for high-performance thin film device**. *Appl. Phys. Lett.*, **94**(5):053109, 2009. 16

[61] B. S. Munge, C. E. Krause, R. Malhotra, V. Patel, Gutkind J. S., and J. F. Rusling. **Electrochemical immunosensor for interleukin-6. Comparison of carbon nanotube forest and gold nanoparticle platforms**. *Electrochem. Comm.*, **11**(5):1009–1012, 2009. 16

[62] L. Zhang and D. E. Resasco. **Single-Walled Carbon Nanotube Mars: A superhydrofobic Surface**. *Langmuir*, **25**(8):4792–4798, 2009. 16

[63] K. B. Mogensen, L. Gangloff, P. Boggild, K. B. K. Teo, W. I. Milne, and J. P. Kutter. **Carbon nanotubes integrated in electrically insulated channels for lab-on-a-chip applications**. *Nanotechnol.*, **20**(9):095503, 2009. 16

[64] G. C. Jensen, X. Yu, J. D. Gong, B. Munge, A. Bhirde, S. N. Kim, F. Papadimitrakopoulos, and J. F. Rusling. **Characterization of Multienzyme-antibody-carbon nanotube bioconjugates for immunosensors**. *J. Nanosci. and Nanotechnol.*, **9**(1 SI):249–255, 2009. 16

[65] E. Gregan, S. M. Keogh, A. Maguire, T. G. Hedderman, . O. Neill, G. Chambers, and H. J. Byrene. **Purification and isolation of SWNTs**. *Carbon*, **42**:1031, 2004. 16

[66] H. J. Li, L. Feng, L. H. Guan, Z. J. Shi, and Z. N. Gu. **Synthesis and purification of single-walled carbon nanotubes in the cottonlike soot**. *Solid State Commun*, **132**:219, 2004. 16

[67] D. Nepal, D. S. Kim, and K. E. Geckler. **A facile and rapid purification method for single-walled carbon nanotubes**. *Carbon*, **43**:651, 2005. 16

[68] S. Kundu, Y. Wang, W. Xia, and M. Muhler. **Thermal Stability and Reducibility of Oxygen-Containing Functional Groups on Multiwalled Carbon Nanotube Surfaces: A Quantitative High-Resolution XPS and TPD/TPR Study**. *J. Phys. Chem. C*, **112**(43):16869–16878, 2008. 16

[69] M. L. Toebes, J. M. P. van Heeswijk, J. H. Bitter, A. J. van Dillen, and K. P. de Jong. **The influence of oxidation on the texture and the number of oxygen-containing surface groups of carbon nanofibers**. *Carbon*, **42**:307, 2004. 16

[70] J.J. Gooding, A. Chou, J. Liu, D. Losic, J.G. Shapter, and D.B. Hibbert. **The effects of the lengths and orientations of single-walled carbon nanotubes on the electrochemistry of nanotube-modified electrodes**. *Electrochemistry Communications*, **9**(7):1677–1683, 2007. 16, 34

[71] F. Patolsky, Y. Weizmann, and I. Willner. **Long-Range Electrical Contacting of Redox Enzymes by SWCNT Connectors**. *Angewandte Chemie*, **116**(16):2165–2169, 2004. 16, 34

[72] A. F. Ismail, P. S. Goh, J. C. Tee, S. M. Sanip, and Aziz M. **A review of purification techniques for carbon nanotubes**. *Nano*, **3**(3):127–143, 2008. 16

[73] P. X. Hou, C. Liu, and H. M. Cheng. **Purification of carbon nanotubes**. *Carbon*, **46**(15):2003–2025, 2008. 16

[74] L. Vaccarini, C. Goze, R. Aznar, V. Michiolet, C. Journet, and P. Bernier. **Purification procedure of carbon nanotubes**. *Synth. Met.*, **103**(1-3):2492–93, 1999. 16

[75] E. Dujardin, T.W. Ebbesen, A. Krishnan, and M. M. J. Treacy. **Wetting of single shell carbon nanotubes**. *Adv. Mater.*, **10**(8):611, 1998. 16

[76] K. Tohji. **Purifying single-walled nanotubes**. *Nature*, **383**(6602):679, 1996. 16

[77] Jie Liu, Andrew G. Rinzler, Hongjie Dai, Jason H. Hafner, R. Kelley Bradley, Peter J. Boul, Adrian Lu, Terry Iverson, Konstantin Shelimov, Chad B. Huffman, Fernando Rodriguez-Macias, Young-Seok Shon, T. Randall Lee, Daniel T. Colbert, and Richard E. Smalley. **Fullerene Pipes**. *Science*, **280**(5367):1253–1256, 1998. 17, 18

[78] D. A. Heller, R. M. Mayrhofer, S. Balk, Y. V. Grinkova, M. L. Usrey, and M. S. Strano. **Concomitant length and diameter separation of single-walled carbon nanotubes**. *J. Am. Chem. Soc.*, **126**:14567–14573, 2004. 17

[79] J. A. Fagan, M. L. Becker, J. Chun, and E. K. Hobbie. **Length fractionation of carbon nanotubes using centrifugation**. *Adv. Mater.*, **20**:1609–1613, 2008. 17

[80] D. Q. Yang and E. Sacher. **Carbon 1s X-ray photoemission line shape analysis of highly oriented pyrolytic graphite: The influence of structural damage on peak asymmetry**. *Carbon*, **22**(3):860–862, 2006. 20, 29

REFERENCES

[81] C. Mattevi, G. Eda, S. Agnoli, S. Miller, K. A. Mkhoyan, O. Celik, D. Mastrogiovanni, G. Granozzi, E. Garfunkel, and M. Chhowalla. **Evolution of electrical, chemical, and structural properties of transparent and conducting chemically derived graphene thin films**. *Adv. Funct. Mater.*, **19**:1–7, 2009. 20, 29

[82] C. Hontoria-Lucas, A. J. L. Peinando, J. D. D. Lopez-Gonzalez, M. L. Rojas-Cervantes, and R. M. Martin-Aranda. **Study of oxygen-containing groups in a series of graphite oxides: physical and chemical characterization**. *Carbon*, **33**:1585–1592, 1995. 20, 29

[83] P. Kruger, R. Knes, and J. Friederich. **Surface cleaning by plasma-enhanced desorption of contaminants (PEDC)**. *Surf. Coat. Technol.*, **112**(1-3):240–244, 1999. 21

[84] Elisa Cimetta, Sara Pizzato, Sveva Bollini, Elena Serena, Paolo De Coppi, and Nicola Elvassore. **Production of arrays of cardiac and skeletal muscle myofibers by micropatterning techniques on a soft substrate**. *Biomedical microdevices*, **11**(2):389–400, APR 2009. 21, 25, 51, 57

[85] Kristiana Kandere-Grzybowska, Campbell Christopher, Komarova Yulia, Grzybowski Bartosz, and Boris Gary. **Molecular dynamic imaging in micro-patterned living cells**. *Cell structure and function*, **30**:115–115, 2005. 21, 25

[86] J.J. Gooding. **Nanostructuring electrodes with carbon nanotubes: A review on electrochemistry and applications for sensing**. *Electrochimica Acta*, **50**(15):3049–3060, 2005. 23, 34

[87] J. H. Du, J. Bai, and H. M. Cheng. **The present status and key problems of carbon nanotube based polymer composites**. *Express Polym. Lett.*, **1**(5):253–273, 2007. 23

[88] W. Xia, C. Jin, S. Kundu, and M. Muhler. **A highly efficient gas-phase route for the oxygen functionalization of carbon nanotubes based on nitric acid vapor**. *Carbon*, **47**:919–922, 2009. 24

[89] Roman Brukh and Somenath Mitra. **Kinetics of carbon nanotube oxidation**. *Journal of Material Chemistry*, **17**:619–623, 2007. 29

[90] H. Shi and J.I. Yeh. **Part I: recent developments in nanoelectrodes for biological measurements**. *Nanomedicine*, **2**(5):587–598, 2007. 34

[91] S.N. Kim, J.F. Rusling, and F. Papadimitrakopoulos. **Carbon nanotubes for electronic and electrochemical detection of biomolecules**. *Advanced Materials*, **19**(20):3214–3228, 2007. 34

[92] W. Yang, P. Thordarson, J.J. Gooding, S.P. Ringer, and F. Braet. **Carbon nanotubes for biological and biomedical applications**. *Nanotechnology*, **18**:412001, 2007. 34

[93] L.Y. Heng, A. Chou, J. Yu, Y. Chen, and J.J. Gooding. **Demonstration of the advantages of using bamboo-like nanotubes for electrochemical biosensor applications compared with single walled carbon nanotubes**. *Electrochemistry Communications*, **7**(12):1457–1462, 2005. 34

[94] B.S. Flavel, J. Yu, J.G. Shapter, and J.S. Quinton. **Electrochemical characterisation of patterned carbon nanotube electrodes on silane modified silicon**. *Electrochimica Acta*, **53**(18):5653–5659, 2008. 34

[95] J. Yu, J.G. Shapter, M.R. Johnston, J.S. Quinton, and J.J. Gooding. **Electron-transfer characteristics of ferrocene attached to single-walled carbon nanotubes (SWCNT) arrays directly anchored to silicon (1 0 0)**. *Electrochimica Acta*, **52**(21):6206–6211, 2007. 34

[96] D.J. Garrett, B.S. Flavel, J.G. Shapter, K.H.R. Baronian, and A.J. Downard. **Robust Forests of Vertically Aligned Carbon Nanotubes Chemically Assembled on Carbon Substrates**. *Langmuir*, **26**(3):1848–1854, 2009. 34

[97] D. Nkosi, J. Pillay, KI Ozoemena, K. Nouneh, and M. Oyama. **Heterogeneous electron transfer kinetics and electrocatalytic behaviour of mixed self-assembled ferrocenes and SWCNT layers.** *Physical chemistry chemical physics*, **12**(3):604, 2010. 34, 37

[98] Z. Wang, M. Li, P. Su, Y. Zhang, Y. Shen, D. Han, A. Ivaska, and L. Niu. **Direct electron transfer of horseradish peroxidase and its electrocatalysis based on carbon nanotube/thionine/gold composites**. *Electrochemistry Communications*, **10**(2):306–310, 2008. 34

[99] Hui Hu, Bin Zhao, Mikhail E. Itkis, and Robert C. Haddon. **Nitric Acid Purification of Single-Walled Carbon Nanotubes**. *The Journal of Physical Chemistry B*, **107**(50):13838–13842, 2003. 34

[100] J.W. Jo, J.W. Jung, J.U. Lee, and W.H. Jo. **Fabrication of Highly Conductive and Transparent Thin Films from Single-Walled Carbon Nanotubes Using a New Non-ionic Surfactant via Spin Coating**. *ACS Nano*, **4**(9):5382–5388, 2010. 35

[101] X. Yu, S.N. Kim, F. Papadimitrakopoulos, and J.F. Rusling. **Protein immunosensor using single-wall carbon nanotube forests with electrochemical detection of enzyme labels**. *Molecular BioSystems*, **1**(1):70–78, 2005. 35

[102] Z. Liu, Z. Shen, T. Zhu, S. Hou, L. Ying, Z. Shi, and Z. Gu. **Organizing single-walled carbon nanotubes on gold using a wet chemical self-assembling technique**. *Langmuir*, **16**(8):3569–3573, 2000. 35

[103] LR Bard, AJ; Faulkner. *Electrochemical Methods, Fundamentals and Applications.* John Wiley & Sons, 2nd edition, 2001. 37

[104] B.B. Parekh, G. Fanchini, G. Eda, and M. Chhowalla. **Improved conductivity of transparent single-wall carbon nanotube thin films via stable postdeposition functionalization**. *Applied Physics Letters*, **90**:121913, 2007. 37

[105] M. Gerritsen, A. Kros, V. Sprakel, JA Lutterman, RJ Nolte, and JA Jansen. **Biocompatibility evaluation of sol-gel coatings for subcutaneously implantable glucose sensors**. *Biomaterials*, **21**(1):71–78, 2000. 50

[106] X. Cui, J. Wiler, M. Dzaman, R.A. Altschuler, and D.C. Martin. **In vivo studies of polypyrrole/peptide coated neural probes**. *Biomaterials*, **24**(5):777–787, 2003. 50

[107] P.M. George, A.W. Lyckman, D.A. LaVan, A. Hegde, Y. Leung, R. Avasare, C. Testa, P.M. Alexander, R. Langer, and M. Sur. **Fabrication and biocompatibility of polypyrrole implants suitable for neural prosthetics**. *Biomaterials*, **26**(17):3511–3519, 2005. 50

[108] H. Li, D.Q. Wang, H.L. Chen, B.L. Liu, and L.Z. Gao. **A Novel Gelatin–carbon nanotubes hybrid hydrogel**. *Macromolecular Bioscience*, **3**(12):720–724, 2003. 50

[109] T. Alfrey Jr, EF Gurnee, and WG Lloyd. **Diffusion in glassy polymers**. *Journal of Polymer Science Part C: Polymer Symposia*, **12**(1):249–261, 1966. 50

[110] X. Cao and MS Shoichet. **Photoimmobilization of biomolecules within a 3-dimensional hydrogel matrix**. *Journal of Biomaterials Science, Polymer Edition*, **13**(6):623–636, 2002. 50

[111] A. Guiseppi-Elie, AM Wilson, and KE Brown. **Electroconductive Hydrogels: Novel Materials for the Controlled Electrorelease of Bioactive Peptides**. *POLYMER PREPRINTS-AMERICA-*, **38**:608–609, 1997. 50

[112] A. Guiseppi-Elie. **Electroconductive hydrogels: Synthesis, characterization and biomedical applications**. *Biomaterials*, **31**(10):2701–2716, 2010. 50, 51

[113] Elena Serena, Susi Zatti, Elena Reghelin, Alessandra Pasut, Elisa Cimetta, and Nicola Elvassore. **Soft substrates drive optimal differentiation of human healthy and dystrophic myotubes**. *Integrative Biology*, **2**(4):193–201, 2010. 51

[114] E.A. Moschou, M.J. Madou, L.G. Bachas, and S. Daunert. **Voltage-switchable artificial muscles actuating at near neutral pH**. *Sensors and Actuators B: Chemical*, **115**(1):379–383, 2006. 51

[115] JP Gong, I. Kawakami, VG Sergeyev, and Y. Osada. **Electroconductive organogel. 3. Preparation and properties of a charge-transfer complex gel in an organic solvent**. *Macromolecules*, **24**(19):5246–5250, 1991. 51

[116] J.H.O. Owino, O.A. Arotiba, P.G.L. Baker, A. Guiseppi-Elie, and E.I. Iwuoha. **Synthesis and characterization of poly (2-hydroxyethyl methacrylate)-polyaniline based hydrogel composites**. *Reactive and Functional Polymers*, **68**(8):1239–1244, 2008. 51

[117] L. Janovák and I. Dékány. **Optical properties and electric conductivity of gold nanoparticle-containing hydrogel-based thin layer composite films obtained by photopolymerization**. *Applied Surface Science*, **256**(9):2809 – 2817, 2010. 51

[118] Q. Tang, J. Lin, and J. Wu. **The preparation and electrical conductivity of polyacrylamide/graphite conducting hydrogel**. *Journal of Applied Polymer Science*, **108**(3):1490–1495, 2008. 51

[119] R.A. MacDonald, C.M. Voge, M. Kariolis, and J.P. Stegemann. **Carbon nanotubes increase the electrical conductivity of fibroblast-seeded collagen hydrogels**. *Acta Biomaterialia*, **4**(6):1583–1592, 2008. 51

[120] J.N. Coleman, S. Curran, AB Dalton, AP Davey, B. McCarthy, W. Blau, and RC Barklie. **Percolation-dominated conductivity in a conjugated-polymer-carbon-nanotube composite**. *Physical Review B*, **58**(12):7492–7495, 1998. 51

[121] O. Meincke, D. Kaempfer, H. Weickmann, C. Friedrich, M. Vathauer, and H. Warth. **Mechanical properties and electrical conductivity of carbon-nanotube filled polyamide-6 and its blends with acrylonitrile/butadiene/styrene**. *Polymer*, **45**(3):739–748, 2004. 51

[122] D.L. Nelson and M.M. Cox. *I principi di biochimica di Lehninger*. Zanichelli, Bologna, febbraio 2002. 57, 76

[123] J. Wang and M. Musameh. **Carbon-nanotubes doped polypyrrole glucose biosensor**. *Analytica Chimica Acta*, **539**(1-2):209–213, 2005. 57

[124] Y. Yao and K.K. Shiu. **Electron-transfer properties of different carbon nanotube materials, and their use in glucose biosensors**. *Analytical and Bioanalytical Chemistry*, **387**(1):303–309, 2007. 57

[125] D. Krinke, H.G. Jahnke, O. P
"anke, and A.A. Robitzki. **A microelectrode-based sensor for label-free in vitro detection of ischemic effects on cardiomyocytes**. *Biosensors and Bioelectronics*, **24**(9):2798–2803, 2009. 58

[126] U.K. Laemmli et al. **Cleavage of structural proteins during the assembly of the head of bacteriophage T4**. *Nature*, **227**(5259):680–685, 1970. 59

[127] B.E.P. Swoboda and V. Massey. **Purification and Properties of the Glucose Oxidase from Aspergillus niger**. *J. Biol. Chem.*, **240**(5):2209–2215, 1965. 60

[128] P.S. Dittrich and A. Manz. **Lab-on-a-chip: microfluidics in drug discovery**. *Nature Reviews Drug Discovery*, **5**(3):210–218, 2006. 74

[129] M.H. Wu, S.B. Huang, and G.B. Lee. **Microfluidic cell culture systems for drug research**. *Lab on a Chip*, **10**(8):939–956, 2010. 74

[130] T.M. Squires and S.R. Quake. **Microfluidics: Fluid physics at the nanoliter scale**. *Reviews of modern physics*, **77**(3):977–1026, 2005. 74

[131] J.H. Choi, S.K. Lee, J.M. Lim, S.M. Yang, and G.R. Yi. **Designed pneumatic valve actuators for controlled droplet breakup and generation**. *Lab on a Chip*, **10**(4):456–461, 2010. 74

[132] M.R. Bringer, C.J. Gerdts, H. Song, J.D. Tice, and R.F. Ismagilov. **Microfluidic systems for chemical kinetics that rely on chaotic mixing in droplets**. *Philosophical Transactions of the Royal Society of London. Series A: Mathematical, Physical and Engineering Sciences*, **362**(1818):1087, 2004. 74

[133] D.B. Weibel and G.M. Whitesides. **Applications of microfluidics in chemical biology**. *Current Opinion in Chemical Biology*, **10**(6):584–591, 2006. 74

[134] D.N. Breslauer, P.J. Lee, and L.P. Lee. **Microfluidics-based systems biology**. *Molecular BioSystems*, **2**(2):97–112, 2006. 74

[135] J. Hong, J.B. Edel, and A.J. deMello. **Micro-and nanofluidic systems for high-throughput biological screening**. *Drug discovery today*, **14**(3-4):134 –146, 2009. 74

REFERENCES

[136] K. Sato, K. Mawatari, and T. Kitamori. **Microchip-based cell analysis and clinical diagnosis system**. *Lab on a Chip*, **8**(12):1992–1998, 2008. 74

[137] JGE Gardeniers and A. Van den Berg. **Lab-on-a-chip systems for biomedical and environmental monitoring**. *Analytical and bioanalytical chemistry*, **378**(7):1700–1703, 2004. 74

[138] G.S. Wilson and R. Gifford. **Biosensors for real-time in vivo measurements**. *Biosensors and Bioelectronics*, **20**(12):2388–2403, 2005. 74

[139] A. Lardner. **The effects of extracellular pH on immune function**. *Journal of leukocyte biology*, **69**(4):522, 2001. 74

[140] J.N. Trochu, J.B. Bouhour, G. Kaley, and T.H. Hintze. **Role of endothelium-derived nitric oxide in the regulation of cardiac oxygen metabolism: implications in health and disease**. *Circulation research*, **87**(12):1108, 2000. 74

[141] O. Geschke, H. Klank, and P. Tellemann. *Microsystem Engineering of Lab-on-a-chip Devices*. Vch Verlagsgesellschaft Mbh, 2004. 74

[142] R.S. Marks. *Handbook of biosensors and biochips*. John Wiley & Sons, 2007. 74

[143] P. H. Seeberger and T. Blume. *New Avenues to Efficient Chemical Synthesis*. Heidelberg: Springer Berlin Heidelberg, 2006. 74

[144] A. Khademhosseini, R. Langer, J. Borenstein, and J.P. Vacanti. **Microscale technologies for tissue engineering and biology**. *Proceedings of the National Academy of Sciences of the United States of America*, **103**(8):2480, 2006. 74

[145] W. Cheng, N. Klauke, G. Smith, and J.M. Cooper. **Microfluidic cell arrays for metabolic monitoring of stimulated cardiomyocytes**. *Electrophoresis*, **31**(8):1405–1413, 2010. 74

[146] I.A. Ges and F. Baudenbacher. **Enzyme electrodes to monitor glucose consumption of single cardiac myocytes in sub-nanoliter volumes**. *Biosensors and Bioelectronics*, **25**(5):1019–1024, 2010. 75

[147] I.A. Ges and F. Baudenbacher. **Enzyme-coated microelectrodes to monitor lactate production in a nanoliter microfluidic cell culture device**. *Biosensors and Bioelectronics*, 2010. 75

[148] J. Gottschamel, L. Richter, A. Mak, C. Jungreuthmayer, G. Birnbaumer, M. Milnera, H. Bru ckl, and P. Ertl. **Development of a Disposable Microfluidic Biochip for Multiparameter Cell Population Measurements**. *Analytical chemistry*, **81**(20):8503–8512, 2009. 75

[149] A. Weddemann, F. Wittbracht, A. Auge, and A. H "utten. **Positioning system for particles in microfluidic structures**. *Microfluidics and Nanofluidics*, **7**(6):849–855, 2009. 75

[150] O. Frey, S. Talaei, P.D. Wal, M. Koudelka-Hep, and N.F. Rooij. **Continuous-flow multi-analyte biosensor cartridge with controllable linear response range**. *Lab on a Chip*, **10**(17):2226–2234, 2010. 75

[151] M. Brivio, W. Verboom, and D.N. Reinhoudt. **Miniaturized continuous flow reaction vessels: influence on chemical reactions**. *Lab on a Chip*, **6**(3):329–344, 2006. 75

[152] S. Natarajan, A. Hatch, D.G. Myszka, and B.K. Gale. **Optimal conditions for protein array deposition using continuous flow**. *Analytical chemistry*, **80**(22):8561–8567, 2008. 75

[153] J.C. Yoo, G.S. La, CJ Kang, and Y.S. Kim. **Microfabricated polydimethylsiloxane microfluidic system including micropump and microvalve for integrated biosensor**. *Current Applied Physics*, **8**(6):692–695, 2008. 75

[154] Z. Li, Q. He, D. Ma, and H. Chen. **On-chip integrated multi-thermo-actuated microvalves of poly (N-isopropylacrylamide) for microflow injection analysis**. *Analytica chimica acta*, 2010. 75

[155] A. van den Berg and T. Lammerink. **Micro total analysis systems: microfluidic aspects, integration concept and applications**. *Microsystem technology in chemistry and life science*, pages 21–49, 1998. 75

[156] P.A. Serra, G. Rocchitta, G. Bazzu, A. Manca, G.M. Puggioni, J.P. Lowry, and R.D. O'Neill. **Design and construction of a low cost single-supply embedded telemetry system for amperometric biosensor applications**. *Sensors and Actuators B: Chemical*, **122**(1):118–126, 2007. 76, 80

[157] J. Melin and S.R. Quake. **Microfluidic large-scale integration: the evolution of design rules for biological automation**. *Biophysics*, **36**(1):213, 2007. 81